2nd SIRINDHORN CONFERENCE ON GEOINFORMATICS 2018

1 - 2 FEBRUARY 2018
09:00 - 17:00

AT CENTRA BY CENTARA GOVERNMENT COMPLEX HOTEL & CONVENTION CENTRE
Chaeng Wattana, Bangkok, Thailand

FOR MORE INFORMATION
Please kindly contact the conference secretariat at **scgi@gistda.or.th**

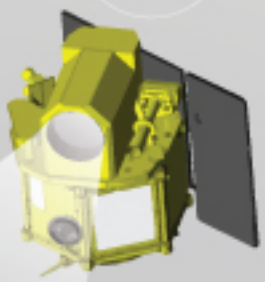

GISTDA

2nd SIRINDHORN CONFERENCE ON GEOINFORMATICS 2018

1-2 FEBRUARY 2018

CENTRA BY CENTARA GOVERNMENT COMPLEX HOTEL

& CONVENTION CENTRE

CHAENG WATTANA, BANGKOK, THAILAND

2nd SIRINDHORN CONFERENCE ON GEOINFORMATICS 2018

1-2 FEBRUARY 2018

WELCOME ADDRESSES

DR. ANOND SNIDVONGS

Chair of Organizing Committee of the Sirindhorn Conference on Geo-informatics & *Executive Director of Geo-Informatics and Space Technology Development Agency Ministry of Science and Technology, Thailand.*

On behalf of the local organizing committee, I would like to welcome all geospatial communities to attend the 2nd Sirindhorn Conference on Geo-informatics during February 1-2, 2018.

The Sirindhorn Conference on Geo-informatics is under the supervision of Sirindhorn Center of Geo-informatics, which aims to increase and improve the capability of personnel knowledge and innovative research development in the region in space and geo-informatics technology. The Sirindhorn Conference on Geo-informatics was first held on March 21, 2015 at the Space Krenovation Park, Sriracha, Chonburi, Thailand. Following the success in 2015, this year's conference was held at Centra by Centara Government Complex Hotel & Convention Centre, Chaeng Wattana, Bangkok, Thailand.

Space and geo-informatics technology have been an important tool to help solving many sustainability issues, such as disaster, agriculture, pollution, and natural resource management. Now, we are moving toward the next era, the geo-intelligence, the platform that integrates human society, security, politics, economics, and engineering solutions for global and regional sustainability. This technology and its innovation become part of everyone life though personal devices using internet of things, drone and crowded sensor networks. The integration among these technologies will elevate the quality of living for humankind in the long term.

The various outstanding papers of this conference highlight new development in this geo-intelligent technology. This is therefore a good sign indicating achievement on the latest advancements in the rapidly changing technology. Additionally, it is a great opportunity for you to discover new innovations and applications from around the Asia countries and to build new connections with them as well as to strengthening scientific and technological collaboration.

Once again, I wish everyone an enjoyable conference and hope that the ideas, knowledge, and experiences on a wide range of subjects will help in paving the way for the future direction of the space and geo-informatics technology.

Best regards,

PROF. DR. RUIZHI CHEN

Director of the State Key Lab of Information Engineering in Surveying, Mapping and Remote Sensing, Wuhan University, China.

Dear colleagues and friends

Geo-informatics is now becoming a hot topic as it will play a pivotal role in the on-coming era of Artificial Intelligence. Global monitoring using high resolution satellite imagery, smart-city, road environment sensing and mapping for autonomous driving and mobile location-based services are good examples that demonstrate the potential of geo-informatics technologies for future AI applications. Geo-informatics covers the topics of sensing and processing geospatial data from global scale based on satellite images to personal scale based on data collected from smartphones. It further discovers knowledge by exploring the geotagged flow big data such as human flows and vehicle flows. Geo-informatics is now entering into a new era along with the development of science and technology. It will serve the World in a more intelligent way.

The 2nd Sirindhorn Conference on Geo-informatics will be held in Bangkok, Thailand, in February 1-2, 2018. This conference is organized by Sirindhorn Center for Geo-Informatics (SCGI), which supported by the Ministry of Science and Technology of the Kingdom of Thailand and Wuhan University of the People's Republic of China. The conferences aims to provide a forum to exchange ideas and experiences on space technology and geo-informatics through applications, study cases and practical experiences. It will improve and enhance the collaboration and cooperation between the intellectuals, professional and government bodies in achieving a common vision towards knowledge sharing of geo-informatics across discipline. Experts, scholars and users from different parts of the world will gather in the beautiful city, Bangkok, to exchange the latest research results, to share successful experiences and to understand the current academic and technical development in geo-informatics. It is an excellent opportunity to meet experts and colleagues in this field. Looking forward to seeing you in Bangkok, Thailand!

Best regards,

SIRINDHORN CONFERENCE ON GEOINFORMATICS 2018

1-2 FEBRUARY 2018

KEYNOTE SPEAKER

PROF. DR. RUIZHI CHEN

Prof. Dr. Ruizhi Chen is currently the Director of the State Key Laboratory of Information Engineering in Surveying, Mapping and Remote Sensing, Wuhan University. He used to work an Endowed Chair and Professor in Texas A&M University Corpus Christ, U.S. and Head & Professor of the Department of Navigation and Positioning at the Finnish Geodetic Institute, Finland. He has published two books: *Geospatial Computing in Mobile Devices* and *Ubiquitous Positioning and Mobile Location-Based Services in Smart Phones*. He is an author/co-author of more than 170 scientific papers and 5 book chapters. His research results have been selected twice as cover stories in "*GPS Worlds*". His Ph.D. students have received 7 international student paper awards, including 3 times of student-wining papers in the Institute of Navigation for 2010, 2012 and 2013. Dr. Chen is the general chair of the IEEE conferences "*Ubiquitous Positioning, Indoor Navigation and Location-based Services*", Editor-in-Chief the *Journal of Global Positioning Systems* and associate editor of the *Journal of Navigation*. Dr. Chen was the President of the International Association of Chinese Professionals in Global Positioning Systems (2008) and board member of the Nordic Institute of Navigation (2009-2012). Dr. Chen's research interests include smartphone positioning indoors/outdoors, context awareness and satellite navigation.

TITLE OF MY PRESENTATION

PRECISE SMARTPHONE POSITIONING INDOORS

Short description of my presentation

Indoor positioning is one of the core technologies of artificial intelligence (AI) and will play a pivotal role in the upcoming era of AI. However, affected by the complexity of the indoor spaces, it is still challenging to develop a smartphone-based real-time positioning solution indoors with high accuracy, lost-cost and large coverage. This presentation introduces a solution of smartphone-based positioning solution indoors by integrating the measurements of built-in sensors and RF radios together with various high precision positioning techniques including camera re-sectioning, acoustic ranging, and Angle of Arrival from Bluetooth antenna array. The high precise positioning techniques are used to control the error propagation in large indoor space, while the built-in sensors including the accelerometer, gyroscope, magnetometer and RF radios are used to fill the gaps among the hot spots covered by the high precise positioning techniques.

2nd SIRINDHORN CONFERENCE ON GEOINFORMATICS 2018

1-2 FEBRUARY 2018

KEYNOTE SPEAKER

PROF. DR. CHIH-HONG SUN

Prof. Dr. Chih-Hong Sun is a professor at Geography Department, National Taiwan University and Past President of Taiwan Geographic Information Society (2005-2006). In 2008 he was appointed as chairman of Taiwan Geographic Information System Center, which is a non-profit organization funded by the Council of Economic Planning and Development, Executive Yuan. Dr. Sun was also elected as president for Asia Geographic Information System Association in 2010. Dr. Sun received his undergraduate education at the National Taiwan University (1977) and his Ph.D. degree in geography from the University of Georgia, USA (1986). He served as director of the Global Change Research Center, National Taiwan University from 1998 to 2004 and the executive secretary of the Commission on Sustainable Development Research, National Science Council from March, 1998 to June, 2000. Prior to that, Dr. Sun also served as chairman of the geography department, National Taiwan University from August 1994 till July 1997. His research specialties are in geographic information system, spatial decision support system, hazards mitigation, and sustainable development. His recent researches are concentrated in developing intelligent spatial decision support system for natural hazards mitigation and for sustainable development issues. Dr. Sun is the project leader for the design of the National Geographic Information System in Taiwan.

TITLE OF MY PRESENTATION

SMART EARTH COLLABORATION PLATFORM

Short description of my presentation

With over half of the world's population now living in cities, the pace of urbanization has been accelerating. As a result, major cities around the world are faced with multiple challenges, including traffic jam, insufficient infrastructure, rising unemployment, environmental pollution, and deteriorating security. How to cope with those challenges has become an inescapable issue for city chiefs. Fortunately, rapid development of information communications technologies, such as the maturing technologies for cloud computing, the Internet of Things (IoT), wireless sensing network, big data analytics, semantic web, social network, and geographic information system, have opened up opportunities for them to cope with the challenges. Smart earth and smart city that deploy these smarter technologies will provide a brighter future for mankind in the near future; however, it requires the world's governments, academia, and business community to work together to face the challenges. This paper presents the concept of Smart Earth Collaboration Platform (SECP) based on semantic web technology and open data policy. We employ the Open Semantic Framework (OSF) to integrate various kind of structured, semi-structured, and unstructured data. OSF integrates many kinds of open source software on the semantic web forming a useful open framework platform for data integration and knowledge management. Via the employment of SECP, the world of information can be combined into a super big data system for common sharing, and academic research results can also be pooled into a sharable knowledge base. Decision makers only need to raise decision-making needs on SECP and decision support system developers will take advantage of this sharable super big data system and sharable knowledge base to develop customized decision support system for decision makers.

SIRINDHORN CONFERENCE ON GEOINFORMATICS 2018

1-2 FEBRUARY 2018

CENTRA BY CENTARA GOVERNMENT COMPLEX HOTEL
AND CONVENTION CENTRE
CHAENG WATTANA, BANGKOK, THAILAND

INTRODUCTION

Sirindhorn Center for Geo-Informatics (SCGI) is established under the cooperation between the Ministry of Science and Technology of Thailand (MOST) by Geo-Informatics and Space Technology Development Agency (Public Organization): GISTDA, and Wuhan University by State Key Laboratory of Information Engineering Surveying, Mapping and Remote Sensing: LIESMARS, the People's Republic of China. The center located at Space Krenovation Park (SKP), Sri Racha, Chonburi, Thailand. HRH Princess Maha Chakri Sirindhorn graciously presided over the inauguration ceremony the center on March 20, 2015.

To promote the center as the international center of technology transfer and capacity building of space technology and geo-informatics, GISTDA, MOST Thailand and Wuhan University, China jointly organize the 1st Sirindhorn Conference on GeoInformatics on March 21, 2015 at the Auditorium of SCGI, SKP, Sriracha, Chonburi, Thailand.

In this year, the 2nd Sirindhorn Conference on Geo-informatics 2018 is held at Centra by Centara Government Complex Hotel & Convention Centre, Chaeng Wattana, Bangkok, Thailand, during February 1-2, 2018. This conference is established in the theme of "Space Technology and Geo-informatics" and encourage submission on research and applications of the new technologies in multidiscipline involve the theme.

OBJECTIVE

The 2nd Sirindhorn Conference on Geo-informatics aims to provide a forum to exchange ideas and experiences on space technology and geo-informatics through applications, study cases and practical experiences. This would improve and enhance the collaboration and cooperation between the intellectuals, professional and government bodies in achieving a common vision towards knowledge sharing of geo-informatics across discipline.

ORGANIZERS

GEO-INFORMATICS AND SPACE TECHNOLOGY DEVELOPMENT AGENCY (GISTDA)

Geo-Informatics and Space Technology Development Agency (Public Organization) or GISTDA is a government organization under the supervision of the Ministry of Science and Technology. It is Thailand's core agency responsible for providing satellite remote sensing and Geographic Information System (GIS) data, applications, solution and services to both public and private sector, nationally and internationally. GISTDA also conducts capacity building programmes in GIS and its applications and actively involves in research and development in space and geo-informatics technology.

GISTDA is the operator of Thaichote, Thailand's first high resolution on Earth Observation satellite. GISTDA has a ground receiving station network and agreements giving access to more than 20 foreign satellites, the largest section in Southeast Asia. Moreover, GISTDA has been working with a variety of data sources including data from airborne sensor, Unmanned Aerial Vehicles (UAVs), coastal radar system, mobile mapping units and ground measuring instruments.

https://www.gistda.or.th

MINISTRY OF SCIENCE AND TECHNOLOGY, THAILAND

The Ministry of Science and Technology (MOST) is presently tasked with forwarding the policy and strategic plan for science, technology and innovation and seeing to its effective and substantive implementation, both in terms of research and development as well as in terms of creating cooperative mechanisms between all sectors of society, with a view to promote economic benefits and enhancing quality of life. Under the vision of "excelling as the steward or main organization in the development of science, technology and innovation", the Ministry of Science and Technology aims to create and enrich the intellect of Thai society.

https://www.most.go.th

WUHAN UNIVERSITY

Wuhan University (武汉大学) is located in Wuhan, Hubei, China.

The University is administered by the Ministry of Education of the People's Republic of China. Wuhan University is the world class comprehensive research university and key national university of China, particular in Geoinfomatics technology. The university is situated at Luojia Hill, with palatial buildings blending the Chinese and Western style. It was commonly regarded as one of the most beautiful campuses and top 10 universities for decades in China.

http://en.whu.edu.cn

CRITICAL DATES

ABSTRACT SUBMISSION DEADLINE
15 December 2017

ABSTRACT ACCEPTANCE
20 December 2017

FULL PAPER SUBMISSION DEADLINE
10 January 2018

REGISTRATION DEADLINE
15 January 2018

REGISTRATION

ONLINE REGISTRATION
Online registration is available via the SCGI website (http://scgi.gistda.or.th) including entire conference information. The cost of registration fee is 100 USD for normal registration includes permission to all technical session, a flash drive includes all accepted abstract and full papers, food, welcome banquet and coffee breaks. Online registration will be closed on January 15, 2018.

FOR MORE INFORMATION
Please kindly contact the conference secretariat at
scgi@gistda.or.th

LOCATION

CENTRA BY CENTARA GOVERNMENT COMPLEX HOTEL & CONVENTION CENTRE CHAENG WATTHANA

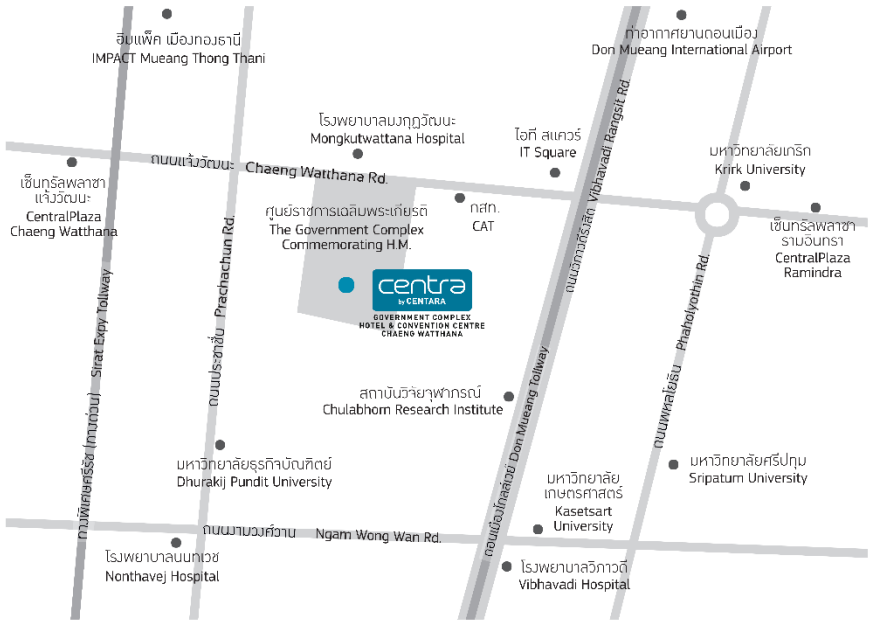

Address: Chaeng Watthana, 120 Moo 3 Convention Centre Building,Bangkok 10210, Thailand

Phone: +66 (0) 2143 1234

Fax: +66 (0) 2143 1235

Email: cgc@chr.co.th

VISA

It is important for those participants from overseas to check their visa require for entry into Thailand. It is strongly recommended that you contact, as soon as possible, the Embassy or Consulate of Thailand in your country to ascertain whether or not you require a visa and to check details of visa requirement, if any. Please note that it may take a few weeks to obtain a visa following the submission of visa application.

List of Thailand Mission Abroad

http://www.thaiembassy.org/main/

List of Countries which have Concluded Agreement on the Exemption of Visa Requirements with Thailand.

http://www.mfa.go.th/main/en/services/4908

Before applying for the visa, please make sure that you have a passport that is valid for at least 6 months counting from the date of arrival in Thailand. Please note that any cost involved in obtaining the visa should be borne by the participant concerned.

Any participants who requires an invitation letters from GISTDA, the local organization in Thailand, for visa application purpose should provide needed information when register for The 2nd Sirindhorn Conference on Geo-informatics 2018.

PROGRAM COMMITTEES

PROF. DR. DEREN LI
Wuhan University, China

PROF. DR. JIANYA GONG
Academician of Chinese Academy of Sciences, Dean, School of Remote Sensing and Information Engineering, Wuhan University, China

PROF. DR. CHEN RUIZHI
Director of LIESMARS, Wuhan University, China

ORGANIZING COMMITTEES

DR. ANOND SANITWONG
Executive Director of Geo-Informatics and Space Technology Development Agency

DR. DAMRONGRIT NIAMMUAD
Director of Space Krenovation Park and Acting Rector GISTDA Academy

MS. PRANPRIYA WONGSA
Acting Director of Knowledge Development and Outreach Office, GISTDA

SCRETARY

DR. TANITA SUEPA
Chief of Instructional Media and Curriculum Development Division

DR. CHANIKA SUKAWATTANAVIJIT
Geo-Informatics Scientist

MS. NATNAPHAT SUBTAWEEPOLLERT
Geo-Informatics Scientist

CONTACT INFORMATION

Dr.Tanita Suepa and Dr.Chanika Sukawattanavijit

Geo-informatics and Space Technology Development Agency (GISTDA)

E-mail: scgi@gistda.or.th

Phone: +66-02-561-4505#231

Fax: +66-02-561-4503

SPEAKER GUIDELINE

Photo by Marcos Luiz Photograph on Unsplash

PLEASE READ ALL OF THE INFORMATION BELOW

BEFORE COMING TO THE CONFERENCE

The following guidelines are provided to assist invited speakers and plenary presenters. By following these important tips, your presentation will go smoothly.

SESSION EQUIPMENT

All of the session room computers will be laptops; therefore, Mac users should review the sections below regarding supported formats and files. If you have any questions, contact us at scgi@gistda.or.th

SLIDE SHARING OPTION

We will share your presentation in our website (available a few weeks after the meeting) for speakers who wish to share their slides with fellow SCGICON2018 attendees. A 16:9 wide screen format will be used for projection of slides in this conference.

PLENARY PRESENTATION

VERY IMPORTANT! Presenters need to turn in their presentation to the registration desk at in front of Room BB404 as scheduled below:

1st February 2018

Registration Time *10:00-12:00*

2nd February 2018

Registration Time *07:30-08:30*

Due to the large volume of presentations, this preparation time is very important for necessary arrangement so that the program can proceed smoothly. In case presenters arrive less than 12 hours in advance, please take your USB flash drive or CD to the registration desk at your presentation room at least 30 minutes before your presentation time – no later than that!

LANGUAGE: All oral presentations must be in English.

LENGTH OF PRESENTATION: A total of 20 minutes (15 minutes for the presentation and 5 minutes for Q & A) has been allocated for each talk. To ensure the session runs smoothly, please respect the time allotted for your presentation. A moderator will be present to manage the time.

SYSTEM REQUIREMENTS:

- Presenters will not be allowed to use their own computers because of the time taken to switch between computers during the sessions and the possibility of crashes with the onsite system.
- Presenters will not be allowed to put their USB Flash driver or CD directly into the session room computer for the same reason as above.
- Presenters should save their PowerPoint presentation on a storage device that can be turned in and left with our staff (ie. CD or USB Flash drive).

VIDEO AND AUDIO FILE SUPPORT FOR PRESENTATIONS

- Considerations for custom fonts: We only supply fonts that are included with normally for Microsoft Office 2013. If you need a specialized font, it should be embedded into your PowerPoint presentation. Some licensed fonts may not embed and should be replaced with a font included with Office.
- Links to Web Pages: Meeting Room computers may be not connected to the Internet. Links to web pages will not function and may cause issues if clicked accidentally during your presentation. We strongly recommend removing all internet links from your presentation.

AUDIOVISUAL EQUIPMENT

The audiovisual equipment available inside the room includes:

- Computer, monitor, and mouse/slide advancer on a lighted lectern
- Data projector
- Screen
- Monitor for speaker presentation mode and notes
- Speaker timer with flashing lights to let you know when your time is almost up
- Lavaliere microphone
- Lectern microphone
- Table microphone
- Aisle microphones will be placed in the audience for the question and answer period

There will *not be an Internet connection.* If you require equipment not listed above or require an Internet connection for your presentation, please contact us at scgi@gistda.or.th prior to January 25.

BACKUP: Please bring a backup copy of your presentation with you to the conference. You should copy your PowerPoint and all movies to a folder on a USB thumb drive. PowerPoint does NOT embed movies. They must be placed in the same folder as your PowerPoint. It is good practice to keep a second copy in your luggage.

ON THE DAY OF PRESENTATION

- Arrive at the meeting room at least 30 minutes before the start of your session (not your talk) and introduce yourself as a speaker to the technical administration and chairpersons. Please sit near the stage to ease the transition between talks.
- It is important that all speakers stay on time. Coordinator has been instructed to stop you from speaking if you go over the allotted time.
- At the lectern, there will be a monitor where you can follow your presentation. Simply click your session time, then click your name on the display, and your PowerPoint will launch automatically.
- Speak directly into the microphone in a normal voice, and do not handle the microphone while speaking.
- If you have any difficulties or need any assistance while you are on presentation, please raise your hand.

TEST YOUR PRESENTATION

Test your presentation on a PC computer to ensure that all videos and photos open correctly.

Please name your file with ONLY the following 3 items:

1. Paper ID
2. Session
3. Presentation room name/number –with an UNDERSCORE between each item.

Please name your PowerPoint file as requested, so that your presentation can be easily identified and loaded to the onsite computers.

GUIDELINES FOR CHAIRPERSONS & CO-CHAIRPERSONS

Photo by Arthur Miranda on Unsplash

The following is a brief description of the functions of the Chairpersons and Co-chairpersons

CONDUCTING THE SESSION

The chairperson is responsible for conducting the session time (a timer device is available in the conference room to help with this). The times indicated in the program schedule for each presentation question-& answer and discussion. The chairperson should open and close the session on time. He or she should ensure that the speakers of the session are present and that they are able to make their presentations without disruption. The chairperson is also responsible for well moderating the question-& answer and discussions.

VERIFICATION OF PRESENTING AUTHORS

Prior to each presentation the chairperson and co-chairperson should verify that the individual to speak is listed in the program as the authors or one of the authors.

RECORDING/COPYING

Due to author's copyright privileges, it is prohibited to copy electronically any scientific material during oral sessions, without the expressed permission of the author(s). The Chairpersons and Co-chairpersons are requested to observe that these rules are adhered to.

TECHNICAL ASSISTANCE

Co-chairpersons are to be present in the presentation rooms. They will help the chairpersons and speakers in setting up the speakers' computers or installing the presentation files on the conference room computer, and will help with slide shows if needed.

TIME SCHEDULE

In view of the multiple parallel sessions, the time schedule of each session should be strictly kept. The co-chairpersons may help the chairperson with the use of the timer device provided in the conference room. Any disruption in the schedule is extremely annoying for those wishing to attend only selected presentations. Therefore, if a gap should occur in the time schedule, it is suggested that the chairpersons stimulate discussion on the previous talks or seek short oral introductions of relevant papers.

ELECTRONIC PRESENTATIONS

Each conference room is equipped with an autonomous presentation set-up. Authors should upload their electronic presentations to the conference room notebook computer for their presentation. Authors should test their presentations prior to the start of their session.

PROGRAM

1ST FEBRUARY 2018

08:00 – 09:00 Registration merged with Geoinfotech2018

09:00 – 10:00 Opening Ceremony by Permanent Secretary of Minister of Science and Technology, Thailand

10:00 – 12:00 Coffee Break & Exhibition

12:00 – 13:00 Lunch

13:00 – 14:40 Sirindhorn Conference S-1
(Room No. BB404)

Plenary Session 1: *Keynote Forum*

Keynote Forum 1:
Precise Smartphone Positioning Indoors
By: Prof. Dr. Ruizhi Chen, Wuhan University, China

Keynote Forum 2:
Smart Earth Collaboration Platform
By: Prof. SUN Chih-Hong, National Taiwan University, Taiwan

14:40 – 15:00 Coffee Break & Exhibition

15:00 – 16:40 Sirindhorn Conference S-2
(Room No. BB404)

Plenary Session 2: *Geo-informatics for Natural Resource and Management*

Chairman: Prof. Dr. Ruizhi Chen

18:00 – 20:00 Welcome Banquet

2ND FEBRUARY 2018

09:00 – 10:40 Sirindhorn Conference S-3
(Room No. BB404)

Plenary Session 3: *Geo-informatics for Disaster and Risk Management/Environmental and Climate Change*

Chairman: Dr.Anuphao Aobpaet

10:40 – 11:00 Coffee Break & Exhibition

11:00 – 12:00 Sirindhorn Conference S-4
(Room No. BB404)

Plenary Session 4: *Environmental and Climate Change*

Chairman: Prof. Dr. Chalermchon Satirapod

12:00 – 13:00 Lunch

13:00 – 14:00 Sirindhorn Conference S-5
(Room No. BB403)

Plenary Session 5: *New Generation Sensors and Innovative Applications/ Web Map Service*

Chairman: Dr. Martin Isenburg

14:20 – 14:50 Coffee Break & Exhibition

14:50 – 16:30 Closing Ceremony

PLENARY SESSION

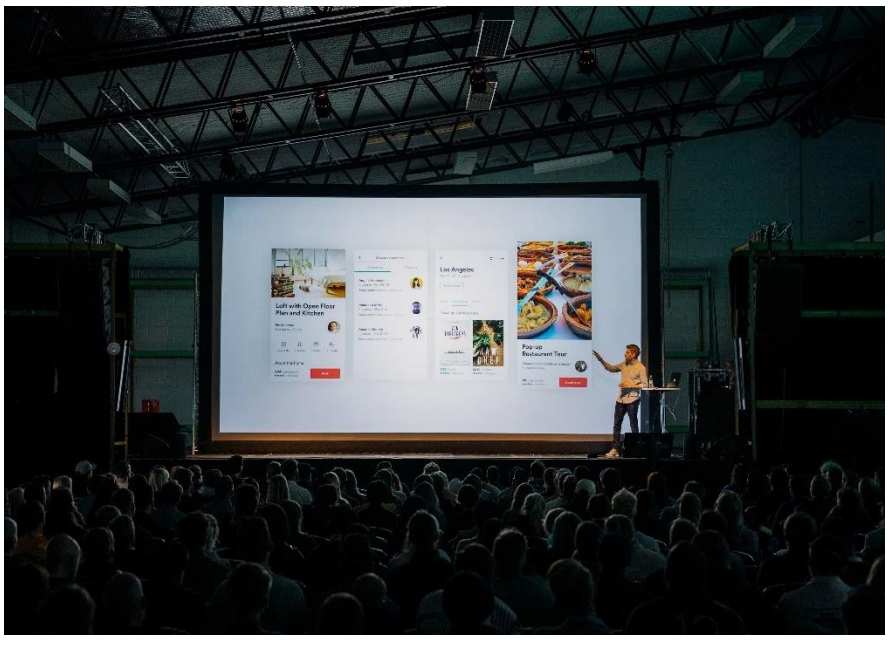

Photo by Teemu Paananen on Unsplash

1ST FEBRUARY 2018

SESSION NO. **S-2** ROOM NO. BB 404 | **15:00 – 16:20**

GEO-INFORMATICS FOR NATURAL RESOURCE AND MANAGEMENT

Prof. Dr. Ruizhi Chen – Chairman | Dr.Chanika Sukawattanavijit – Secretary

S – 2 – 1 SCGI006

Applied Geo-Informatics Technology to Urban Green Space Management on Role of Stormwater Runoff Reducing and Increasing of Subsurface Water

Yaowaret Jantakat

S – 2 – 2 SCGI009

Coastal Resources Mapping in the Philippines

Charmaine Cruz

S – 2 – 3 SCGI016

Geographic Information System Analysis of Shoreline Change Using Digital Shoreline Analysis System (DSAS): A Case Study of Tambon Songkhong, Amphoe Bangpakong, Chacheongsoa, Thailand.

Janejira Khunpai

S – 2 – 4 SCGI019

Detection of Mangrove Forest Changes and Assessment of Carbon Stock and Economics Values in Samuth Songkram, Thailand Using Remote Sensing and GIS Techniques

Kamonporn Upakankaew

2ND FEBRUARY 2018

SESSION NO. **S-3** ROOM NO. BB 404 | **09:00 – 10:40**

GEO-INFORMATICS FOR DISASTER AND RISK MANAGEMENT/ ENVIRONMENTAL AND CLIMATE CHANGE

Dr. Anuphao Aobpaet – Chairman | Panicha Nopjiradej – Secretary

S – 3 – 1 SCGI013

High Spatial Worldview 2-A for Tsumami Vulnerability Mapping Using Spatial Multicriteria Evaluation (Smce): Case Study Pangandaran Regency

M Zayyanul Afwani

S – 3 – 2 SCGI010

Spatial Factors Affecting the Landslide via Logistic Regression Model in Nanglae Nai Village, Chiang Rai Province

Krittawit Suk-ueng

S – 3 – 3 SCGI011

Impacts of Land Use and Land Cover Change on Runoff and Soil Erosion in Small Watershed

Komsan Kiriwongwattana

S – 3 – 4 SCGI014

Climate Change GIS-based Modelling of Thailand Malaria Outbreak

Chirakorn Seangprong

S – 3 – 5 SCGI007

An analysis of Land use change at the Peri-Protected area: A case study of Phu Kradueng National park and Surrounding areas during 1952 - 2016

Mayuree Nasa

Photo by Daria from TaskArmy.nl on Unsplas

SESSION NO. **S-4** ROOM NO. BB 404 | **11:00 – 12:00**

ENVIRONMENTAL AND CLIMATE CHANGE

Prof. Dr. Chalermchon Satirapod – Chairman | Sapsathit Phansri – Secretary

S – 4 – 1 SCGI020

Detecting the El Niño's Induced Changes in Phenology of A Secondary Dry Dipterocarp Forest by Using Remote Sensing

Rungnapa Kaewthongrach

S – 4 – 2 SCGI023

Towards An Automatic Change Detection System for Land Use Land Cover

Cheng Chien Liu

SESSION NO. **S-5** ROOM NO. BB 403 | **13:00 – 14:00**

NEW GENERATION SENSORS AND INNOVATIVE APPLICATIONS/ WEB MAP SERVICE

Dr. Martin Isenburg – Chairman | Dr.Chanika Sukawattanavijit – Secretary

S – 5 – 1 SCGI002

Median Ground Models for Drone LiDAR from Velodyne Puck Systems

Martin Isenburg

S – 5 – 2 SCGI022

A Cross-Anchor UWB Locating Scheme in TDOA Mode for Wide Area UWB Network

Xiaoguang Zhang

S – 5 – 3 SCGI015

Model and Framework of Real-time Flood Process Detection under the Sensor Web Environment

Wenying Du

S – 5 – 4 SCGI021

Development of Spectral Library for Trace Detection of Explosives Using Hyperspectral Sensor

Siddharth Chaudhary

2nd SIRINDHORN CONFERENCE ON GEOINFORMATICS 2018

1-2 FEBRUARY 2018

FULL PAPER

CENTRA BY CENTARA GOVERNMENT COMPLEX HOTEL

& CONVENTION CENTRE

CHAENG WATTANA, BANGKOK, THAILAND

TABLE OF FULL PAPER

THE 2nd SIRINDHORN CONFERENCE ON GEO-INFORMATICS 2018

APPLIED GEO-INFORMATICS TECHNOLOGY TO URBAN GREEN SPACE MANAGEMENT ON ROLE OF STORMWATER RUNOFF REDUCING AND INCREASING OF SUBSURFACE WATER

Yaowaret Jantakat [1]
Information and Communication of Technology, Faculty of Sciences and Liberal Arts, Rajamangala University of Technology Isan, yaowaret.ja@rmuti.ac.th
Pongpun Juntakut [2]
Department of Civil Engineering, Academic Division of Chulachomklao Royal Military Academy, juntakut37@gmail.com
Sanun Kranka [3]
Information and Communication of Technology, Faculty of Sciences and Liberal Arts, Rajamangala University of Technology Isan, yaowaret.ja@rmuti.ac.th

ABSTRACT

This study aimed to determine spatially geographical locations for managing urban green space based on the relationships between urban greenness, storm water runoff reduction and subsurface water increase in the past 11 years (2006-2016) in the Nakhonratchasima Municipality (NM). The SWAT model and GIS was used in this study. As results, 6 sub-sites of NM were totally analyzed for classifying into 2 levels: priority (higher runoff and lower infiltration into subsurface or more requirement of the urban green space management) and minority (lower runoff and higher infiltration into subsurface or less requirement of the management). The level of priority was in the middle part of NM (urban and built-up land, recreation area, and golf course) and the northern NM (urban and built-up land, recreation area, vegetable crop behind the mall department store), while other sites were manipulated on monitoring level. The results also indicated the most significant factors affecting higher runoff and lower infiltration into subsurface are elevation and land use (urban green space). However, these mentioned areas are not fully understood yet, particularly at spatial and temporal scales relevant to managing urban green area. As such, a reliable land use of urban greenness for storm water and subsurface water control depends on improved understanding of how and to what extent urban greenness (plant species) interact with storm water and subsurface water, and the context-specific consideration of optimal arboriculture practices and NM frameworks to maximize the storm water and subsurface water benefits trees should provide.

Keywords: Geo-Informatics, Urban Green Space, Stormwater Runoff, Subsurface Water

1. INTRODUCTION

Increasing urban population has affected to expansion of urbanization especially built-up land such as buildings, residents, roads, etc. Green-dominated land covers are being converted to built-up areas. In fact, some areas in urban still have green land covers, but some areas have no green sites. It depends on planning of the urban management. Moreover, development of urban society still has to be inescapably prepared for growing of ASEAN Economic Community (AEC), it consists of growth of buildings and public utilities. In the past of Thailand, an dramatically economic development had an impact on directionless urban land use patterns [4] as well as, in the present, it still faces problem of urban land use changes especially green areas where have become more built-up areas [10]. Consequently, stormwater runoff occurs severer and oftener a rapid flooding (flash flood) in low-lying areas such as a case of flooding in Nakhon Ratchasima and Bangkok in year 2010 and 2011. Furthermore, these flooding also most likely can cause water pollution in urban areas, particularly sites without green spaces and planting, according to the study of ,[1], [2], [7], and [15].

Geo-informatics has not only become very important technology to decision-makers across a wide range of disciplines, industries, commercial sectors, environmental agencies, local and national government, research, and academia national survey and mapping organizations, etc. but also geospatial-temporal data has become infused into many aspects of our daily life and the major driver of today's information society [11] and [12]. Basically, geo-informatics technology focuses on 3 fields: remote sensing (RS), geographical information system (GIS), and global position system (GPS). The examples of benefits of geo-informatics application includes cost saving with greater efficiency, better decision making, improved communication, better geographic information recordkeeping and managing geographically, have been evidenced by relevant papers such as [5], [3], and [8]. In addition, the geo-informatics also can be an efficiently techniques for analyzing input data into the Soil and Water Assessment (SWAT) tool, or called 'ArcSWAT' for use with ArcGIS in order to evaluate and plan water management in a watershed The ArcSWAT and SWAT model have been applied in many studies of water management. An example of studies include [6], [9], [13] and [14].

As mentioned above, this article mainly aimed to determine spatially geographical locations for the urban green management by considering on the relationships between urban greenness, storm water runoff reduction and increasing subsurface water for 11 years (2006-2016) in the Nakhonratchasima Municipality (NM). Due to the 2010 flash flooding in NM, NM authorities have attempted to find the best and most suitable policies and practices in the sustainable protection of flooding in NM. Development of urban green spaces (UGSs) is a potential approach that is created in 3-year continuous plan with periods of 2016-2018, 2017-2019 and 2018-2020. Therefore, this paper will be a guideline for the UGSs management in NM and also will be utilization for the management in other urban areas of Thailand.

2. OBJECTIVES

This study aims to determine spatially geographical locations for managing urban green spaces by considering on the relationships between urban greenness, storm water runoff reduction and increasing subsurface water for 11 years (2006-2016) in the Nakhonratchasima Municipality (NM). The objectives of this research are as the following:

(1) To estimate UGSs based on remote sensing,

(2) To apply the ArcSWAT model for estimating stormwater runoff and subsurface water recharge based on changes of estimated UGSs,

(3) To study the relation of stormwater runoff, subsurface water and UGSs,

(4) To determine identification of specific areas for improving and restoring UGSs

3. METHODOLOGY

3.1 Study site

The study area is Nakhonratchasima Municipality or shortly, "NM" as shown Fig. 1. NM site is located in Muang district of Nakhon Ratchsiam province at 14' to 16'N and 101' to 103'E and occupies a total area of 37.5 km^2 (4.96 and 0.18 percent of Muang district and Nakhon Ratchasima province) with sea level 174-206 m. NM is far from Bangkok by vehicles about 255 km., by rails about 264 km. NM topography is characterized by most plain, a little slope in eastern direction, low land in the NM north and high land in the southern west. Most of soils are loamy sand. The main river is Lum Ta Klong (the major of Mun river) where flows through the NM north with length about 12 km. Authority of NM comprises of the north adjacent to 3-subdistrict administrative organization (SAO): Muen Wai, Nongkratum and Bankoh, the south adjoining 2-subdistrict municipality and 1 SAO: Nong Phailom, Pho Klang and Nong chabok, the east close to Hau THale subdistrict municipality, and the west next to 2- SAO and 1 subdistrict municipality: Ban Mai, Suranari and Pru Yai.

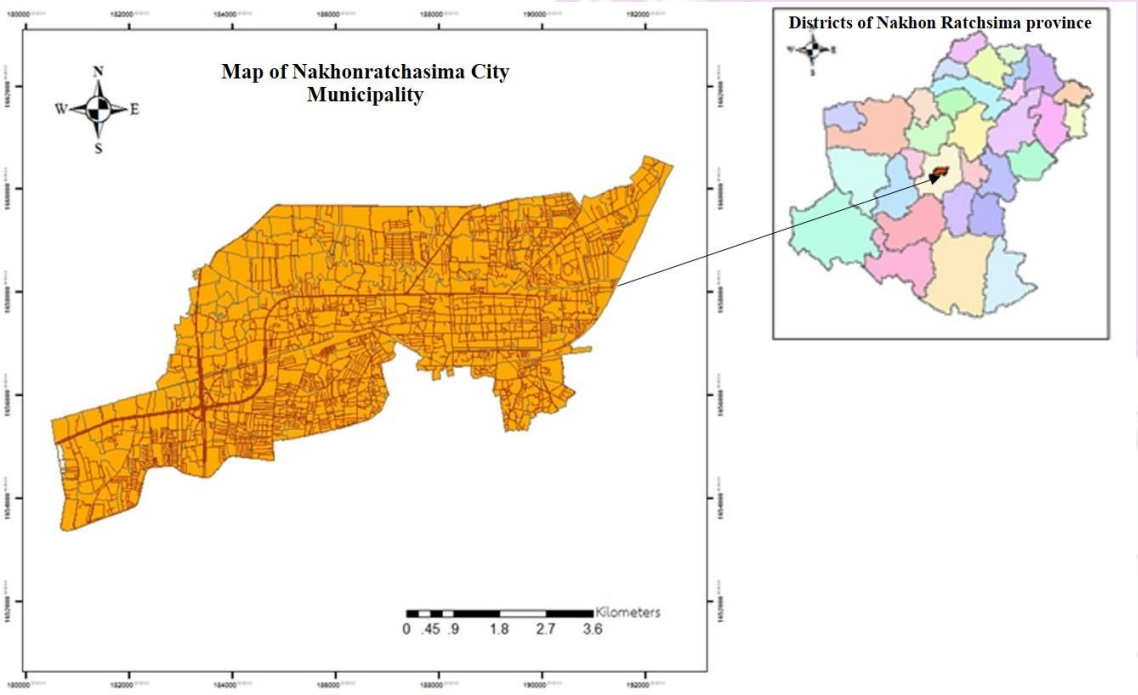

Fig.1 Area of Nakhonratchasima Municipality

3.2 Study Procedure

3.2.1 Data collection

In this study, we collected data during 2006 to 2016 from many sources including:

(1) Remotely sensed data is in form of aerial photos and satellite images from Land Development Department (LDD), Geo-Informatics and Space Technology Development Agency (Public Organization) (GISTDA), U.S. Geological Survey (USGS) and Google Inc.

(2) Land use/land cover data of Muang Nakhonratchasima district, Nakhon Ratchasima province is in form of polygon-based vector layer from Land Development Department (LDD)

(3) Climate data is in form of attribute of rainfall data from Nakhon Ratchsima Meteorological Observation Station and The Thai Meteorological Department

(4) Subsurface water data is in form of attribute of groundwater wells and volume and point-vector layer of wells from Bureau of Groundwater Conservation and Restoration, Department of Groundwater Resources and Office of Groundwater Resource Area 5

(5) Boundary and land use of Nakhonratchasima municipality is in form of polygon-vector layer from Office of Nakhonratchasima City Municipality

3.2.2 Application of ArcSWAT model for determining specific areas and managing urban green spaces

In this section, we applied the ArcSWAT model to estimate stormwater runoff and subsurface water recharge and investigated the relationship with urban greenness during 2006 to 2016 in NM. The steps of method are described as the following:

(1) Defining site boundary with direction of water flow in the study area.

(2) Classifying sites for estimating stormwater runoff and subsurface water recharge.

(3) Ranking index for UGSs management on role of stromwater runoff reducing and increasing of subsurface water.

(4) Evaluating the accuracy of modeling by using calibration and validation.

4. RESULTS

4.1 Directions of water flow

Based on the ArcSWAT model, site boundary with water flow directions was defined and evaluated from considering DEM and land use as shown in Fig. 2. We found that water flows from the western part (higher elevation) to eastern part (lower elevation) of the study area and the southern (higher) to northern (lower) of NM area.

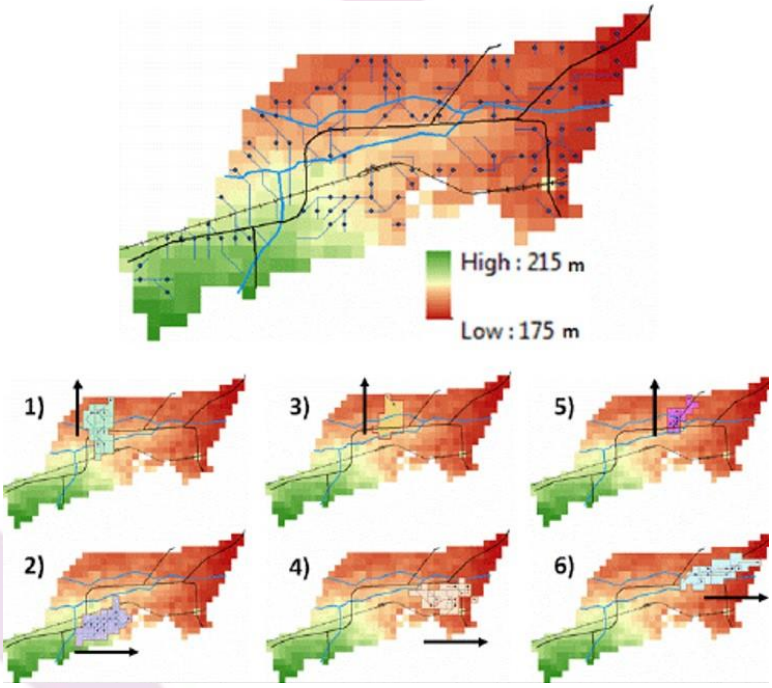

Fig. 2 Output of site boundary and direction of water flow in the study area

4.2 Sites with Stromwater Runoff

Stormwater runoff in NM was estimated based on land use, soil characteristics, and rainfall data in the ArcSWAT model. This model elaborately classified the study area into 6 sub-sites based on water flow directions (Fig. 3) as described in the following:

Site no.1: community of Ban Kham Thuat, low land and agricultural land, with the direction of stormwater runoff towards the north.

Site no.2: area of city, town and commercial, recreation area and golf course with the direction of stormwater runoff towards the east.

Site no.3: area of city, town and commercial, recreation area, agricultural area (such as vegetation and truck crops behind the mall department store) and low land with the direction of stormwater runoff towards the northern west.

Site no.4: area of city, town and commercial, recreation area and low land with the direction of stormwater runoff towards the southern east.

Site no.5: area of city, town and commercial and water body with the direction of stormwater runoff towards the north.

Site no.6: area of city, town and commercial, recreation area and low land with the direction of stormwater runoff towards the east.

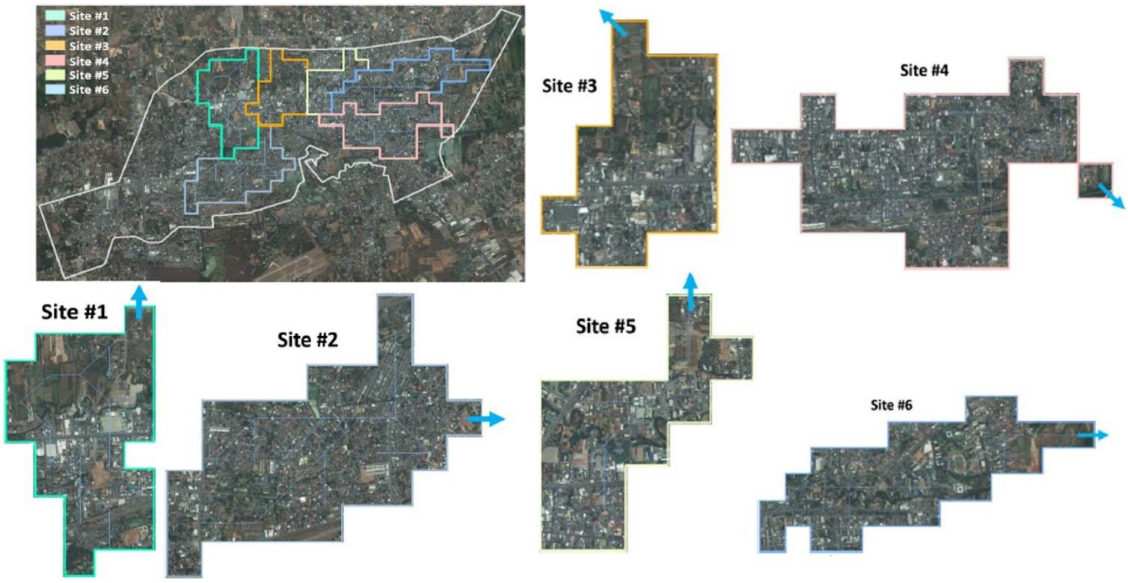

Fig. 3 Sites for estimating stromwater runoff and subsurface water recharge

4.3 Ranking Index

The indices of stormwater runoff and subsurface water recharge in 6 sub-sites were executed in ranking at risk of a stormwater runoff is in high level and a subsurface water recharge is in low level. Fig. 4 presents the indices of stormwater runoff and percolation (subsurface water) for 6 sub-sites.

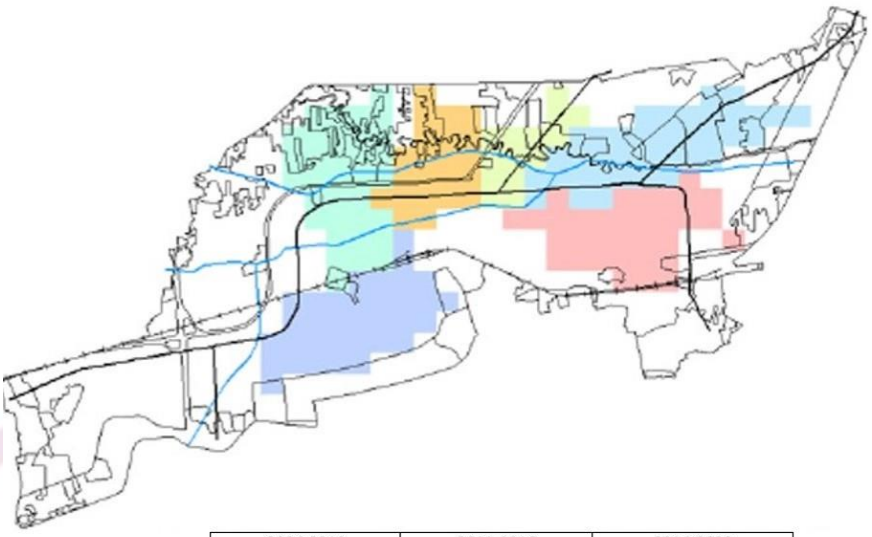

		2006-2010		2011-2015		2016-2020	
		Runoff Index	Percolation Index	Runoff Index	Percolation Index	Runoff Index	Percolation Index
	Site no.1	6	2	5	3	5	1
	Site no.2	1	3	1	5	2	3
	Site no.3	2	4	2	4	1	6
	Site no.4	4	1	3	2	4	2
	Site no.5	5	6	4	6	6	4
	Site no.6	3	5	6	1	3	5

Note: - Index no.1 defines the highest level for stormwater runoff reducing or percolation increasing
- Index no.2 defines the high level for stormwater runoff reducing or percolation increasing
- Index no.3 defines the moderate for stormwater runoff reducing or percolation increasing
- Index no.4 defines the lower moderate for stormwater runoff reducing or percolation increasing
- Index no.5 defines the low for stormwater runoff reducing or percolation increasing
- Index no.6 defines the lowest for stormwater runoff reducing or percolation increasing

Fig. 4 Index of stromwater runoff reducing and Percolation

4.4 Calibrating and Validating Model

For evaluating the model, observed water discharge at the Assumption College station (Fig. 5a) was used to estimate statistically error of modeling. Basically, the evaluation of a model consists of 2 steps: calibration and validation. Fig. 5b and Fig. 5c show the result of calibration during 2001 to 2014 with 0.54 of R^2 and the result of validation from 2015 to 2016 with 0.79 of R^2, respectively.

5. CONCLUSION AND DISCUSSION

This study analyzed spatially geographical locations for managing urban green space based on the relationships between urban greenness, storm water runoff reduction and subsurface water increase in the past 11 years (2006-2016) in the Nakhonratchasima Municipality (NM). The SWAT model and GIS was used in this study. Consequently, there were 6 sites of NM were obtained and analyzed for classifying into 2 levels: priority (higher runoff and lower infiltration into subsurface or more requirement of the urban green space management) and minority (lower runoff and higher infiltration into subsurface or less requirement of the management). The level of priority was in the middle part of NM (urban and built-up land, recreation area, and golf course) and the northern NM (urban and built-up land, recreation area, vegetable crop behind the mall department store), while other sites were manipulated on monitoring level. The results also indicated the most significant factors affecting higher runoff and lower infiltration into subsurface are elevation and land use (urban green space).

(5a)

(5b)

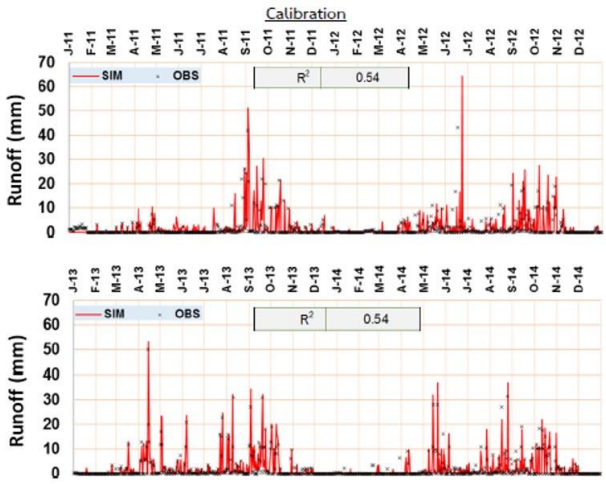

(5c)

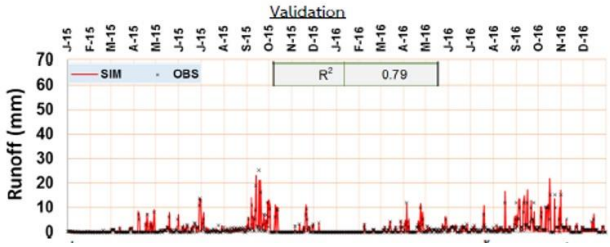

Fig.5 Gauging station, Calibration and Validation

6. RECOMMENDATION

The prior and minor areas were mentioned above should be not fully understood yet, particularly at spatial and temporal scales relevant to managing urban green area. As such, a reliable land use of urban greenness for stormwater and subsurface water control depends on improved understanding of how and to what extent urban greenness (plant species) interact with storm water and subsurface water, and the context-specific consideration of optimal arboriculture practices and NM frameworks to maximize the storm water and subsurface water benefits trees should provide.

REFERENCES

[1] Armson, D., Stringer, P. and Ennos, A. R. "The effect of street trees and amenity grass on urban surface water runoff in Manchester, UK. Urban" Urban Forestry & Urban Greening, Vol.12, Issue 3, pp.282-286, 2013.

[2] Inkiläinen, E. N. M., McHale, M. R., Blank, G. B., James, A. L., & Nikinmaa, E. "The role of the residential urban forest in regulating throughfall: A case study in Raleigh, North Carolina, USA." Landscape and Urban Planning, 119, 91–103, 2013. Barten et al. (2008),

[3] Kumar, A. and Krishna, A. P. "Winter seasons assessment of atmospheric aerosol over Coalfield region of India using geoinfomatics." Urban Climate, Vol.20, 94-119, 2017.

[4] Khongouan, W. and Sitachitta, P. "The management of Green Area in Educational Institutions in accordance with the Action Policy of Green Area Management in Sustainable City." Academic Journal of Architecture, Vol. 1, pp. 141-150, 2010.

[5] Lal, K., Kumar, D. and Kumar, A. "Spatio-temporal landscape modeling of uran growth ptterns in Dhanbad Urban Agglomeration, India using geoinformatics techniques." The Egyptian Journal of Remote Sensing and Space Sciences, Vol.20, 91-102, 2017.

[6] Luo, Y., Su, B., Yuan, J., Li, Hui, and Zhang, Q. "GIS Techniques for Watershed Delineation of SWAT Model in Plain Polders." Procedia Environment Science 10, pp. 2050-2057, 2011.

[7] Mentens, J., Raes, D., and Hermy, M. "Green roofs as a tool for solving the rainwater runoff problem in the urbanized 21st century?" Landscape and Urban Planning, Vol.77, pp. 217-226, 2006.

[8] Narmada, K., Gobinath, K. and haskaran, G. "An Assessment of Resources Potential for Sustainable Development of Micro-Watershed in Tirunelveli District Using Geoinformatics-A Case of Nambiyar Micro-Watershed in Tirunelveli District, Tamil Nadu, India." Aquatic Procedia, Vol.4, 1299-1306, 2015.

[9] Santra, P. and Das, B. S. "Modeling runoff from an agricultural watershed of western catchment of Chilika lake through ArcSWAT." Journal of Hydro-environment Research 7, pp. 261-269, 2013.

[10] Silapacharanan, S., Sajjakul, V., Peerapun, W., Rattanagomut, S., Osiri, N., Buachaiboon, K., Supapunmanee, S. and Pipatvong, N. (2008). "Action Plan Project for Compete Green Areas in Sustainable Ecosystem." Retrieved on December 7, 2017. From http://chm-thai.onep.go.th/chm/city/document/03.sustrainpowercitygreenarea.pdf

[11] The University of Iowa. (2017). "Geoinformatics." Retrieved on December 10, 2017. From https://informatics.uiowa.edu/study-opportunities/graduate-program/geoinformatics

[12] The Univesity of Twente. (2017). "Learn to develop technologies required for analyzing, distribution and visualizing geo-spatial data." From https://www.utwente.nl/en/education/master/programmes/geo-information-science-earth-observation/specialization/geoinformatics/

[13] Winchell, M., Srinivasan, R., Di Luio, M. and Arnold, J. (2010). "ArcSWAT Inerface for SWAT2009: User's Guide." Retrieved on December 10, 2017. From https://www.researchgate.net/...modeling...SWAT.../ArcSWAT2009English+textbook.pdf

[14] Zhang, L., Karthikeyan, R., Bai, Z. and Srinivasan, R. "Analysis of streamflow response to climate variability and land use change in the Loess Plateau region of China. " Catena 154, pp. 1-11, 2017.

[15] Zhang, B., Xie, G., Li, N., and Wang, S. "Effect of urban green space changes on the role of rain water runoff reduction in Beijing, China." Landscape and Urban Planning, Vol. 140, pp. 8-16, 2015.

COASTAL RESOURCES MAPPING IN THE PHILIPPINES

Charmaine Cruz[1]
University of the Philippines Diliman, cacruz7@up.edu.ph
Kristina Di Ticman, Gay Amabelle Go, Rudolph Peralta, Mark Vener Vergara, Jaime Guihawan, Al Jayson Songcuan, Mia Shaira Estabillo, Ivy Elaine Cadalzo, Rey Rusty Quides, Rey Jalbuena, Alexis Richard Claridades, Ayin Tamondong, Ariel Blanco 2
University of the Philippines Diliman

ABSTRACT

The Philippines, being an archipelago with more than 7,600 islands, is considered as home of rich and high productive marine habitats. Despite their economic and ecological importance, reports on the declining coastal resources have increased in numbers in recent years. With the advance technological approaches on research such as remote sensing and geographic information system, mapping the coastal resources in the Philippines is not too farfetched to obtain the inventory and spatial extent information which are important for resource management. This paper describes the nationwide mapping of coastal resources in the Philippines using remote sensing, and discusses how these maps could contribute to the conservation and protection of these resources.

The Nationwide Detailed Resources Assessment using LiDAR Surveys Program (Phil-LiDAR 2) was implemented by fifteen universities throughout the country which aimed to produce high resolution coastal resources maps using the available LiDAR and other remotely-sensed datasets. Object-based image analysis (OBIA) technique was applied to extract the resource features based on its spatial and spectral attributes. Image was first segmented into objects based on homogeneity criteria. A supervised classification was performed using a support vector machine (SVM) classifier to categorize the objects into different classes. Field surveys to collect training and validation points were done to calibrate the classification process and validate the output. The maps produced were distributed to stakeholders once standards of accuracy had met. These would be beneficial for the planners and coastal managers by providing comprehensive spatial and land cover information which could be used to extract other science-based information such as identifying vulnerable coastal resources to impacts of climate change and anthropogenic disturbance. The maps would also aid them in monitoring activities and management strategies. Overall, this is expected to recognize the importance of space technologies in mapping the country's natural resources.

Keywords: remote sensing, object-based image analysis, LiDAR, coastal resources

1. INTRODUCTION

1.1. The Philippine Coasts

The Philippines, being an archipelagic country with more than 7,600 islands and located at the apex of the Coral Triangle also known as the World's Centre of Marine Biodiversity, is rich in coastal ecosystems characterized by dense mangrove forests, and large areas of seagrass and coral **[1]**. With approximately 60% of the country's total population living along coastal communities **[2]**, the people depends on the country's coastal and marine resources for sustainance and livelihood. Despite its ecological and economic services for the people, the coastal resources of the country continue to experience serious threats of degradation over the years, mainly because of the unsustainable human exploitation but progressively by global climate change-related stressors. With the growing concern of protecting the country's coastal resources, there is a need to accurately map the coastal environment to provide rapid assessment of these habitats which is critical for developing management strategies and marine spatial planning. Mapping of coastal resources using the traditional field-based method produces high accuracy. However, to cover a larger area, the activity would be expensive and would need a longer time. Approach on researches using latest technologies such as remote sensing provides information that could support the wide-scale mapping of these resources for monitoring, protection, and conservation.

Light Detection and Ranging or LiDAR technology has become increasingly well known as an accurate mapping tool. The use and demand for the technology increased because of its ability to map or spatially reference physical features at high accuracy for a large geographic area. This technology was used to map the Philippines' coastal resources along with hyperspectral and multispectral images.

1.2. Nationwide Coastal Resources Mapping

The University of the Philippines Training Center for Applied Geodesy and Photogrammetry (UP TCAGP) implemented a directed research program entitled "Detailed Resources Assessment using LIDAR (Phil-LiDAR 2)". It was a three-year program which started last July 2014. The Phil-LiDAR 2 Program aimed to complement on-going programs of government agencies (e.g. Department of Agriculture, Department of Environment and Natural Resources, Department of Energy, etc.) by utilizing LiDAR data and developed methodologies for extracting resource features from LiDAR and other remote sensing data for various applications such as production of high value crops, irrigation assessment, coastal resource conservation, aquaculture production, forest protection and discovery of renewable energy sources. As part of the program's objective, high resolution resource maps and vulnerability assessment maps for high-value crops and coastal resources were produced to aid in the recommendations addressing future local supply and demand in agriculture, coastal, forest, and renewable resources.

The program was driven by the collaborative efforts of the fourteen (14) other State Universities and Colleges (SUCs) and Higher Educational Institutes (HEIs) in the different regions of the country. The SUCs and HEIs were clustered into three, representing the major groups of islands in the Philippines: Luzon cluster, Visayas

cluster, and Mindanao cluster. The fourteen partners were Mariano Marcos State University (MMSU), Isabela State University (ISU), Central Luzon State University

(CLSU), Mapua Institute of Technology (MIT), University of the Philippines Los Banos (UPLB), Ateneo de Naga University (ADNU), University of the Philippines Cebu (UP Cebu), University of San Carlos (USC), Visayas State University (VSU), Ateneo de Zamboanga University (ADZU), Central Mindanao University (CMU), Mindanao State University – Illigan Institute of Technology (MSU-IIT), UP Mindanao (UP Min) and Caraga State University (CSU). These SUCs and HEIs committed to deliver the coastal resources maps for their assigned provinces and municipalities. They also coordinated with the provincial and local government of their study areas in conducting field surveys and gathering secondary data.

Figure 1. Phil-LiDAR 2 partner universities and their assigned regions

2. OBJECTIVE

The Program was composed of five components: Project 1: Agricultural Resources Extraction from LiDAR Surveys (PARMap), Project 2: Aquatic Resources Extraction from LiDAR Surveys (CoastMap), Project 3: Forest Resources Extraction from LiDAR Surveys (FRExLS), Project 4: Development of the Philippine Hydrologic Dataset for Watersheds from LiDAR Surveys (PHD), Project 5: Philippine Renewable Energy Resource Mapping from LiDAR Surveys (REMap). This paper discusses the Project 2 of Phil-LIDAR 2 Program. The Project 2 or the Aquatic Resources Extraction using LiDAR Surveys aimed to provide an updated and detailed inventory of high valued coastal resources in the Philippines by developing methodologies for mapping such resources using LiDAR and other geospatial technologies such as optical imagery and multi beam

echo sounder. Specifically, the project aimed to develop algorithms and workflows for

extracting and characterizing coastal resources using LiDAR and other remotely sensed data, and field measurements; production of high resolution and high accuracy maps of coastal resources; and vulnerability assessment of different coastal resources. Among the expected outputs of the Project were the algorithms and workflows for data processing, output maps, geodatabases, and spectral library of various coastal resources such as mangroves, corals and seagrass.

3. METHODOLOGY

3.1. Data

LiDAR is an emerging remote sensing technology which is used to accurately map the topography of the Earth's surface. It is an active type of remote sensing that uses laser pulses to compute for distances of objects on the ground. The distance is computed by measuring the time it takes for a laser to hit the ground and sent back to the sensor. The aircraft is installed with a laser device which scans the Earth, the global positioning system receiver that tracks the altitude and position of the aircraft at the time of measurement, the Inertial Measurement Unit that records the attitude or orientation (yaw, pitch, heading) of the plane which is important for accurate elevation computation, and a computer and software for navigation and flight management and data records and storage.

Topographic LiDAR uses near infrared light to map the ground features, while the bathymetric LiDAR system uses both green and near infrared lights. The bathymetric LiDAR system collects simultaneous land and water depth measurements. An aerial camera is also mounted on the aircraft to capture orthophoto simultaneously with the acquisition of LiDAR point cloud.

In the Philippines, the LiDAR system was set to produce an up-to-date and detailed elevation dataset with 1-meter horizontal resolution (2 data points per square meter) for flood plain areas, and 20-centimeter vertical accuracy. This was to cover major river systems in the country for the purpose of flood hazard assessment. On the other hand, the data was also used to produce inventory and assessment for natural resources such as agricultural, coastal, forest, and renewable energy. The LiDAR data being utilized for the project was obtained from the Data Acquisition Component of the UP DREAM/Phil-LiDAR 1 Program. The data delivered by this component have already been corrected for acquisition errors and processed to the standard LAS file format.

For areas without LiDAR coverage or had no available high-resolution satellite images, the project used freely downloadable Landsat satellite imagery from the U.S. Geological Survey (USGS) website. Landsat images are composed of multispectral image bands with 30m by 30m pixel resolution. The coastal features extracted from these images provide a good measure of the available resources for areas without high resolution LiDAR or satellite image data.

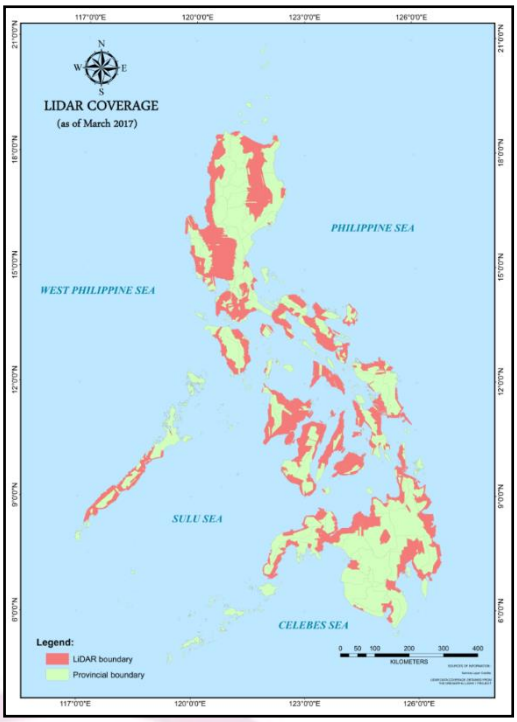

Figure 2. LiDAR Coverage in the Philippines

3.2. Processing

To extract aquaculture ponds and mangroves, an object-based image analysis (OBIA) was employed. Image layers such as digital surface model (DSM), digital terrain model (DTM), number of returns, canopy height model (CHM), slope, hillshade and intensity were derived from LiDAR point clouds. Available orthophotos were also added in the layers for OBIA along with the field data and other secondary references. The processing started with grouping the image pixels by segmentation based on spectral similarities and object's properties such as texture, context, and geometry. The image segmentation is a critical step as the objects segmented were used as basis for the classification. Assigning classes using threshold values of objects obtained from the derivatives was done to extract some of the classes. Similarly, Support Vector Machine (SVM) a type of supervised classification method was used for the extraction of the remaining classes needed. Two (2) different sets of points, training and validation, were used in the methodology. Training points were used in the SVM classification while the validation points were used to determine the accuracy of the classification. These set of points were gathered through the field and supplemented by satellite images. Lastly, an assessment was done to test how accurate the classification was.

3.3. Data Validation

The Project employed various methods of field data collection in order to produce detailed maps of the coastal resources. Field surveys are integral part of the mapping process as these provide supplementary datasets that aid classification and ensures accuracy of maps produced. Training data collection was done to gather reference data to be used in subsequent image classification while field validation was implemented to determine the accuracy of the classification results. The field techniques used in both types of survey include point observation using handheld GPS and underwater video tow.

A reconnaissance was conducted before the actual fieldwork to have an idea of the benthic feature locations. In the field, a stratified random sampling design was used in obtaining sampling points for training data collection. Using this method, a specific number of sample points in a predetermined category is assigned. Study sites were mapped out as well. The pre-selected points were pre-loaded in the handheld GPS. Underwater features are more difficult to identify compared to ground features. As such, assistance of locals and further research were needed in order to correctly identify the said features.

The sampling points were individually located and marked in the field. Pre-identified validation points were also located to compare the results of the classification with the actual ground feature. After point data collection, video tow was conducted to acquire continuous shots of the benthic features or features submerged in water. Data and other relevant observations were recorded in the field data sheets along with the data-gathering equipment. Proper planning and adherence to field techniques guidelines ensure efficient and effective field data collection.

Figure 3. Field techniques employed in the Phil-LiDAR 2 Project 2; sampling location for mangroves (upper left, lower right), aquaculture structures (upper right) and benthic habitats (lower left)

3.4. Capacity Building

Training programs were developed to upgrade knowledge and skills in geospatial technologies for mapping natural resources. Training on basic remote sensing and GIS was also provided to the project staff. Aside from the development of the standard coastal resources extraction methodologies, the Project was also able to introduce these workflows to the different State Universities and Colleges (SUCs) and the Higher Education Institutions (HEIs). The project members conducted trainings and demonstrations to the SUCs and HEIs on how to implement the algorithms and perform the data gathering techniques.

Figure 4. Training and mentoring sessions for the partner SUCs and HEIs

The University of the Philippines also conducted field visits to the partner universities at least twice a year to monitor their progress, present processing updates, and discuss other project implementation concerns.

4. RESULTS

Classification maps were generated after obtaining an acceptable accuracy assessment following the image classification procedures. The class shapefiles were exported in the GIS software to prepare the final classification maps that show the following coastal resources: mangroves, aquaculture structures (fish ponds, fish traps), and the benthic features like seagrass, corals, sand, rubbles, and rocks. Non-coastal features were also presented in the map for reference which include other vegetation covers and non-vegetation features such as buildings, bare soil, and water.

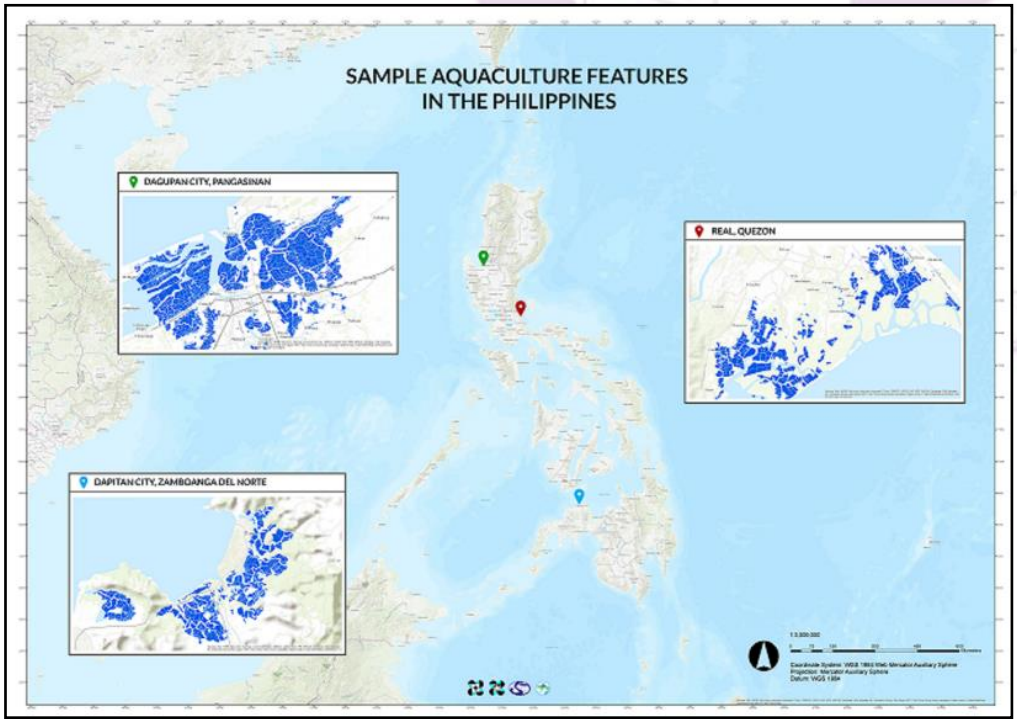

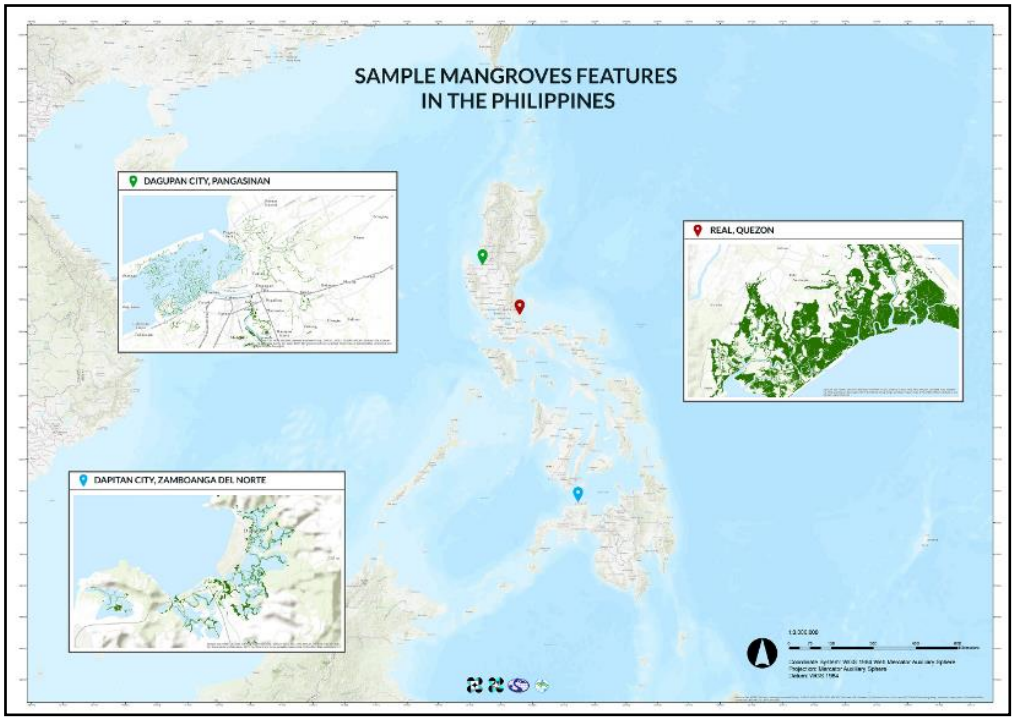

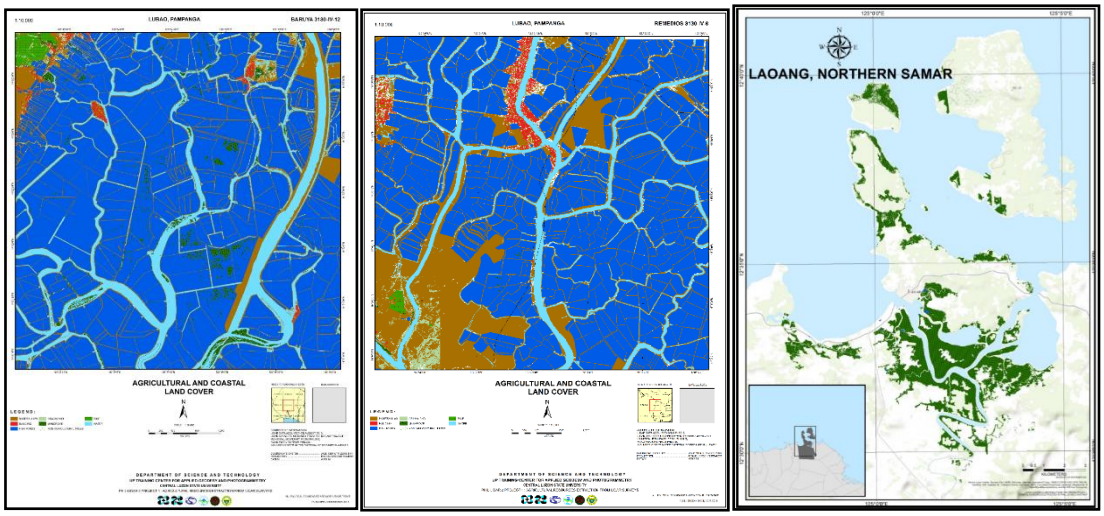

Figure 5. Sample Coastal Resource Maps using Remote Sensing Data

The project employed a quick deployment of maps to the local government units and national government agencies for their use in planning, resource monitoring and management. To further facilitate the distribution of maps, the partner SUCs and HEIs were tasked to turnover their products to their respective government units. They were required to conduct orientation and short GIS training courses for the stakeholders. These aimed to discuss to them the usage of maps, its limitations, and how to update the products.

Figure 6. Resource Maps Turnover to Government Units

5. CONCLUSION AND DISCUSSION

The Project, consisting of 15 universities, was able to produce maps of coastal resources from the available LiDAR data in the country. The produced resource maps are used not only to provide comprehensive spatial and land cover information but also to extract information like coastal areas vulnerable to impacts of climate change and anthropogenic disturbances. These resource vulnerability maps are very essential in identifying areas that need urgent decisions and to assess gaps. Thus, it strengthens existing environmental policies and programs, address the gaps and loopholes in management system and create strategic actions in addressing different issues in fisheries and coastal environment. With this type of information, the interplay between these factors to climate change impacts can be used to properly manage coastal areas.

The Project was also successful in human resource development and capacity building. Many young researchers and students who were part of the program were trained in remote sensing and geographic information systems. Similarly, the collaboration between government units and academic institutions was enhanced which could improve the natural resource management in the country.

REFERENCES

[1] Department of Environment and Natural Resources, Bureau of Fisheries and Aquatic Resources, Department of Agriculture and Department of the Interior and Local Government, "Philippine Coastal Management Guidebook Series No. 1: Coastal Management Orientation and Overview," Cebu City, Philippines, 2001.

[2] "The World Factbook," [Online]. Available: https://www.cia.gov/library/publications/the-world-factbook/geos/rp.html. [Accessed 2018].

APPLICATION OF GEOGRAPHIC INFORMATION SYSTEM FOR COASTAL EROSION ANALYSIS USING DIGITAL SHORELINE ANALYSIS SYSTEM (DSAS): A CASE STUDY OF SONGKLONG SUB-DISTRICT, BANG PAKONG DISTRICT, CHACHOENGSAO PROVINCE, THAILAND

Janejira Khunpia [1],
Department of Natural Resources and Environment, Faculty of Agriculture Natural Resources and Environment, Naresuan University, janejane.kpx@gmail.com

Tanyaluck Chansombat [2],
Department of Natural Resources and Environment, Faculty of Agriculture Natural Resources and Environment, Naresuan University, tanyalak.sp@gmail.com

ABSTRACT

This study aims to analyze the change of shoreline over the period of the year of 2002-2016 (15 years) by using Geographic Information System together with Digital Shoreline Analysis System (DSAS). The study was conducted at Songklong district, Amphoe Bangpakong, Chacheongsoa, Thailand with the coastal distance of 16.28 kilometers. Satellite imagery and aerial photography were used to analyze the coastal change in the study area. The statistics that were selected to evaluate the change of shoreline are included of Net Shoreline Movement (NSM), Shoreline Change Envelop (SCE) and Linear Regression Rate (LRR). The results show that in 2017 the average Net Shoreline Movement was -66.86 meters which means that the shoreline has been decreased continuously in the past 15 years due to coastal erosion. The Shoreline Change Envelop was 84.60 meters. The Linear Regression Rate results indicate that the average erosion rate was -5.62 m yr^{-1}. The high erosion rate area occupies the distance of 4.21 kilometers (40%), the moderate erosion rate area was 4.74 kilometers (45.01%), the stable coastal area was 1.25 kilometers (11.9%) and the coastal accretion rate area was 0.33 kilometer (3.09%), respectively. In conclusion, the coastal erosion situation of the study area can be defined as high erosion area because it has coastal erosion rate more than 5 m yr-1 (Department of Marine and Coastal Resources, 2013). Furthermore, the results can provide the contribution to practices of coastal planning and management in a coastal area, moreover, historical shoreline change statistics can be used to monitor coastal environmental changes such as climate change, global warming, sea level change, and sedimentation accumulation rates.

.

Keywords: coastal erosion, Digital Shoreline Analysis System (DSAS), shoreline change analysis

1. INTRODUCTION

The coast of Thailand covers a total area of about 2,600 km covering 23 provinces. The coastal distance of the Gulf of Thailand is approximately 1,650 km long covering coastal areas in 17 provinces including Bangkok, Samut Prakan, Samut Sakhon, Samut Songkhram, Phetchaburi, Prachuap Khiri Khan, Trat, Chanthaburi, Rayong, Chonburi, Chachoengsao, Chumphon, Surat Thani. Songkhla, Pattani and Narathiwat. Whereas the Andaman coast line has a length of about 950 km covering the coastal areas of six provinces including Ranong, Phangnga, Phuket, Krabi, Trang and Satun [1].

At present, Thailand's coastline is experiencing coastal erosion as well as coastal countries around the world. The erosional situation has continued throughout the Gulf of Thailand and the Andaman Sea. In the part of the Gulf of Thailand, the coastal erosion occurs along the coastline from the coast of Trat Province to Narathiwat Province. At present, many areas with severe erosional situation are in critical condition resulting in destruction to coastal resources, for instance, houses, buildings, habitats, quality of life and even local cultures of the community. Coastal erosion also affects the scenery of the coast. The government spent a lot of money in order to prevent and solve the coastal erosion problem.

Bang Pakong district, Chachoengsao province is situated in the coastal area of the Gulf of Thailand (figure 1) which is classified as a critical areas of high erosion rate at 5 m yr^{-1} [1]. The coastline of Bang Pakong district is 16.28 km in lenght which is characterized by a mudflat marine clay soil type covered by mangrove forests. At present, coastal erosion situation in Bang Pakong district is occurring continuously and coastal areas are severely eroded [1].

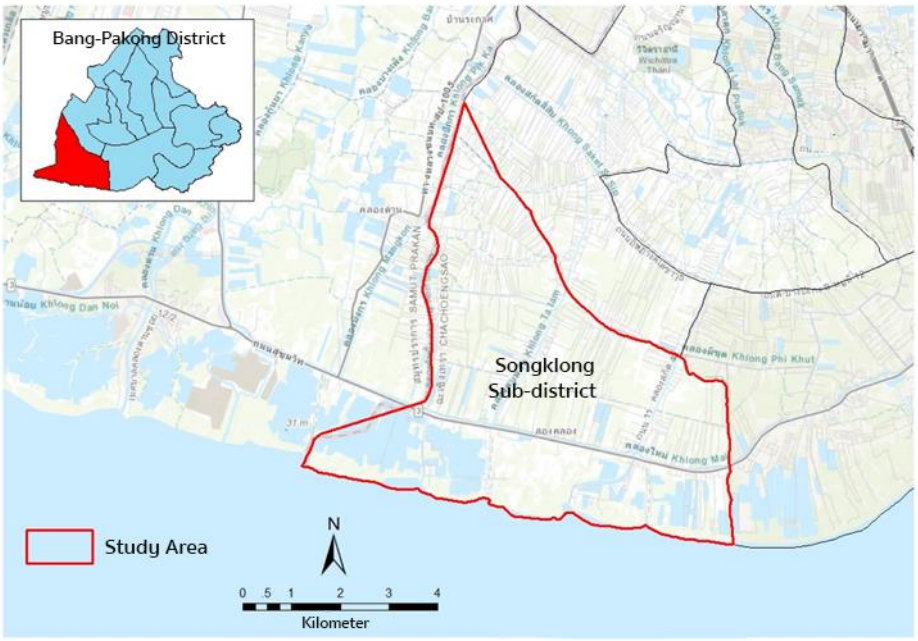

Figure 1. Map of the study area location at Songklong district, Amphoe Bangpakong, Chacheongsoa, Thailand

Digital Shoreline Analysis System (DSAS) is a computer software extension in ArcGIS that can be used to calculate the rate of change of coastline positions over several periods of time using Geographic Information System (GIS). It is also useful to calculate the rate of change of other boundaries with clearly defined positions in discrete time [3]. This study is focuses on analyzing the shoreline changes situation in the area of Songklong sub-district, Bang Pakong district, Chachoengsao Province using Digital Shoreline Analysis System (DSAS) and GIS to study the severity rate of coastal erosion. The results of this study provide useful information for the community, local government and government authorities and private organization to formulate policies and plans for coastal erosion management and protection. It also reduces the impact of coastal, economic, social and environmental erosion in the future. Furthermore, the results can provide the contribution to practices of coastal planning and management in a coastal area, moreover, historical shoreline change statistics can be used to monitor coastal environmental changes such as climate change, global warming, sea level change, and sedimentation accumulation rates.

2. OBJECTIVE

2.1 To analyze the changes of shorelines over a 15-year period in Songklong sub-district, Bang Pakong district, Chachoengsao Province from the year of 2002 to 2016.

2.2 To assess the erosion situation of Songklong sub-district, Bang Pakong district, Chachoengsao Province.

3. METHODOLOGY

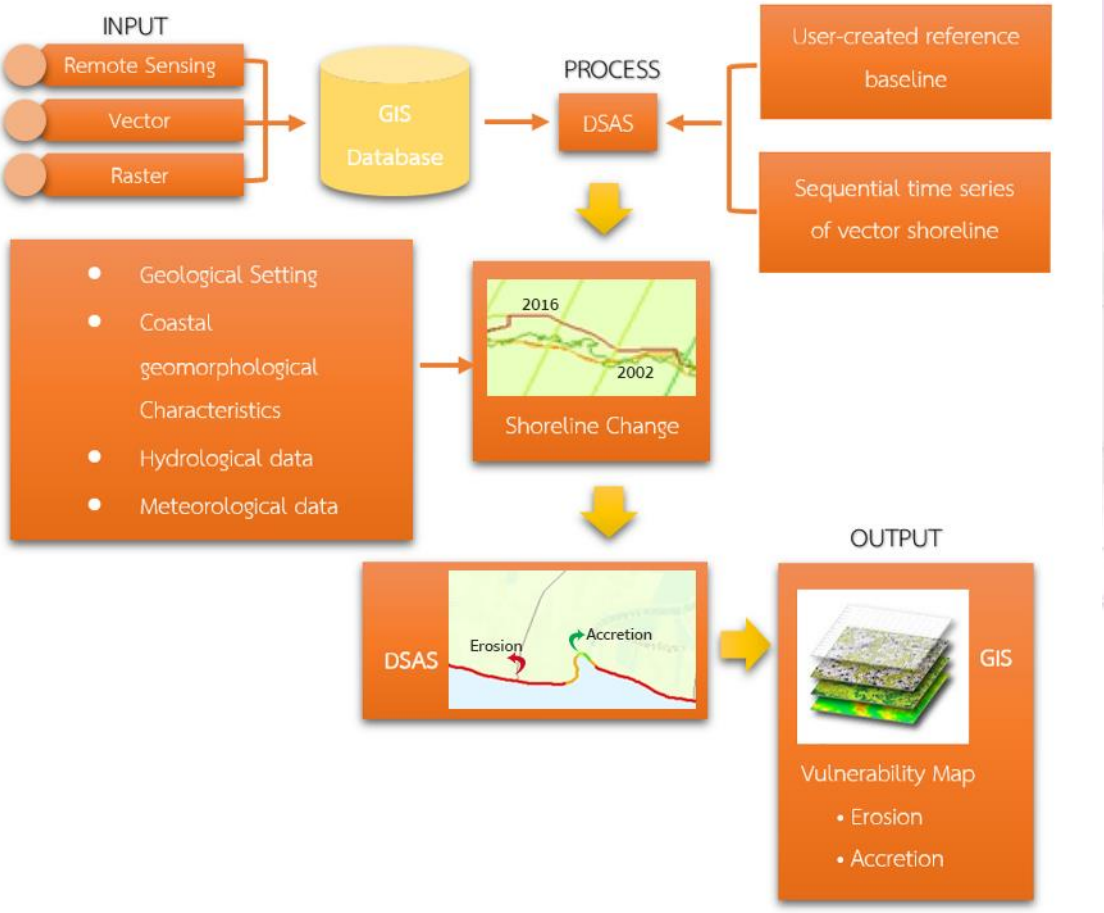

Figure 2. Conceptual framework of the study of Application of Geographic Information Systems for Coastal Erosion Analysis Using Digital Shoreline Analysis System (DSAS): A Case Study of Songklong sub-district, Bang Pakong district, Chachoengsao Province, Thailand

Conceptual framework of the study of Application of Geographic Information Systems for Coastal Erosion Analysis Using Digital Shoreline Analysis System (DSAS): A Case Study of Songklong sub-district, Bang Pakong district, Chachoengsao Province represents the process of the study. This can be explained as shown in figure 2. GIS database consists of Remote Sensing (RS), Vector (Vector), and Raster data. Then, data is imported into the digital shoreline analysis system (DSAS) using following methods; 1) User defined baseline and 2) Define multiple coastline dataset 3) Then, the coastline analysis was performed by comparing shoreline movement in DSAS. 4) The map of coastal erosion and shoreline change is generated from digital shoreline analysis system in geographic information system environment.

The investigation of changes in shoreline positions in Songklong sub-district's muddy coastal area is carried out using Satellite imagery (Landsat5 and Landsat8) and aerial photography available for the period between 2002 and 2016. Shoreline movements were measured from historical vegetation line index by digitizing in GIS using the DSAS extension developed by the *United States Geological Survey* (USGS). In this study, the Digital Shoreline Analysis System (DSAS) was used to analyze shoreline changes. The

statistics that were used to analyze are as follows; 1) Shoreline Change Envelope (SCE), 2) Net Shoreline Movement (NSM), 3) Linear regression rate (LRR)

The choice of DSAS statistical parameters in the case study has been able to explore the temporal and spatial dynamics of the coastal change and the geomorphic variability along the beach because of their ability in making use of all shoreline positions (SCE), the cumulative shoreline movement (NSM) and Linear regression rate (LRR) which summarize the rate-range of the historical dataset.

Shorelines were digitized from each Satellite image and aerial photograph. The standard DSAS shoreline change measures - Net Shoreline Movement (NSM) was calculated. Net Shoreline Movement (NSM): reports the distance between the oldest (2002) and the youngest (2016) shorelines, which presents the overall change in shoreline position for the 15 year period.

4. RESULTS

4.1) Shoreline Change Envelope (SCE)

Table 1. Shoreline Change Envelope (SCE) of Songklong sub-district

Level of change	**interval (m)**	**Average distance (m)**
Very low	0-50	3,985.65
Low	50.01-100	2,742.64
Moderate	100.01-150	1,364.99
High	>150.01	1,781.20

Shoreline Change Envelope reports the distance between shorelines measured furthest and closest to the baseline for each transect. This represents the total change in movement and is not governed by the age of the shorelines. The average coastline of 84.60m was moved as shown in figure 3. The results show that changes of coastline during the period of 15 years from 2002 to 2016 can be classified into 4 levels (table 1): 1) Very low level change of coastline ranges from 0 to 50 m with an average distance of 3,985.65 m. 2) Low level change of coast line ranges from 50.01 to 100m, with an average distance of 2,742.64m. 3) Moderate level of coastal change variates in the range of 100.01 to 150 meters, with an average distance of 1,364.99m. And 4) High level of the shoreline change ranges from 150.1 to 213.43m with an average distance of 1,781.2 m.

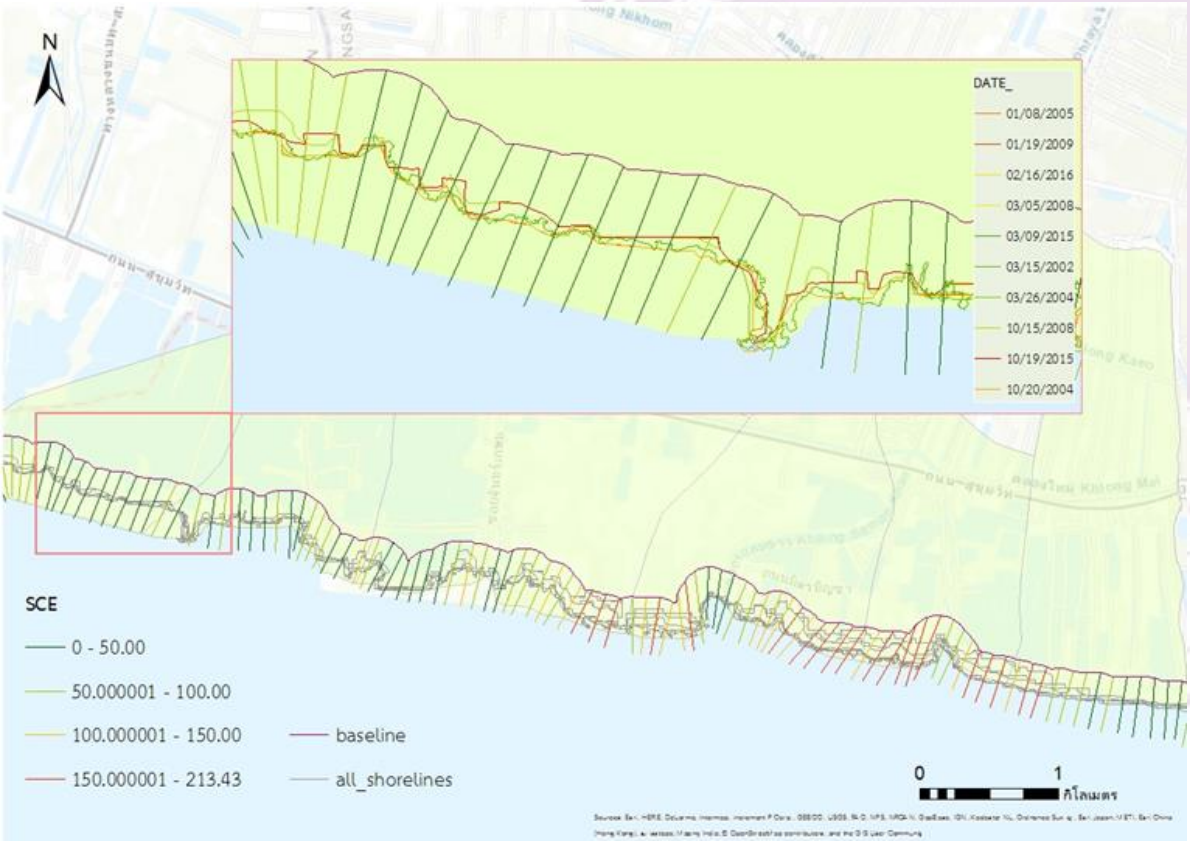

Figure 3. Map of Shoreline Change Envelope (SCE) of Songklong sub-district

4.2) Net Shoreline Movement (NSM)

The Net Shoreline Movement reports the distance between the oldest and youngest shoreline features for each transect. The results indicate that net shoreline movement in the area of Songklong sub-district during the period of 15 years from 2002 to 2016 can be classified into 4 levels (table 2), which are 1) Very low level of net shoreline movements are in the range of 0.01 to 50 meters, with an average distance of 1,581.19 meters. 2) Low level of net shoreline movement is in the range of -49.99 to 0 meters with an average distance of 3,685.65 meters. 3) Moderate level of net shoreline movement ranges from -99.99 to -50 meters, with an average distance of 1,766.65 meters. 4) High level of net shoreline variation ranges from -19.22 to -100 meters, with an average distance of 2,940.75 meters. The average net shoreline movement in the study area is 66.86 meters shown in figure 4.

Table 2. Net Shoreline Movement (NSM) of Songklong sub-district

NSM	interval (m)	Average distance (m)
Very low	0.01 to 50	1,581.19
Low	-49.99 to 0	3,685.65
Moderate	-99.99 to -50	1,766.65
High	< -100	2,940.75

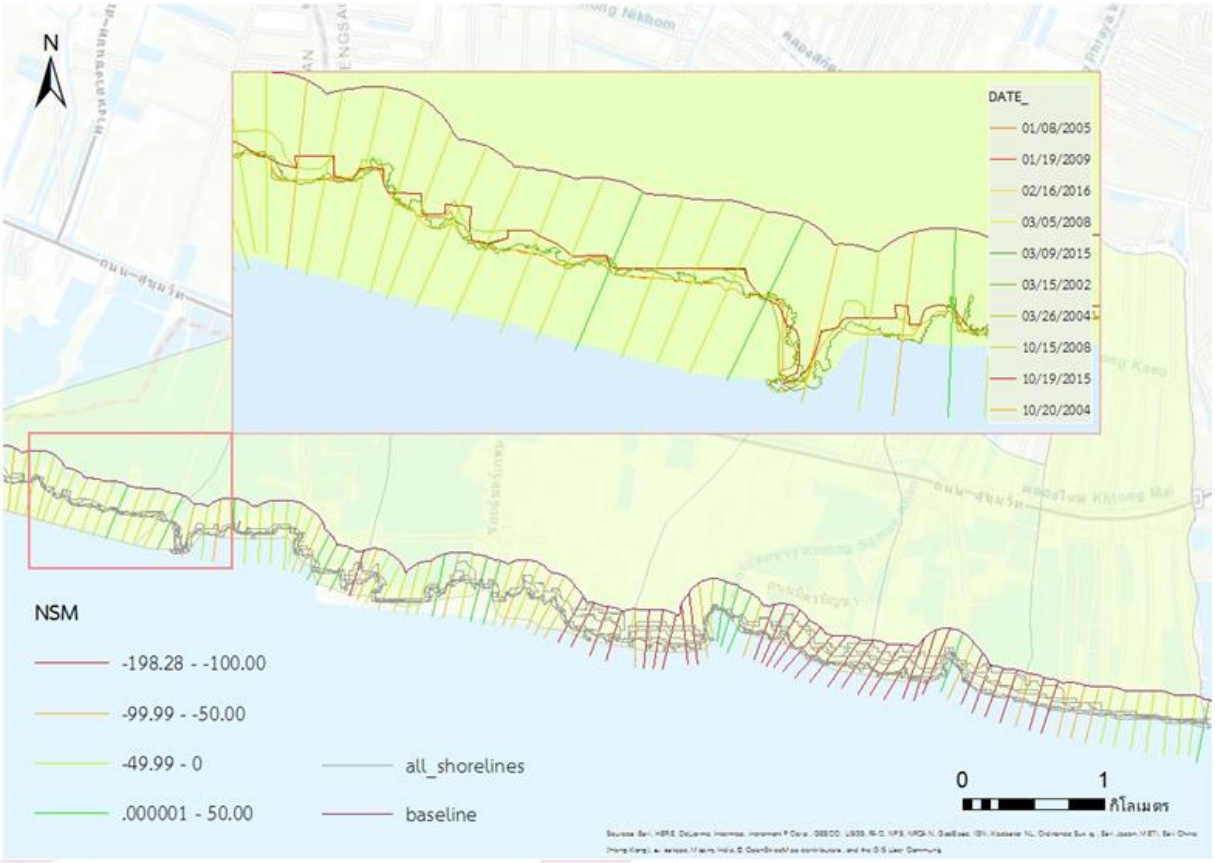

Figure 4. Map of Net Shoreline Movement (NSM) of Songklong sub-district

4.3) Linear regression rate (LRR)

The R-squared statistic, or coefficient of determination, is the percentage of variance in the data that is explained by a regression. It is a dimensionless index that ranges from 1.0 to 0.0 and measures how successfully the best fit line accounts for variation in the data. In other words, it reflects the linear relationship between data sets. The r-squared value quantifies the proportion of the variability in the dependent variable (Y) that is explained by the regression model through the independent variable (X). The smaller the variability of the residual values around the regression line relative to the overall variability, the better the prediction. The results show that the erosion rate of the study area over the 15 years from 2002 to 2016 can be divided into 4 levels (table 3): 1) Accretion coastline is rated over 1 m yr^{-1} with the average distance of 330m. 2) Stable coastline is rated between -0.99 and 0 m yr^{-1}, with an average distance of 1,250m. 3) Low erosion is rated between -4.99 and -1 m yr^{-1}, with an average distance of 4,740m. 4) High erosion is rated between -15.99 - 5 m yr^{-1}, with an average distance of 4,210m. The study found that the study area has erosion rate of -5.62 m yr^{-1} with R2=0.9819 (figure 5 and figure 6)

Table 3. The table shows the erosion rate of the study area over the 15 years from 2002 to 2016

Erosion Rate	Interval (m yr^{-1})	Distance (m)
Accretion	< 1	330
Stable coastline	-0.99 to 0	1,250
Low erosion	-4.99 to -1	4,740
High erosion	-15.99 to -5	4,210

Figure 5. The map summarizes the scales and rates of change in shoreline position at Songklong sub-district beach with the average erosion rate of -5.62 m yr^{-1} with R2=0.9819.

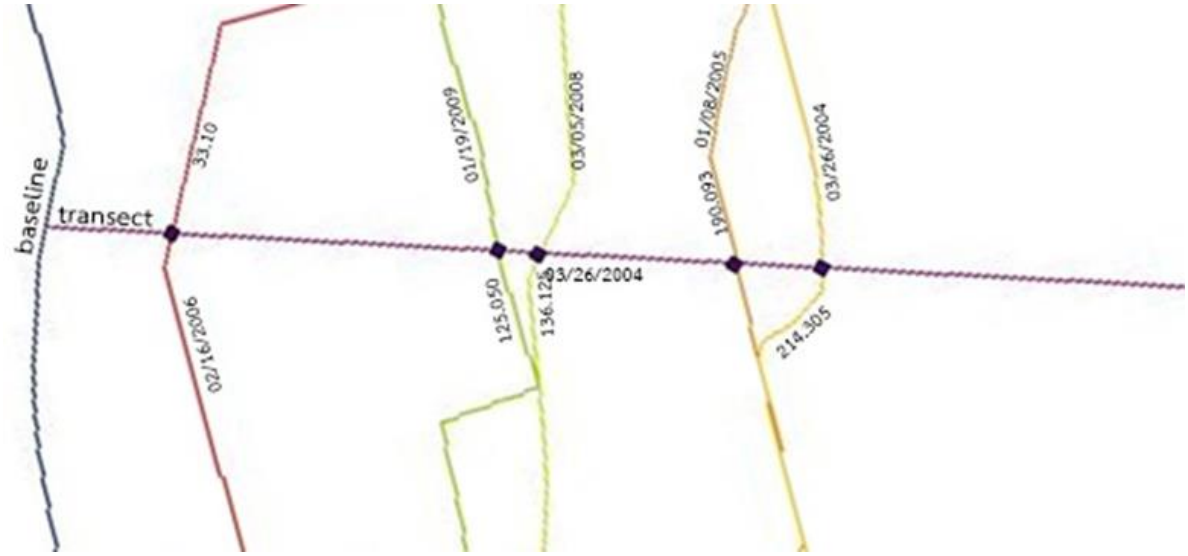

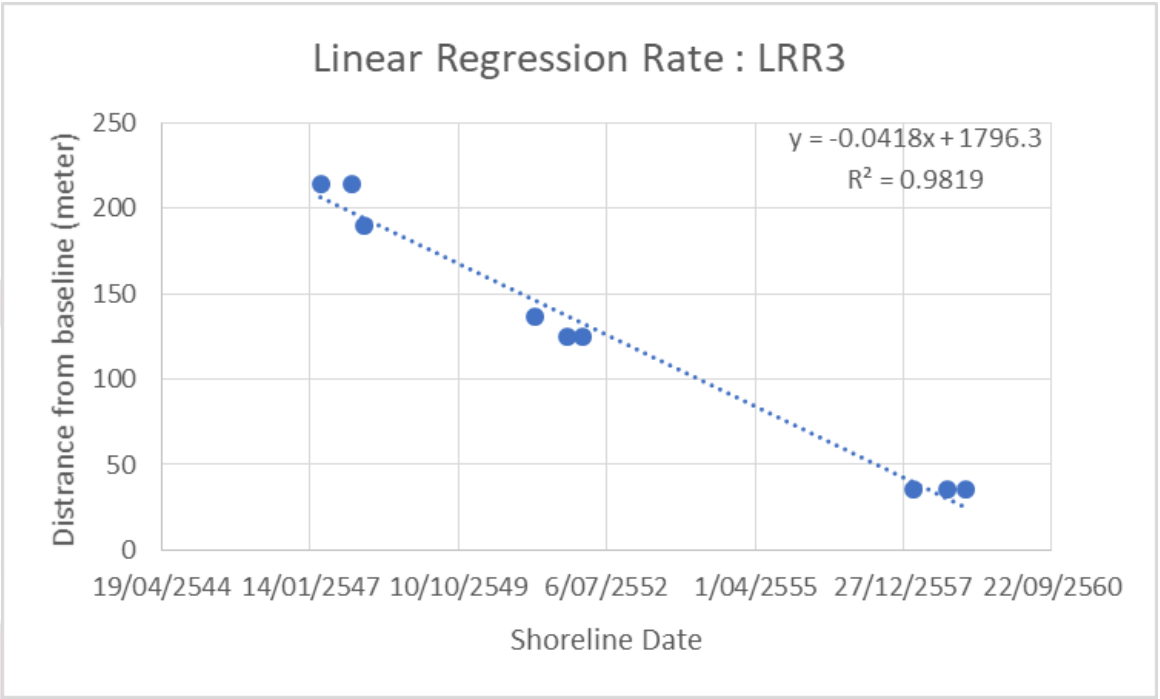

Figure 6. The figure shows Linear Regression Rate: LRR at Songklong sub-district beach with the average erosion rate of -5.62 m yr^{-1} with R2=0.9819.

5. CONCLUSION AND DISCUSSION

Application of Geographic Information System for Coastal Erosion Analysis using Digital Shoreline Analysis System (DSAS): A Case Study of Songklong Sub-district, Bang Pakong District, Chachoengsao Province utilized the satellite imagery and aerial photos to analyze the change of shoreline over the period of the year of 2002-2016 (15-year period). The study found that the study area has erosion rate of -5.62 m yr^{-1} with R2=09819, which indicates that area is classified into the level of severe erosion with erosion rates of more than 5 m yr^{-1}.

The coastal area of Songklong sub-district is characterized by a mudflats covered by mangrove forest during the high tide it will be submerged and will emerge when the water is low. The sediment dated less than 5,000 years old with gray or greyish green, consisting of a large amount of organic matter. The area is abundant of many living organisms with a complex ecosystem. This area is the most sensitive and prone to erosion area because of the sediment transportation activities [1].

The situation observed here can be compared to what S. Oraon and K. Nakapakorn (2014) [2], who applied geographic information system to the erosion situation of the coast. The study found that the coastal area of Phetchaburi was eroded at a total distance of 11,638 m. The coastline eroded severity by more than 4 m yr^{-1}, which is different from the results of Songklong Sub-district, Bang Pakong District, Chachoengsao Province.

6. RECOMMENDATION

DSAS is a computer software that calculates the rate of change in coastline positions over several periods of time using GIS for data analysis. The software developed by U.S. Geological Survey is a reliable institution. Accuracy and accuracy are reliable in the middle. DSAS can also be used to calculate the rate of change of other boundaries that are clearly marked in a discrete time. In this research, it is only an analysis and evaluation of the erosion situation using statistical methods. Fieldwork should be studied in the actual area in order to obtain accurate information.

REFERENCES

[1] Department of Marine and Coastal. “Coastal erosion”, Central Database and Standards for Marine and Coastal Resources, 2013

[2] S. Oraon and K. Nakapakorn, “Geo-information Application for Coastal Erosion Situation, Phetchaburi Province”, Thammasat Journal of Science and Technology 22(6), pp.789-800, 2014

[3] U.S. Geological Survey, “Digital Shoreline Analysis System”, NOAA, 2016

DETECTION OF MANGROVE FOREST CHANGES AND ASSESSMENT OF CARBON STOCK AND ECONOMICS VALUES IN SAMUTH SONGKRAM, THAILAND USING REMOTE SENSING AND GIS TECHNIQUES

Kamonporn Upakankaew
Department of Geography, Faculty of Arts, Silpakorn University
6 Rajamankha Nai Road, Amphoe Muang, Nakhon Pathom, 73000, Thailand.
nest06th@gmail.com

Rajendra Prasad Shrestha
School of Environment, Resources and Development, Asian Institute of Technology. P.O. Box 4, Khlong Luang, Pathumthani 12120, Thailand. Rajendra@ait.asia

ABSTRACT

Thailand has introduced and implemented numerous policies to protect and restore the mangrove forests which provided mixed results. To maintain the trend of the increase of mangrove forest cover as well as to increase the possibilities of obtaining financial support under the REDD+ scheme or carbon offsetting scheme, assessment of the changes of forest cover and related carbon stocks becomes needed. This study estimated area changes of mangrove forest in Samuth Songkhram province using Remote Sensing and forest carbon stocks using forest inventory data. Five carbon pools were considered and respective allometric equations were used to derive carbon pools. Carbon emission reductions and removals were estimated 2030, based upon which economic potentials from carbon-based revenues were derived.

This study found that area of mangrove forests in Samuth Songkram had increased since 2001. In terms of carbon stocks, 2.9 million MgC were stored in the mangrove in 1973 but declined to 1.6 million MgC in 2001 and to 2.1 million MgC in 2016. For tree species in conservation zone was dominated by Avicennia alba (64.4%). In management zone, Rhizophora apiculata was dominated. Projection to the future suggested that conservation and management have resulted in carbon emission reductions and removals and therefore the carbon-based economic values were estimated at $4.4 million in 2021-2030 at the price $3.3 /tCO2. With the costs of conservation and management of $2.51/tCO2, the net economic values for this province were $1 million over the same period between 2021 and 2030. If the current management and conservation continue to succeed, there are huge carbon benefits. To benefit from the REDD+ scheme, project design document along with transparent monitoring, reporting and verification systems need to be developed.

***Keywords**: remote sensing, carbon stock, mangrove forest, GIS, biomass*

1. INTRODUCTION

Due to mismanagement, the global mangrove areas are less than half of their original cover in the last 50 years and mostly in the last two decades (Mangrove action project, 2016) [37]. The use of Global Forest Watch (GFW) found that 192,000 ha (1.38%) of mangrove forest were lost from 2001 to 2012 (Strong and Minnemeyer, 2015) [65]. The main causes of mangrove deforestation were the conversion of mangroves to different land uses or purposes such as aquaculture, charcoal, agriculture, urban expansion and selling wood. In Thailand, the early plans of economic development led to overexploitation of natural resources without any planning of their effects (Office the National Economic and Social Development Board, 2015) [44].

Mangrove areas had been sharply exploited due to the need for fast economic development and mismanagement. This overexploitation resulted in the loss of mangrove areas about 50.93% between 1961 and 1989 (Suwannakon, 1991) [67]. The goals of the 1st – 7th of Thai National Economic and Social Development (1961 – 1996) were to develop basic infrastructures and to support economic development but they did not concern about environment. Realizing the danger to its natural resources, this Thai National Economic and Social Development (1997-2001) was revised to include sustainable were managed of natural resources. This revising was included in the 8th – 11th plans.

Because of the reforms, mangrove forests were classified according to conservation and management. The former is the natural mangrove, while the latter is the restored mangrove whose management purposes are mainly for charcoal production (Jintanukun, 1997; Marine Knowledge Hub. 2010) [29] [39].

Although, forest areas of mangrove has increased in Samuth Songkhram Province, the increase is in the expense of natural mangrove forest because the province needs to conserve the mangrove forest, at the same time to manage other areas to support economic development. To understand the effects of conservation and management on mangrove forest, forest cover change needs to be understood. However, such information in currently is not available in sustainable management.

In addition, as REDD+ is permanent based payment, to obtain such payments at in required trend information on carbon stock emission reduction be made available. However, this information is also not available. As REDD+ scheme requires biodiversity be protected, information of carbon stock relative to species is also needed.

Therefore, to ensure long-term effective of conservation and organization mangrove forest in sustainable, assessment of the change in areas of mangrove and carbon stock need to be undertaken. Such large scale assessment is very expensive and time consuming. The use of remote sensing is the one of most efficiency technique in surveying and monitoring due to their highly accuracy, rapid and cost effective (Aschbacher, 1993)[6]. Therefore, appropriate conservation measures can not be achieved without identifying the area changes.

Once area changes are identified, total carbon stock can also be calculated by additionally using carbon stock per ha obtained from forest inventory. In addition, in knowing carbon stock changes and emission reductions, carbon-based revenues can

also be estimated. Accordingly, these revenues can be used for conservation. Then the appropriate management in this area is discussed.

2. OBJECTIVE

1. Assess the changes in mangrove areas between 1996 to 2016
2. Assess the carbon stock relative to trees in mangrove forest
3. Assess the carbon stock in mangrove forest between 2017 and 2030
4. Estimate the economic potential of carbon stock in mangroves for future under

3. METHODOLOGY

3.1 Study area

3.1.1 The criteria for selection of study area

Samuth Songkhram Province is one example mangrove areas that gaining less mangrove forest increasing (Marine Knowledge Hub, 2010) [39]. One popular reason of gaining less or stable mangrove forest is that the mangrove lands are in the private hands. Most land owners do not want to remain the mangrove forests because they provide less direct income comparing to other land use such as shrimp farming and residence areas. The last criteria of selecting this area is that the size of the area. According to employing remote sensing technique to extract the mangrove forest (Landsat satellite has 30*30 meters spatial resolution), the small areas are not appropriated.

3.1.2 Geography of selected area

The study area is located in the coastal of Samuth SongKhram Province, around the gulf of Thailand. The area of this province is 87,200.30 hectares. The south areas of Samuth Songkhram province is the coastal areas. The length of coastal area is around 41.80 kilometers.

3.2 Methodology

The overall approaches of this study to assess carbon stock and economic revenues using remote sensing and geographic information system techniques are divided to

four parts (1) Data collection (2) Satellite image preparation (3) Image processing, and (4) Data analysis as shown in figure 1

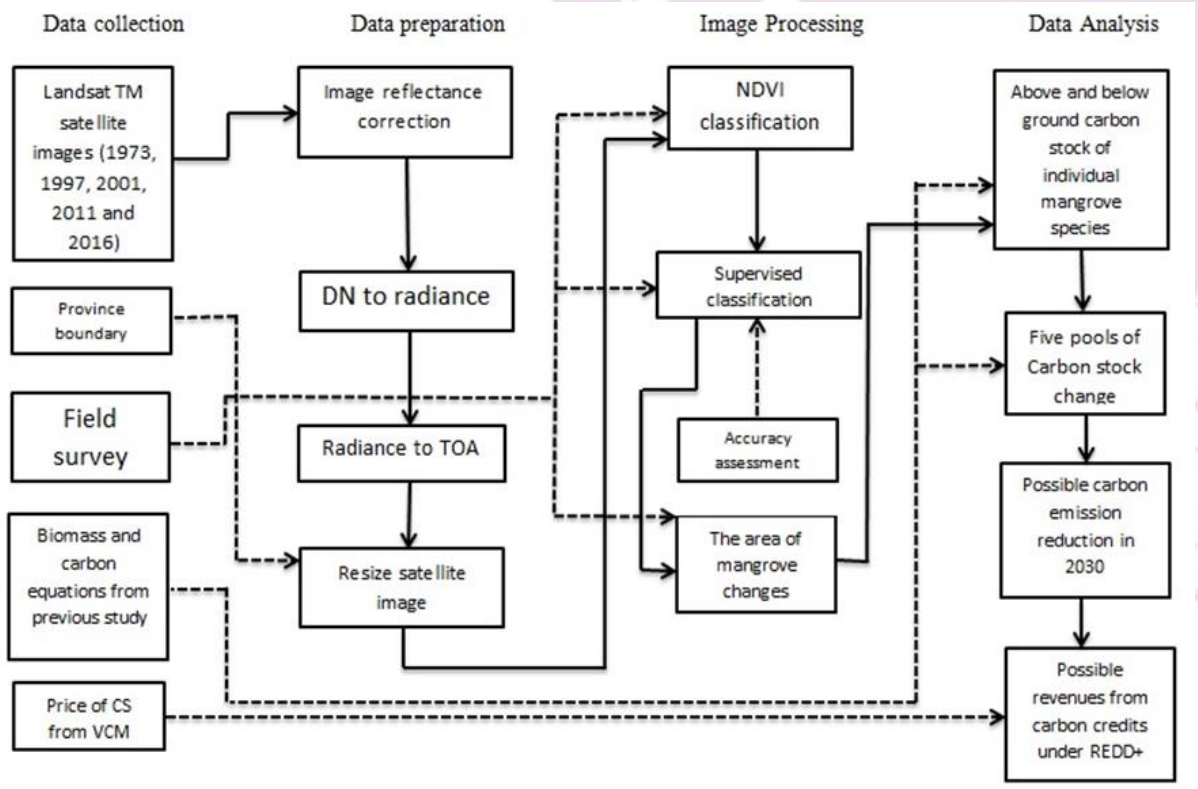

3.2.1 Data collection

The Landsat satellite images were downloaded from United States Geological Survey. The above ground biomass values of specific mangrove species were collected from previous study which are located in Thailand and have similar climate conditions. The price of carbon credit is also based on the price of voluntary market in 2016.

The satellite images were mostly downloaded in the winter season because it is clear from cloud. The images were downloaded in the year 1973, 1997, 2001, 2011 and 2016. These periods were selected to monitor the mangrove area changes before the forest restoration policies (the eight plan of the Office of the National Economic and Social Development) had implemented in 1997. After the year 1997, the mangrove area changes were also classified to see the trend of changes. Moreover, the satellite image of year 2016 was classified to identify mangrove species related with ground survey because specific mangrove species content different amount carbon stock.

Field surveys were conducted three times. The first time was pre-survey assessment prior to plan for plot setting and tree measurement. Secondly, ten plots were designed according to purposive sampling to measure mangrove tree diameter and their species. These mangrove areas mostly are the mangrove plantations that have two main zones. These unique two zones have two main objectives; the first one is for mangrove conservation and the second purpose is for charcoal production. The plot size was 10*10 meters and ten plots were set up that the trees in conservation zone were measured at DBH ≥ 4.5 cm and all trees in second zone were measured. All tree species

in both two zones were recorded. The last survey is for checking accuracy assessment that 99 ground points were identified systematically.

3.2.2. Satellite image preparation

NDVI is one of most effective formula to classify vegetation. Then it employed only Red band and NIR band. Moreover, supervised classification is one of the most popular applications that are often used to classify land use and land cover. Before each band was composited to enhance the objects, each band in Landsat satellite images was rescaled to Top of Atmospheric reflectance. This process has a two-step process. First the DNs must be converted to radiance values, and then these radiance values are needed to convert to reflectance values. For each scene, the sun, earth in astronomical units, the day of the year, the distance and solar zenith angle are provided in metadata.

3.2.3 Image processing

Satellite images were needed to resize or crop before they were composited because the large images consumed more time in analyzing process.

3.2.3.1 Remote sensing for mangrove forest classification

Remote-sensing images were used to classify mangrove forests in different years by analyzing NDVI and using supervised classification. Biomass could be estimated by regression equations among their band ratio indices using Normalized Difference Vegetation Index (NDVI).

NDVI formula;

$$NDVI = (NIR-RED) / (NIR+RED) \quad (1)$$

In mangrove species identifying process, the mangrove forest was surveyed to identify their major mangrove specie distributions. The field surveys were conducted in 2016 to identify mangrove species related with satellite images using GPS. The mangrove field surveys were taken two times in different mangrove forest. It will survey mangrove species around the forest and following the nature trail. According to the nature of mangrove species, each species grow in their specific natural condition

3.2.3.1.2 Supervised classification

Then NDVI classified images were used as the base in supervised classification to identify the areas of interest using their values. Future more, the major mangrove specie distributions from field survey will be used to identify mangrove species in satellite images as giving examples of the area of interest in supervised classification process.

3.2.3.1.3 Post classification

In order to check the accuracy of image classification, 99 points of ground survey were checked systematically using Kappa analysis.

Kappa analysis: Khat Coefficient of Agreement

$$\widehat{K} = \frac{N\sum_{i=1}^{k} xii - \sum_{i=1}^{k}(xi+ + x+i)}{N - \sum_{i=1}^{k}(xi+ \times x+i)} \quad (2)$$

Where $\widehat{K}$ is the number of rows (land-cover classes) in the matrix.

X_{ii} = the number of the observation in row i and column i
X_{i+} = the marginal totals for row i
X_{+i} = the marginal totals for column i
N = the total number of observations

$\widehat{K}$ values > 0.80 represent strong agreement or accuracy between the classification map and the ground reference information.

Finally, the mangrove areas were extracted and calculated from other land covers to assess the changes of mangrove areas and their species from 1973 to 2016 in the ArcGis application.

3.2.4 Data Analysis

3.2.4.1 The change of mangrove area from 1973 to 2016

The areas were calculated form satellite images in the year 1973, 1997, 2001, 2011 and 2016. From the year 1997 to 2016, the mangrove areas were divided to two main zones; the first zone has purpose for mangrove conservation and the second zone is for charcoal production. According to different spatial resolution of Landsat 1, the mangrove area in 1973 was not divided.

3.2.4.2 Assess the above and below ground of biomass and carbon stock according to their individual mangrove species

The above and below ground biomass and carbon of individual mangrove trees were assessed using the equations from previous studies. Formulas for assessment above and below ground biomass and carbon stock per hectares

$$\mathrm{AGB}_{\mathrm{plot}} = \frac{\sum \mathrm{AGB}_{\mathrm{i}}}{\mathrm{PlotSize}} \quad (3)$$

$$\mathrm{AGB}_{\mathrm{average}} = \frac{\sum \mathrm{AGB}_{\mathrm{plot}}}{\mathrm{TotalPlot}}$$

$$\mathrm{CAGB} = \mathrm{AGB}_{\mathrm{average}} \times \mathrm{CT}$$

(4)

(5)

(6)

(7)

(8)

3.2.4.3 Assess biomass and carbon stock of mangrove trees

As the above and below ground of biomass and carbon stock were already assessed, then litter, dead wood and soil organic carbon that also store large amount of carbon stock were estimated using equations. The areas of mangrove which were already classified in objective 1 were used to estimate carbon stock in the equations.

For litter and dead wood carbon stock were calculated using the average carbon stock values from previous studies. Litter and dead wood biomass are 13.24 MgC/ha or 14.1%, 16.34 MgC/ha or 17.4%, and 369 MgC/ha for the average soil carbon stock.

3.2.4.4 Making mangrove forest baseline and projectline for estimating mangrove forest in the future

To get the incentive support from REDD+, the baseline and projectline were needed to be developed. Therefore, two scenarios (baseline and projectline) are considered for 1973-2030 (Chheng et al., 2016) [12].

3.2.4.4.1 The baseline of mangrove forests without conservation and management

Formula:

$$FA_b(t) = FA_b(t_0) \times e^{-a_b \times t} \quad (9)$$

Data: 1973, 1997 and 2001

Where;

$FA_b(t)$ = Forest area cover under no conservation or baseline scenario

t = Time step (year)

$FA_b\ t_0$ = Forest area at starting time (i.e. 1973, 1997 and 2001)

a_b = Deforestation rate

3.2.4.4.2 The projectline of mangrove forests with conservation and management

Formula:

$$FA_p(t) = \frac{FA_{max} \times FA_p(t_0) \times e^{-a_p \times t}}{FA_{max} + FA_p(t_0) \times (e^{-a_p \times t} - 1)} \quad (10)$$

Data: 2001, 2011 and 2016

Where;

$FA_p(t)$ = Forest cover under conservation and management or projectline at time step

$FA_p(t_0)$ = Forest cover under conservation and management or projectline at staring time (i.e. 2001, 2011 and 2016

FA_{max} = The maximum area of mangrove in the whole province

a_p = Rate of increase

3.2.4.4.3 Weighted average of carbon stock

Formula;

$$CS_{WA} = \frac{(CS_{conservation} \times FA_{conservation}) + (CS_{management} \times FA_{management})}{FA_{total}} \quad (11)$$

Where;

CS_{WA} = Weighted average of carbon stock of two zones

FA_{total} = Total Forest area

$CS_{conservation}$ = Carbon stock in conservation zone

$CS_{management}$ = Carbon stock in management zone

$FA_{conservation}$ = Forest area in conservation zone

$FA_{management}$ = Forest area in management zone

3.2.4.4.4 Carbon stock changes and their credits (1973-2030)

$$CS_b(t) = FA_b(t_0) \times CS_{WA} \quad (12)$$

$$CS_p(t) = FA_p(t_0) \times CS_{WA} \quad (13)$$

$$CC = \left[\Delta CS_b(t) - \Delta CS_p(t)\right] \times \frac{44}{12} \quad (14)$$

Where;

CS_b = Baseline of carbon stock

CS_p = Projectline of carbon stock

CC = Carbon credit

ΔCS_b = The difference of carbon stock without conservation and management

ΔCS_p = The difference of carbon stock with conservation and management

3.2.4.5 Economic potential of carbon stock

To assess the potential economic from carbon emission reduction this study is based on the price of carbon in 2015 under voluntary carbon market of REDD+ scheme that it costs $3.3/ tone of CO_2 emission reduction. In addition, $10 and $20 /tone of CO_2 emission reduction were compared for the possible future prices and the cost for conserving and managing mangrove forest were also calculated. The formula in assessment of potential revenues from carbon stock is following.

Formula for carbon revenues;

$$NCR = CC * (CP - RC) \quad (15)$$

Where;

NCR = Net carbon revenue

CC = Carbon credit

CP = Carbon price

RC = Reduction cost (*RC=US$2.51/tCO2)

*RC refers to conservation and management costs for mangrove were estimated at $2.51 by Ammar et. al. (2015)[3].

4. RESULTS

4.1 The mangrove areas in 1973 to 2016

The overall accuracy assessment of the mangrove images in 1973, 1997, 2001, 2011 and 2016 are 87%, 84%, 88%, 81% and 82%, and their kappa analysis are 82%, 79%, 84%, 76% and 75%.

The areas of mangrove are divided to two zones in different years. According to the limitation of satellite Landsat 1, their bands are limited and resolutions are rougher than Landsat 5-8. Then the mangrove area image in 1973 which was recorded by Landsat 1 was classified to only mix species of mangrove. Therefore, in 1973, the mangrove areas were 5,479.14 ha.

This study found that most mangroves in Samuth Songkhram province are secondary mangroves or mangrove plantation but they could be classified to two main categories; the first zone is for mangrove conservation purpose and the second mangrove plantation is for charcoal production.

Table 4.1 *Change in mangrove area*

Year	Species	Area(ha)	Total(ha)
1973	Mixed mangroves	5,479.14	5,479.14

1997	*A. alba*, *X. granatum*, *S. caselaris* *Rhizophora apiculata*	540.73 3,264.99	3,805.71
2001	*A. alba*, *X. granatum*, *S. caselaris* *Rhizophora apiculata*	654.91 2,723.43	3,378.34
2011	*A. alba*, *X. granatum*, *S. caselaris* *Rhizophora apiculata*	655.36 3,056.08	3,711.45
2016	*A. alba*, *X. granatum*, *S. caselaris* *Rhizophora apiculata* *Sonnerata caselaris*	642.74 3,815.89 16.77	4,475.41

4.2 Assess the carbon stock relative to trees in mangrove forest

In order to reduce the variance of their carbon content and their specie richness, two zones are identified.

As shown in table 4.2, this study found that in conservation zone, *A. alba* is the most found in this zone (64.4%), followed by *S. caselaris*, *R. apiculata*, *X. granatum* (20.3%, 13.6% and 1.7%), and their average carbon stock of above ground and below ground is 236.82 MgC/ha. In management zone, Most specie is *R. apiculata* that their average carbon stock is 102.8 MgC/ha for above and below ground carbon stock.

Table 4.2 *The above and below ground carbon stock of individual mangrove species*

Zone	Species	Kg/m	Mg/ha	MgC/ha
Conservation	*Avicennia alba*	2,444.76	244.48	114.90
	Rhizophora apiculata	285.23	28.52	13.41
	Xylocarpus grnatum	3.08	0.31	0.14
	Sonneratia caselaris	2,305.56	230.56	108.36
Sum		**5,038.63**	**503.86**	**236.82**
Management	*Rhizophora apiculata*	**2,187.18**	**218.72**	**102.80**

For conservation zone, the average aboveground and below ground carbon stock is 138.1 ± 67.1 MgC/ha and 102.8 ± 7.9 MgC/ha in management zone. The weighted average of carbon stock in five pools of two zone is 505.0 MgC/ha. Where other previous studies found that the amount of above ground and below ground carbon stock in mangrove plantation for charcoal in Yeesan, Samuth Songkhram Province, Thailand is 141.56 MgC/ha (Kridiborworn et. al., 2012) [32].

4.3 The carbon balance in mangrove forest

Mangrove biomass was calculated using previous allometric equations relative with individual mangrove species (all sample plots). Firstly, above ground biomass and below ground biomass were calculated from diameters that were measured from the plots. Then they were converted to carbon stock.

The confidence interval of carbon stock in the conservation zone is 293.79 ± 142.72 or 48.58%. The average above ground and below ground biomass of the conservation zone is 293.79 $\pm$142.72 Mg/ha. Then the upper above ground and below ground biomass is 436.52 Mg/ha and the below above ground and below ground biomass is 151.07 Mg/ha (table 4.3).

Table 4.3 *Biomass calculation from sampling plots in conservation zone*

Plot no.	DBH (cm)	ABG (Kg/ha)	BGB (Kg/ha)	AB+BG biomass (Kg/ha)	AB+BG biomass (Kg/ha)	AB+BG biomass (Mg/ha)
1	16.21	4,018.87	1,364.03	5,382.90	538,290.79	538.292
2	16.06	4,139.75	1,567.83	5,707.58	570,758.85	570.75
3	21.02	3,312.56	1,242.94	4,555.50	455,550.06	455.55
4	12.53	1,966.96	822.74	2,789.71	278,971.28	278.97
5	14.32	608.94	253.56	862.51	86,251.16	86.25
6	6.35	156.00	24.53	180.53	18053.67	18.05
7	10.34	788.81	298.27	1,087.08	108,708.88	108.70
SUM	**96.86**	**14,991.92**	**5,573.92**	**20,565.84**	**2,056,584.72**	**2,056.58**
AVERAGE	**13.83**	**2,141.70**	**796.27**	**2,937.97**	**293,797.81**	**293.79$\pm$142.72**

The confidence interval, of carbon stock in management zone is 218.72 ± 16.92 or 17.74%. The average above ground and below ground biomass of this zone is 218.72 $\pm$16.92 Mg/ha. Then the upper above ground and below ground biomass is 235.64 Mg/ha and the below above ground and below ground biomass is 201.80 Mg/ha (table 4.4).

Table 4.4 *Biomass calculation from sampling plots in management zone*

Plot no.	DBH (cm)	AGB (Kg/ha)	BGB (Kg/ha)	AB+BG Biomass (Kg/ha)	AB+BG Biomass (Kg/ha)	AB+BG Biomass (Mg/ha)
8	5.18	1,774.34	321.65	2,095.99	209,599.25	209.60
9	3.24	2,026.62	365.85	2,392.47	239,246.72	239.25
10	3.02	1,758.95	314.11	2,073.07	207,306.72	207.31
SUM	**11.45**	**5,559.91**	**1,001.62**	**6,561.53**	**656,152.70**	**656.15**
AVERAGE	**3.82**	**1,853.30**	**333.87**	**2,187.18**	**218,717.57**	**218.72$\pm$16.92**

The following table 4.5 showed the carbon stocks in different years based in respective zones. The carbon stocks in conservation zone have slowly increased since 1997. For the management zone, carbon stocks had lost about 272,677 MgC from 1997 to 2001. However, the carbon stocks in have increased again in 2011 and continuously to 2016.

Table 4.5 *All carbon stocks divided by two zones*

Year	Conservation zone (MgC)	Management zone (MgC)	Total (MgC)
1973	2,952,076.85		2,952,076.85
1997	291,338.78	1,643,938.22	1,935,277.00
2001	352,863.16	1,371,260.56	1,724,123.73
2011	353,105.84	1,538,753.02	1,891,858.85
2016	354,525.72	1,921,32 2.73	2,275,848.45

4.4 The economic potential of carbon stock in mangrove for the future

In estimate economic potential for mangrove forest conservation and management, baseline and projectline were estimated (figure 4.1).

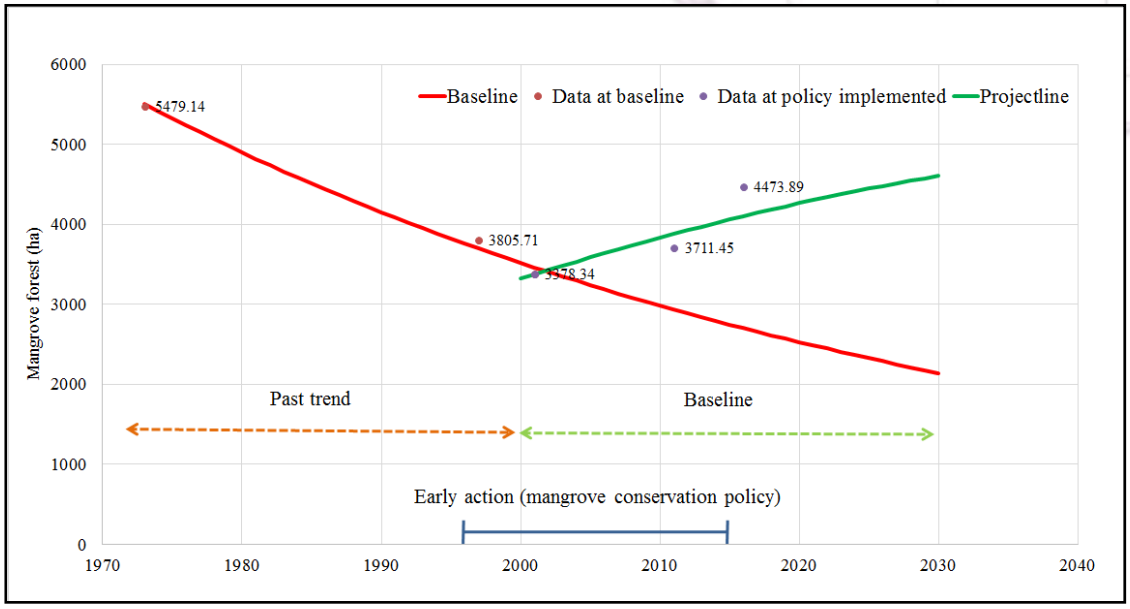

Figure 4.1 Baseline and projectline of mangrove forest changes

As showing in figure 4.1, without early action policies, deforestation rate is 45.49 ha/year^{-1} under baseline from 1973 to 2001 but forest areas increase about 42.42 ha/year^{-1} under projectline from 2001 to 2030. The mangrove areas, cabon stock, and carbon credit change with and without conservation from 2001 to 2030 are shown in the table 4.9. The mangrove forests had decreased to 3,378 ha in 2001 and have divertly increased since mangrove forest conservation policies have implemented in 1997 and 2000. From the projectline trend in 2001 to 2030, the situation of mangrove forests have been increasing because some policies have implemented in this period such as mangrove conservation policy of the eight plan of the Office the National Economic and Social Development in 1997 and the mangrove conservation policy of cabinet resolution in 2000. This increasing period of mangrove forest has been resulted from early action (some policies implemented)(Table 4.7). If there has not implemented any policy, the mangrove areas in Samuth Songkhram would have around 2,001 ha in 2030 (based on past trend baseline).

Table 4.6 These mangrove forests increasing significantly are the result of early action policies.

Furthermore, from this mangrove area projectline estimates that in 2030 with the current policies and management (Table 4.7), Mangrove forest in Samuth Songkhram Province would be 4,608 ha. This etmated that mangrove forests could be reasonable to ask for incentives under REDD+ for carbon emission reduction.

These early policy introduced in Thailand could be considered as early action under the REDD+ scheme, and therefore the carbon emission reduction or removals resulting from increasing forest cover could be eligible for funding.

Table 4.7 These mangrove forests increasing significantly are the result of early action policies

Year	Policies	Eligibility
1973	*Business as usual*	*Baseline*
1991	*Mangrove conservation and restoration led by local leader in Khlong Khon district*	*Baseline*
1997	*Mangrove forest conservation plans of the Thai National Economic and Social Development*	*Early action*
2000	*Mangrove conservation policy of cabinet resolution*	*Early action*

However, emission reduction vary depends on the chosen baseline scenario. For example, if baseline based on past trend is compared, the emission reduction is 2.1 million ton between 2016 and 2030. If the baseline based on linear projection is compared, the emission reduction is only 1 million ton.

Then the carbon revenues were estimated using the priced $3.3 /tCO2 (price in 2015) (Carbon Marketplace, 2016), under past linear baseline about $4.7 million could be get in 2001 – 2016 from REDD+ due to successful conservation and restoration mangrove

Year	Species	Area(ha)	Total(ha)
1973	Mixed mangroves	5,479.14	5,479.14
1997	*A. alba, X. granatum, S. caselaris* *Rhizophora apiculata*	540.73 3,264.99	3,805.71
2001	*A. alba, X. granatum, S. caselaris* *Rhizophora apiculata*	654.91 2,723.43	3,378.34
2011	*A. alba, X. granatum, S. caselaris* *Rhizophora apiculata*	655.36 3,056.08	3,711.45
2016	*A. alba, X. granatum, S. caselaris* *Rhizophora apiculata* *Sonnerata caselaris*	642.74 3,815.89 16.77	4,475.41

forest (early action policies). Based on this price, between 2017 and 2020, $0.9 million can be the compensation for conservation mangrove forest, and $2.1 million is the

compensation of the period 2021-2030. If the price is based on past trend baseline, between 2021 and 2030, $4.4 million could be get from selling carbon credits. The compared prices of carbon credits and their carbon credits in different periods are shown in the table 4.8.

Table 4.8 *Comparing with different price of carbon credit and the baseline*

Carbon credit	Based on linear baseline ($ million)			Based on past trend baseline ($ million)		
	3.3	$10	$20	$3.3	$10	$20
2001-2016	4.7	14.3	28.7	9.7	29.5	59
2017-2010	0.9	3	6	2	6.2	12.4
2021-2030	2.1	6.3	12.7	4.4	13.5	27

Furthermore, if the cost of conservation and management mangroves is $2.51/ton (Conservation and management costs for mangrove were estimated at $2.51 by Ammar et. al., 2015) [3], their revenues based on linear baseline between 2021 and 2030 would be $1 million from REDD+ supporting. If it is based on past trend baseline, the revenues would be $0.5 million from 2021 to 2030

During the Paris agreement period, average reductions and removals are 60 MgCO2 /ha/year and therefore net revenues is $47-1042/ha depending on carbon prices.

5. CONCLUSION AND DISCUSSION

Using RS and GIS techniques, mangrove area changes were estimated between 1973 and 2016. This study found that the mangrove forests in Samuth Songkhram province had decreased from 5,479 ha to 3,378 ha between 1973 and 2001, but according to the main mangrove conservation and restoration policies from local leader and government found that the mangrove had increased to 4,473 ha in 2016. This study divided the mangrove areas in this to two zones due to their management and species which the first is for mangrove conservation and the second is for mangrove management. This dividing also reduces the variance of biomass and carbon stock calculation in mangrove trees. In comparing the mangrove areas changes found that mangrove areas in conservation zone have increased toward the sea, while the mangrove in management zone mostly found in the same places because their cycling cutting is 12 years. These continuously increasing of mangrove forest in conservation zone is the of mangrove conservation policy that has led by local people. As the mangrove is their sources of income, they help to look after mangrove forests including the mangrove conservation law from government. For example, when local people see the cutting or disturbing of mangrove forests they will inform officers to catch the invaders. As a result of effective laws, no one in the local community cut or invades the mangrove forests. Furthermore, in this conservation zone, there are ecotourism and mangrove plantation programs so mangroves in this area have increased continuously.

In order to maintain the successful conservation and expand the areas of mangrove forests, the following activities should continuously implemented;

1. Local participation in the conservation of the mangrove forests

2. Good local leadership that have attracted support from the local community, Royal Department of Forestry (at initial), and government

3. Creation of local conservation-based employment to generate more incomes

4. Community partolling

5. Voluntary restoration of mangrove species

6. Environmental education to raise the awareness of the importances of mangrove forest ecosystems for local livelihood

According to the two mangrove forest divided and using forest inventory, carbon stock by species were estimated. In this step, only above ground and below ground carbon stock were calculated. This study found that the most specie that is found in mangrove conservation zone is *Avicennia alba* which has carbon stock content 114 MgC/ha, following by *Sonneratia caselaris* (108.36 MgC/ha), *Rhizophora appiculata* (13.41 MgC/ha) and *Xylcarus granatum* (0.14 MgC/ha). The average above ground and below carbon in this zone is 138 MgC/ha. In the management zone, mostly found *Rhizophora appiculata* which this species are planted for charcoal production. It contents carbon stock about 102.80 MgC/ha. This information is important for biodiversity safeguarding under the REDD+ scheme. As the mangrove species are not only content large amount of carbon stock, but also provide the large ecosystem services and biodiversity which directly impact on local livelihood and their resources. For example, local fisheries in this areas have an income from collecting cockle or fishing fish around the mangrove forest as nearby mangrove forest provide more fish than far away areas (Mumby et al., 2004) [41]. Moreover, in comparison of mangrove carbon stocks in this study with other studies such as in Yeesan district, Samuth Songkhram province, Thailand and in Vietnam found that the carbon stocks on this area is less than the other studies due to less density and some dead mangrove trees in conservation zone. In order to increase carbon stock in conservation zone, the density of mangrove trees should be considered.

In term of carbon stock changes, Samuth Songkhram province had lost about 37,071 tonC/year between 1973 and 2000 but gained about 41,423 tonC/year between 2001 and 2016. Based on linear baseline between 2017 and 2030, this province will get about 1 million tons CO2 emission reduction. If the carbon emission is based on projectline with the current policy implementation, between 2017 and 2030, this province can get more 0.9 million ton CO2 removal. Therefore, from 2017 to 2030 with the current policy implementation and practices, this mangrove forest can reduce CO2 emission about 1.9 million ton from the atmosphere.

For economic potential, based on the current policies, their practices and the price of carbon credit as $3.3/ton (Voluntary carbon market price in 2015), $2 million will be got between 2017 and 2020. About $4.4 million will be got between 2021 and 2030. If the management cost is $2.51 /tCO2, they could get about $0.8 million between 2017 and 2030 based on linear trend and about $1.8 million based on past trend. Moreover, this province also can ask for the incentive support for successful mangrove

conservation and restoration between 2001 and 2016 from REDD+. These successful in increasing mangrove forests and their carbon stock from early action can be asked for compensation in conservation and management under REDD+. However, the amount of carbon credits is depends on which baselines are chose to estimate the future carbon emission.

This study found that mangrove forest both in conservation and management are likely to increase carbon stock in the forests. Therefore, mangrove conservation and management activities can provide huge benefits in terms of carbon-based financial supports

6. RECOMMENDATION

6.1 Policy recommendations

To obtain financial support for conservation and management, project design document (conservation plan) is needed. In order to design the effective policies to conserve mangrove forest, the areas which mangroves are able to grow should be identified for planning suitable areas for mangrove conservation. Moreover, the understanding of mangroves density is also important in designing mangrove restoration and conservation measures to enhance carbon stock and estimate the future carbon stocks and for preparing report to get financial support under REDD+.

Current successful conservation policies need to be maintained in order to increase area of mangrove as well as carbon stocks. As a result of effective policies in conserving mangrove, the early action policies should be continuously implemented.

The comparison of carbon stock in mangrove forest in conservation zone is less than carbon stock in mangrove in other areas. Then the restoration such as enrichment planting can result in even more carbon stock increase because current stocks are still low

This assessment study may be used to develop a mechanism for obtaining economic values under the REDD+ scheme.

6.2 Recommendations for future research

Future research on local perception on their current conservation and management would provide insights for effective conservation and management planning.

Direct measurement of other carbon pools would give better results for overall carbon assessment.

REFERENCES

[1] Aheto, D. W., Kankam, S., Okyere, I., Mensah, E., Osman, A., Jonah, F. E., et al, (2016). Community-based mangrove forest management: Implications for local livelihoods and coastal resource conservation along the Volta estuary catchment area of Ghana. Ocean & Coastal Management, 127, 43-54.

[2] Aksornkaew, S., (1998). Mangrove forests, Ecology Management (ป่าชายเลน นิเวศวิทยาป่าชายเลน). Bankkok, Thailand, 277.

[3] Almeida, A. R, Novais, A. T., Flavio, H., Oliverira, S. S., Pereiea, R. and Santos, P. T., (2016). Madeira morta: uma revisão da importância da sua conservação. Revista Captar: Ciência e Ambiente para Todos 6.2.

[4] Alongi, D. M. (2014). Carbon Sequestration in Mangrove Forests. *Carbon Management*. 3: 313-322.

[5] Aquatoyou. (2016). Plant Species of Mangrove forests in Thailand. Retrieved on August 2016, from Aquaculture Learning Sources, http://www.aquatoyou.com/index.php/2013-02-20-07-46-16/436-2013-04-01-03-23-55

[6] Aschbacher, J, Ofren, R. Delsol, J. P., Suselo, T. B., Vibulsresth, S. & Charrupat, T. (1993). An integrated comparative approach to mangrove vegetation mapping using advanced remote sensing and GIS technologies: preliminary results. Asia-Pacific Symposium on Mangrove Ecosystems. 106: 285-294.

[7] Baatarbileg and Gerelbaatar (2016). Some Results of Forest Carbon Stock Calculation in Northern Mongolia. Retrieved on April 2016, from National University of Mongolia, www.unredd.net/index.php.

[8]Barbier, Edward, and Mark Cox, (2002). Economic and demographic factors affecting mangrove loss in the coastal provinces of Thailand, 1979–1996. AMBIO: A Journal of the Human Environment 31.4: 351-357.

[9] Badola, Ruchi, and Syed A. Hussain, (2005). Valuing ecosystem functions: an empirical study on the storm protection function of Bhitarkanika mangrove ecosystem, India. Environmental Conservation 32.1: 85-92.

[10] Boonsong, Kanokporn, Somkiat Piyatiratitivorakul, and P. Patanaponpaiboon, (2003). Potential use of mangrove plantation as constructed wetland for municipal wastewater treatment. Water Science and Technology 48.5: 257-266.

[11] Brower, K., (2012). Mesoamerican Reef. National Geographic. Retrieved on April 2016, from WWF Global, http://wwf.panda.org/about_our_earth/blue_planet/coasts/mangroves/mangrove_importance/

[12] Chheng, K., Sasaki, N., Mizoue, N., Khorn, S., Kao, D., and Lowe, A., (2016). Assessment of carbon stocks of semi-evergreen forests in Cambodia. Global Ecology and Conservation 5: 34-47.

[13] Claudia, K., Ochieng, E., Tieszen, L. L., Zhu, Z., Singh, A., Loveland,, T. et al., (2011). Remote sensing of mangrove ecosystems: A review. Remote Sensing 3.5: 878-928.

[14] Clough, B. F., and K. Scott, (1989). Allometric relationships for estimating above-ground biomass in six mangrove species. Forest Ecology and Management 27.2: 117-127.

[15] Comley B. W. T. & McGuinness K. A., (2005). Above and below ground biomass, and allometry of four common northern Australian mangroves, in northern Australia., Australian Journal of Botany. 53: 431–436.

[16] Department of Marine and Coastal Resources (2016). The Mangrove area in Thailand between 2000 and 2009 – Marine Knowledge Hub. Retrieved on April 2012, from Department of Marine and Coastal Resources.

[17] De Sy, V., Herold, M., Achard, F., Asner, G. P., Held, A., Kellndorfer, j., et al., (2012) Synergies of multiple remote sensing data sources for REDD+ monitoring. Current Opinion in Environmental Sustainability 4.6: 696-706.

[18] Donato, D. C., Kauffman, J. B., Murdiyarso, D., Kurnianto, S., Stidham, M. & Kanniene, M. (2011). Mangroves Among the Most Carbon-rich Forests in the Tropics. Nature Geoscience. 4: 293–297.

[19] Duke, N. C., Meynecke, J. O., Dittmann, S., Ellison, A. M., Anger, K., Berger, U., et al. (2007). A World Without Mangroves?. Science. 317(5834): 41-2.

[20] Ellison, Joanna C, (1993). Mangrove retreat with rising sea-level, Bermuda. Estuarine, Coastal and Shelf Science 37.1: 75-87.

[21] FAO, (2013). Climate change guidelines for forest managers. FAO Forestry Paper No. 172. Rome, Food and Agriculture Organization of the United Nations.

[22] Florida Museum of Natural History, (2016). Mangrove Species Profiles. Retrieved on August 2016, from University of Florida, https://www.flmnh.ufl.edu/southflorida/habitats/mangroves/species/

[23] Franco, L. et al, (2016). Kyoto: Think Global, Act Local. Retrieved on August 2016, from Global Community Carbon Forestry Alliance (GCCFA), http://www.communitycarbonforestry.org/

[24] Forest Trends' Ecosystem Marketplace, (2016). Ahead of the Curve: State of the Voluntary Markets 2015. Retrieved on August 2016, from Ecosystem Marketplace, http://forest-trends.org/releases/uploads/SOVCM2015_FullReport.pdf

[25] Grant, M., (1999). Thailand's Disappearing Mangroves: Factors in the Destruction of a Resource. Retrieved on April 2017, from Endangered species, http://connection.ebscohost.com/c/articles/8094033/thailands-disappearing-mangroves-factors-destruction-resource

[26] Holguin, G., Vazquez, P., Bashan, Y., (2001). The Role of Sediment Microorganisms in the Productivity, Conservation, and Rehabilitation of Mangrove Ecosystems: an Overview. Biology and Fertility of Soils. 33(4): 265-278.

[27] Hutchison, J., Manica, A,. Swetnam, R., Balmford, A. & Spalding, M., (2013). Predicting Global Patterns in Mangrove Forest Biomass. Conservation Letters. 7(3): 233–240.

[28] Jardine, Sunny L., and Juha V. Siikamäki, (2014). A global predictive model of carbon in mangrove soils. Environmental Research Letters 9.10: 104013.

[29] Jinta nukun, J., (1997). The Management of Mangrove Forest in Thailand (การจัดการป่าชายเลนในประเทศไทย). Bangkok, Thailand: Forestry Technical Department.

[30] Kennedy, R. E., Townsend, P. A., Gross, J. E., Cohen, W. B., Bolstad, P., Wang, A. Q., et al., (2009). Remote Sensing Change Detection Tools for Natural Resource Managers: Understanding Concepts and Tradeoffs in the Design of Landscape Monitoring Projects. 113(7): 1382-1396.

[31] Komiyama, Akira, Sasitorn Poungparn, and Shogo Kato, (2005). Common allometric equations for estimating the tree weight of mangroves. Journal of Tropical Ecology 21.04: 471-477.

[32] Kridiborworn, P., Chidthaisong, A., Yuttitham, M., Tripetchkul, S., (2012). Carbon Sequestration by Mangrove Forest Planted Specifically for Charcoal Production in Yeesarn, Samut Songkram. Journal of Sustainable Energy & Environment. 3: 87-92.

[33] Kristensen, E.,bouillon, S., Dittmar. T. & Marchand, C., (2008). Organic carbon dynamics in mangrove ecosystems: a review. Aquatic Botany. 89(2): 201-219.

[34] Liu, K., Li, X., Shi, X. & Wang, S., (2008). Monitoring Mangrove Forest Changes Using Remote Sensing and GIS Data with Decision-tree Learning. Wetlands. 28: 336.

[35] Long, J., Giri, C., Primavera, J., Trivedi, M., (2015). Damage and Recovery Assessment of the Philippines' mangroves Following Super Typhoon Haiyan. Marine Pollution Bulletin. 109(2): 734-743.

[36] Malik, A., Fensholt, R. &Mertz, O., (2015). Mangrove Exploitation Effects on Biodiversity and Ecosystem Services. Biodiversity and Conservation. 24(14): 3543-3557.

[37] Mangrove Action Project, (2016). Mangrove-loss. Retrieved on August 2016, from Mangrove Action Project, http://mangroveactionproject.org/mangrove-loss/

[38] Marco A. N., Eid, T. E., Zahabu & Malimbwi, R., (2015). Procedures for quantification of belowground biomass of three mangrove tree species, Tanzanian coastline from north Kenya to south of Mozambique. Wetlands Ecol Manage., 23: 749–764.

[39] Marine Knowledge Hub., (2010). Mangrove in Thailand. Retrieved on August 2016, from Aquatic Resources Research Institute. Chulalongkorn University, http://www.mkh.in.th/index.php/2010-03-22-18-04-43/2010-03-25-13-46-26

[40] Meepol, W., (2010). Carbon Sequestration of Mangrove Forests at Ranong Biosphere Reserve. Journal of Forest Management., 4(7): 33-47.

[41] Mumby, P. J., Edwards, A. J., Arias-Gonzalez, J. E., Lindeman, K. C., Blackwell, P. G., Gall, A., et. al., (2004). Mangrove Enhance the Biomass of Coral Reef Fish Communities in the Caribbean. Letters to Nature. 427: 533-536.

[42]National Statistical Office, (2007). Mangrove Forest Situation in Thailand - National Statistical Office. Retrieved on April 2012, from National Statistical Office, http://service.nso.go.th/nso/nsopublish/servGis/Report_stat/10_2.htm.

[43] Natural Resources Management and Environment Department, (2016). Assessment of biomass and carbon stock in present land use – FAO Corporate Document Repository. Retrieved on April 2012, from FAO, http://www.fao.org/docrep/007/y5490e/y5490e07.htm

[44] Office the National Economic and Social Development Board, (2015). Mangrove Forest Situation in Thailand – Marine Knowledge Hub. Retrieved on April 2012, from Knowledge Management for Marine Interest Project, http://www.mkh.in.th/index.php/2010-03-22-18-04-43/2010-03-25-13-46-26.

[45] Office of Environmental Policy and Planning, (2000). Thailand's Initial National Communication under the United Nations Framework Convention on Climate Change. Ministry of Science, Technology and Environment: Bangkok, Thailand, 100.

[46] Office of Natural Resources and Environmental Policy and Planning, (2014). Thailand's First Biennial Update Report Under the United Nations Framework Convention on

Climate Change. Office of Natural Resources and Environmental Policy and Planning: Bangkok, Thailand, 74.

[47] Ong, J. E., W. K. Gong, and C. H. Wong, (2004). Allometry and partitioning of the mangrove, Rhizophora apiculata. Forest Ecology and Management 188.1: 395-408.

[48] Ozesmi, S. L, & Bauer, M. E., (2002). Satellite Remote Sensing for Wetlands. Wetlands Ecology and Management, 10(5): 381-402.

[49] Pattanaik, C. & Prasad, N., (2011). Assessment of aquaculture impact on mangroves of Mahanadi delta (Orissa), East coast of India using remote sensing and GIS. Ocean & Coastal Management. 54, 789-795.

[50] Phan, Nguyen Hong, (1996). Mangrove destruction for shrimp rearing in Minh Hai, Viet Nam: its damage to natural resources and the environment." SEAFDEC Asian Aquaculture 18.3: 6-11.

[51] Phongsuksawat, P. (2002). Determination of tree biomass in the mangrove habital study area, changwat phangnga. Diss. Master Thesis, Kasetsart University, Bangkok, Thailand.

[52] Prasita, V. D., (2014). Determination of Shoreline Changes from 2002 to 2014 in the Mangrove Conservation Areas of Pamurbaya Using GIS. Procedia Earth and Planetary Science. 14, 25-32.

[53] Restoring Guyana's Mangrove Ecosystem, (2014). Types of Mangroves. Retrieved on August 2016, from National Agricultural Research Institute, http://www.mangrovesgy.org/home/index.php/2014-04-27-16-39-08/types-of-mangroves.

[54] Richards, Daniel R., and Daniel A. Friess, (2016). Rates and drivers of mangrove deforestation in Southeast Asia, 2000–2012. Proceedings of the National Academy of Sciences 113.2: 344-349.

[55] Poungparn, S., Komiyama, A., Intana, V., Piriyaota, S., Sangtiean, T., Tanapermpool, P., et al., (2002). A quantitative analysis on the root system of a mangrove, Xylocarpus granatum Koenig. Tropics 12.1: 35-42.

[56] Rogers, K., Boom, P. L., Branigan, S., Duke, N. C., Field, C. D., Fitzsimons, J. A, et al., (2016). The state of legislation and policy protecting Australia's mangrove and salt marsh and their ecosystem services. Marine Policy. 72, 139-155.

[57] Salam, M.A., Ross, L. & Beveridge, M.C.M., (2007) The use of GIS and remote sensing techniques to classify the Sundarbans mangrove vegetation. Journal of Agroforestry and Environment, 1 (1): 7-15.

[58] Satapathy, D.R., Krupadam, R.J., Kumar, L.P., and Wate, S. R., (2007). The application of satellite data for the quantification of mangrove loss and coastal management in the Godavari estuary, East Coast of India. Environmental Monitoring and Assessment. 134, 453.

[59] Sathirathai, Suthawan, (1998). Economic valuation of mangroves and the roles of local communities in the conservation of natural resources: case study of Surat Thani, South of Thailand. South Bridge: Economy and Environment Program for Southeast Asia.

[60] Sari, S. P. & Rosalina, D., (2016). Mapping and Monitoring of Mangrove Density Changes on tin Mining Area. Procedia Environmantal Sciences. 33: 436-442.

[61] Sheng, J., Cao, J., Han, X. & Miao, Z., (2016). Incentive modes and reducing emissions from deforestation and degradation: who can benefit most?. Journal of Ocean Production. 129: 395-409.

[62] Siriwat, 1989 and Supachai, (1999). Mangrove Restoration Project. Retrieved on April 2012, from Slide Share, http://www.slideshare.net/MaiiTy/ss-15583454.

[63] Sitoe, Almeida, A., Luís, J. C. M., and Benard S. G., (2014)"Biomass and carbon stocks of Sofala bay mangrove forests." Forests 5.8: 1967-1981.

[64] Stanley, P., (2011). Back to the Future: State of the Voluntary Markets *2011*. Forest trends, Ecosystem Marketplace.

[65] Strong, A. and Minnemeyer, S., (2015). Satellite Data Reveals State of the World's Mangrove Forests. Retrieved on August 2016, from Word Resources Institute, http://www.wri.org/blog/2015/02/satellite-data-reveals-state-world%E2%80%99s-mangrove-forests.

[66] Spalding, M., Francois, B., and Colin F., (1997). World mangrove atlas.

[67] Suwannakon, P., (1991). The situation of Mangrove Forest in Thailand (สถานการณ์ป่าเลนในประเทศไทย). Thailand. Forestry Department.

[68] Truong, S.H.; Ye, Q., and Stive, M.J.F., (2017). Estuarine mangrove squeeze in the Mekong Delta, Vietnam.

[69] The Institute for the Promotion of Teaching Science and Technology (IPST)., (2016). Plants and Animal in Mangrove forests. Retrieved on August 2016, from Field Trip,http://fieldtrip.ipst.ac.th/intro_sub_content.php?content_id=24&content_folder_id=295

[70] UNFCCC, (2016). Biennial Update Report. Retrieved on April 2016, from Submitted biennial update reports (BURs) from non-Annex I Parties, http://unfccc.int/national_reports/non-annex_i_natcom/reporting_on_climate_change/items/8722.

Php.

[71] Walters, B.B., Ronnback, P., Kovacs, J. M., Crona, B., Hussain, S. A., Basola, R., et al., (2008). Ethnobiology, socio-economics and adaptive management of mangroves: a review. Aquatic Botany. 89(2): 220-236.

[72] Wang, Y., Bonynge, G., Nugranad, J., Traber, M., Ngusaru, A., Tobey, J., et al., (2010). Remote Sensing of Mangrove Change Along the Tanzania Coast. Marine Geodesy. 26: 35-48.

[73] Weiss, C., Weiss, J., Boy, J., Iskandar, I., Mikutta, R., & Guggenberger, G., (2016). Soil organic carbon stocks in estuarine and marine mangrove ecosystems are driven by nutrient colimitation of P and N. Ecology and Evolution 6.14: 5043-5056.

[74] World Resources Institute, (1996). United Nations Environment Programme, United Nations Development Programme and the World Bank. 400.

[75] WWF, (2016). Mangrove Forest Ecosystem Services. Retrieved on August 2016, from world wildlife, https://www.worldwildlife.org/

S – 3 – 1

SCGI013

HIGH SPATIAL RESOLUTION IMAGERY WORLD VIEW 2-A FOR TSUNAMI VULNERABILITY MAPPING USING SPATIAL MULTICRITERIA EVALUATION (SMCE): CASE STUDY PANGANDARAN REGENCY

Muhammad Zayyanul Afwani[1]

zayyanul.afwani@mail.ug.ac.id
Adriati Annisa Utami[2]
Aannisau41@gmail.com
Adistina Lailia F[3]
adistina.lailia.f@mail.ugm.ac.id
Rani Rahim Suryandari[4]
rara.suryandari@mail.ugm.ac.id
Miftakhul Munir[5]
mfmunir@gmail.com
Totok Wahyu Wibowo[6]
totok.wahyu@ugm.ac.id

ABSTRACT

Pangandaran Village is a vulnerable village to tsunami disaster as happened to 2006 with tsunami-earthquakegenic type. This is caused by the meeting of oceanic plates and continental plates located in the south of Java Island . This study aims to map the degree of vulnerability to tsunami disaster by taking into account the parameters of physical , social and economic vulnerability . WorldView 2 A imagery is used to map building density , road network , and distance from shoreline to land , as a parameter of physical vulnerability . The social vulnerability parameter consists of the number of dependency on life , as well as the parameters of economic vulnerability consisting of economic area and minimum wage of work sourced from local village government . Analysis of various parameters was done by Spatial Multi-Criteria Evaluation (SMCE) method because it was expected to produce a balanced decision . The results showed that West Pangandaran Hamlet had high vulnerability value , while the other two hamlet's had medium and low vulnerability value .

Keywords: *tsunami-earthquakegenic, SMCE, Vulnerability, WorldView 2A, Pangandaran*

1. INTRODUCTION

Pangandaran is a district in West Java Province located in the south of Java Island. Geographically Pangandaran Regency is at 108 ° 30 'to 108 ° 40 "East Longitude and 7 ° 40'20" to 70 50'20' 'South Latitude. Pangandaran is directly adjacent to the Indian Ocean. Based on Regional Disaster Management Agency data, Pangandaran had experienced a tsunami disaster in July 17, 2006 with a strength of 6.8 SR which caused 659 casualties. Reflecting from the study, this research examines the vulnerability in Pangandaran. Vulnerability mapping of settlements was conducted in Pangandaran Village located in the tombolo and settlement areas in the northern part. The total area of this village is 667.87 ha. 137.87 ha utilized for settlement, and 530 ha as nature

reserve. In general, Pangandaran village is located in lowland and coastal areas with an altitude of 0-25 m above sea level about 18%, on a relatively flat coastal area with a slope of 0 - 3 degrees, an average temperature of 27 degrees Celsius.

Tsunami is a series of giant waves of ocean waves that appear due to a shift in the seabed due to earthquakes (BNPB No.8 Year 2011). Tsunami waves that ever occurred in Indonesia reached 26 meters (Istianto, et al. 2003). Tsunamis are not caused by wind. Tsunami is one type of natural disaster that occurs in coastal areas.

Vulnerability is the degree of ability of a system or part of a system to be able to react with a dangerous event (Usamah, et al, 2014). According to BAKORNAS PB (2007) in Danianti and Sariffuddin (2015) vulnerability is a condition of society that leads or causes an inability to deal with the threat of danger. Meanwhile, according to UN / ISDR (2005) in Jaswadi, dkk (2012) vulnerability as a condition determined by physical, social, economic and environmental factors or processes, which can increase the vulnerability of a community to the impact of hazards. Factors affecting vulnerability include being in hazardous locations (volcanic slopes, in the vicinity of river embankments, in unstable slopes, etc.), poverty, rural to urban migration, environmental degradation and degradation, rapid population growth, changes culture, and lack of information and awareness (UNDP / UNDRO, 1992) in Jaswadi, et al (2012).

In this research, from the condition of Pangandaran area adjacent to coastal area and vulnerability study area are in keo, hence vulnerability seen from physical aspect, social, and economy. Physical vulnerability describes the condition and number of buildings with density results in threatened areas. Social demographic vulnerability describes the characteristics of the population in the affected areas. The indicators include population size, age-old age ratio so as to obtain productive and non productive age information. Economic vulnerability describes the level of economic fragility in the face of threats, in this case using the parameters of income and distribution of work / profession.

This research uses a quantitative approach with spatial analysis techniques, such as SMCE (Spatial Multi Criteria Evaluation) in ILWIS. SMCE is one of decision making techniques by considering the importance (priority) of certain criteria (Sharifi, Mohammed and Retsios, 2004). The advantages of SMCE analysis is that it is able to integrate spatial data with non-spatial data such as statistical data and field survey data. So that new information can be generated that shows spatial distribution of phenomena.

Spatial Multi-criteria Evaluation (SMCE) is a framework, which defines the concept of evaluation as a mixture of representation, assessment and quality check connected with a given policy problem, based on a specified objective (Munda, 2008). SMCE aims to foster transparency, reflection and learning in MCA decision processes, simultaneously integrating political, socio-economic, as well as ecological, cultural and technological dimensions of the problem. For the purpose of obtaining evaluation criteria, SMCE examines stakeholders' objectives and expectations, trying to avoid as much as possible a technocratic approach.

2. OBJECTIVE

The aim of this research is :

1. Knowing the level of vulnerability to tsunami disaster through three factors: physical vulnerability, social vulnerability and economic vulnerability.
2. Determine the location of vulnerability levels that are divided into high, medium and low vulnerability.

3. METHODOLOGY

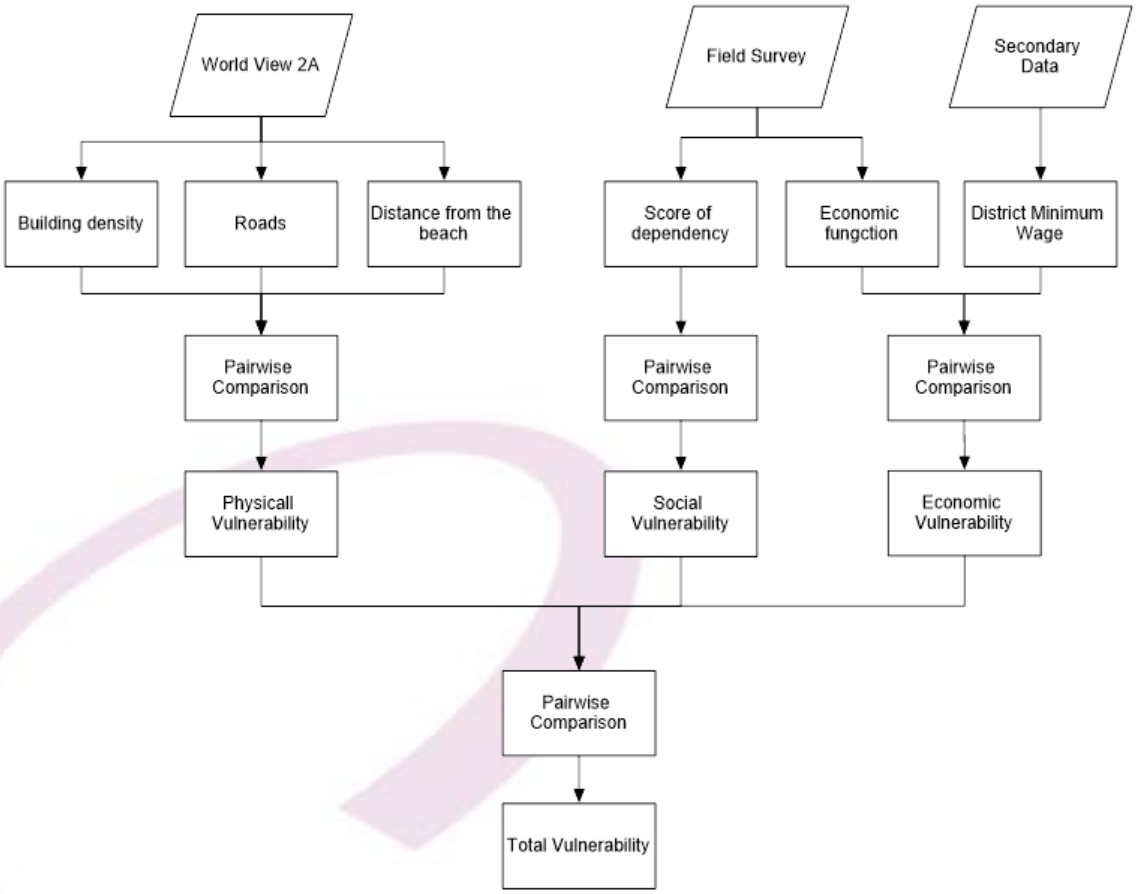

3.1 Primary Data Collection

The primary data required in this study is the density of buildings, road networks, and distance from the coast. For these needs a high resolution image that is worldview 2A. Through the image is done visual interpretation of the building blocks that are separated by the road, and digitized on the building itself. So estimates of building density are obtained using the following technical assumptions (Lo, 1986; 1995; Haack et al., 1997):

$$Building\ Density = \frac{total\ area\ of\ building}{area\ of\ block\ building}$$

The road network is the number of paths per block obtained through on-screen digitization. Then, the distance from the shoreline is struck by the buffer zone, 100m zone including high vulnerability, 300m vulnerability zone and low zone 500m vulnerability. In addition, there are population income data obtained from sampling interviews of some residents with the method of Proportionate Stratified Random Sampling, because the population in each block has members / elements that are not homogeneous and stratified proportionally.

3.2 Secondary Data Collection

Secondary data related to vulnerability parameters such as number of population based on productive and non-productive age and population density, sourced from Pangandaran Village Profile 2016.

3.3 SMCE Execution

The evaluation of the physical vulnerability parameters is used as a block of settlement settlements. Social vulnerability is based on dependency numbers that are divided into high, low and moderate dependencies. Economic vulnerability uses economic, economic and non-economic functions as well as District Minimum Wages where people who have above average earnings are considered capable, and those on average are considered incapable.

The standardization process is required to facilitate the risk assessment analysis (Abella and Westen, 2007). Standardization is done by taking into account the minimum value. If the minimum value of a data has absolute 0 then the maximum method is used, while if it has no absolute value then the interval method is used (Wibowo, 2015). The vulnerability curve used in this study is linear curve. Then the result is a vulnerability value that has a value of 0 to 1.

Determination of weights for each criterion using pairwise comparison. Pairwise Comparison is used because this method refers to each process comparing each paired variance to judge which of each variant has better performance. (Oswaldo, 2014).

4. RESULTS

The parameters of physical vulnerability are weighted according to their degree of effect on the material loss determined by the pair-wise method. The weighting for each parameter is determined by the operator. The highest weight is the density of buildings because the buildings in this area is a solid building and vertical buildings are vulnerable when exposed to tsunami waves, the weight of the building density of this physical vulnerability is 0.66. Furthermore, the distance from the beach, which is bounded by

zone buffers 100 meters, 300 meters and 500 meters. The weight of the distance from this beach is 0.19. the last parameter on the physical vulnerability of the road network, the path has the lowest weight because the road is considered the most recently affected with a value of 0.16.

4.1 Phisically Vulnerability Map

The result of the mapping of physical vulnerability, indicating that West Pangandaran hamlet is generally categorized as medium vulnerability. East Pangandaran hamlet there is a category of high to low vulnerability because in the village of East Pangandaran rare building. Parapat hamlet belongs to the lowest vulnerability category among the two other hamlets because there is still a lot of vacant land and its distance is relatively far from the beach.

Social vulnerability is processed into dependency ratio. The higher the dependency ratio indicates the higher burden that the productive age population has to pay for the lives of unproductive and unproductive populations, meaning that the higher the dependency ratio the more vulnerable to the tsunami disaster. High population density leads to higher vulnerability because it can cause a lot of casualties in the event of a disaster. The weight for this social vulnerability parameter has a value of 1.00 because it is a single parameter.

The results of social vulnerability mapping indicate that the Western Pangandaran hamlet includes high vulnerability, followed by the Eastern Pangandaran hamlet, and the lowest vulnerability of Parapat hamlet. This is caused by high population density in West Pangandaran hamlet to the lowest in Parapat village. In addition, dependency ratio in West Pangandaran hamlet is highest, Pangandaran hamlet is second, and last is Parapat hamlet. The high dependency ratio in Western Pangandaran hamlet is due to

the large number of non productive age population compared to the productive age population which can be affected by the birth rate.

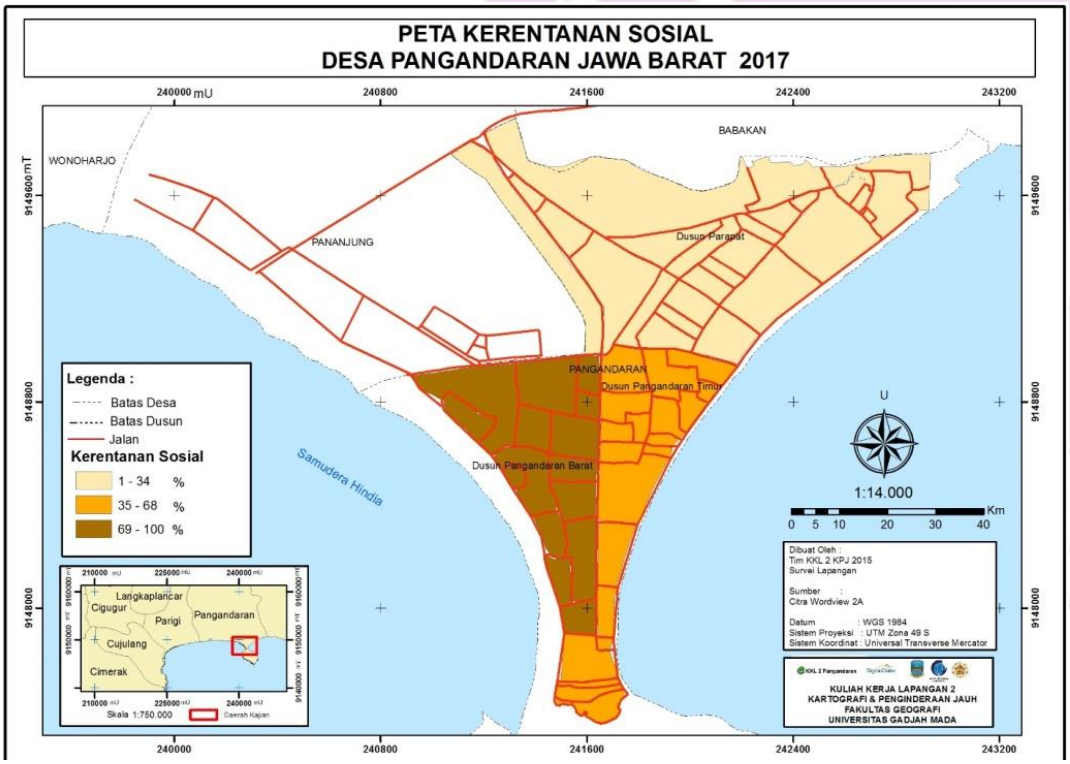

4.2 Social Vulnerability Map

Economic vulnerability is linked to building blocks with economic functions as well as people's incomes. Economic functions such as hotel blocks and shopping blocks, in the event of a tsunami, have a direct impact on the economic activities of the community as it may lead to the temporary disruption of people's economic activity. The weight for this economic function is 0.25. The economic vulnerability parameter associated with District Minimum Wage is a benchmark for the welfare of the local people to meet their daily needs. People who are earning less than MSE are vulnerable in the event of a tsunami, as the recovery of their economies takes a long time and is generally given funding from other parties, while people living on MSEs can recover their economies faster. The weights for the Kabupaten Minimum Wage are 0.75 higher than the parameters of the economic function area.

The result of mapping of economic vulnerability shows that West Pangandaran Hamlet belongs to high vulnerability category because seen from its economic function block, more than two other hamlets. In addition to the economic function block, income also affects economic vulnerability, the income of the people in the West Pangandaran hamlet are mostly small traders with income below Regency Minimum Wage, whereas in Parapat Hamlet is largely a building block with economic function, the vulnerability of the economy and the area of Parapat hamlet is still in the form of open land.

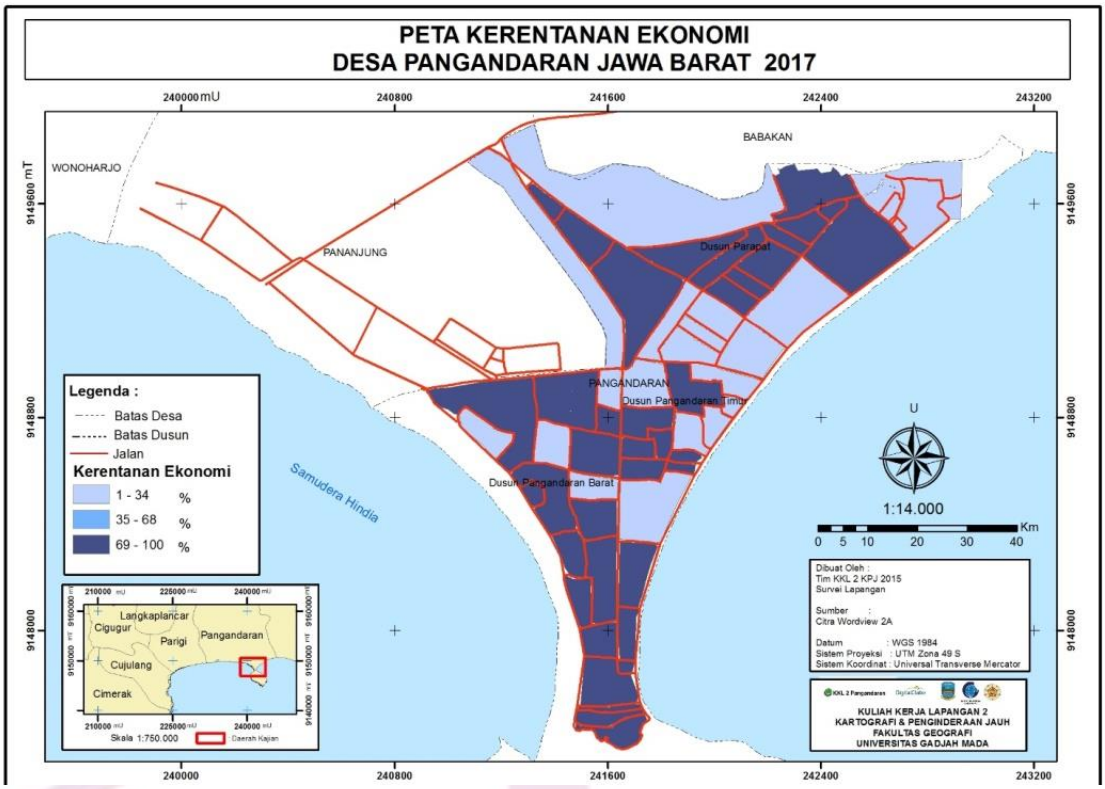

4.3 Economic Vulnerability Map

The three parameters of physical vulnerability, economic vulnerability and social vulnerability are then re-weighted using pairwise comparison. Pair-wise comparison is the basic concept of AHP (Analytical Hierarchical Process) that is by comparing criteria with one criterion to another to obtain results in the form of problem solving. AHP itself is one of the multi-criteria decision-making methods developed by Prof. Thomas L. Saaty in the 1970s (Teknomo, 2010). The pair-wise comparison method in this vulnerability mapping is part of the spatial multi-criteria evaluation which is a commonly dispensed AHP method of ILWIS software (Shomat et al., 2017). The result of weighting of these three parameters is shown in Figure 3.1.

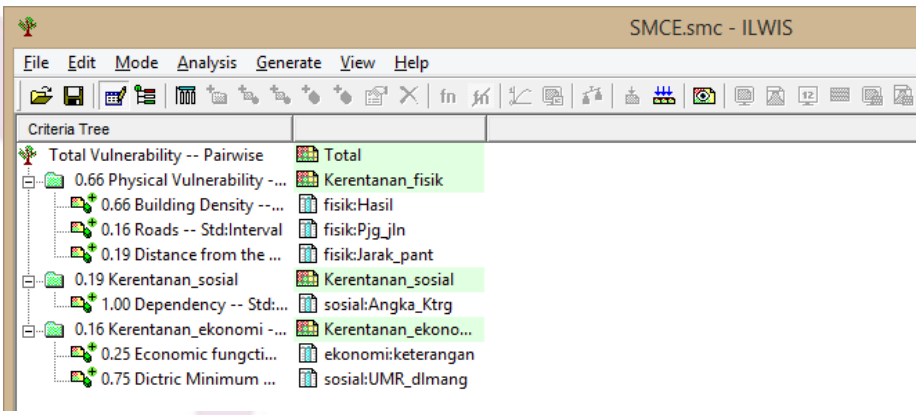

4.4 Criteria Tree

These physical, social, and economic vulnerability mappings are combined into a total vulnerability. The results show that the western Pangandaran hamlet belongs to the highest vulnerability category, second order is East Pangandaran Hamlet, and the

lowest vulnerability is Parapat Hamlet. Seen from the building blocks, West Pangandaran hamlet mostly have building blocks with high vulnerability category, East Pangandaran hamlet mostly have building blocks with medium vulnerability category, and Parapat hamlet mostly have building blocks with low vulnerability category. This is because West Pangandaran hamlet has high physical, social and economic vulnerability, so that West Pangandaran is the most vulnerable category for tsunami disaster, and Parapat hamlet is a hamlet with low vulnerability category, because the three aspects of its vulnerability indicate low vulnerability.

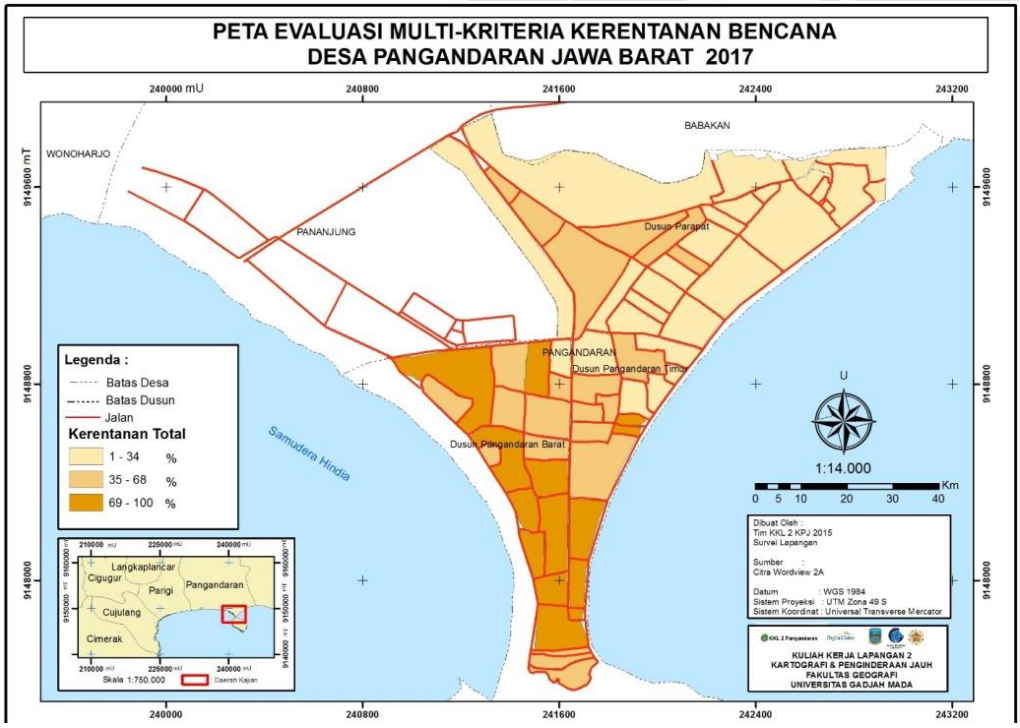

4.5 Disaster Vulnerability Map

This vulnerability mapping can be used as a first step in tsunami disaster mitigation in Pangandaran Village to reduce physical, social and economic losses, where disaster mitigation in the most vulnerable hamlet of West Pangandaran Hamlet is prioritized by not neglecting the other two hamlets, especially East Pangandaran hamlet is equally located in the keyo.

The risk of losses due to the potential tsunami disaster in Pangandaran Village located in this keo area can be reduced by mitigating the tsunami disaster to a safer evacuation route in accordance with existing mitigation measures, which indicate that the mitigation path in the event of a tsunami in the village Pangandaran is heading to the Nature Reserve area in the south. This is because the area of the Nature Reserve is an area that has a relief higher than the area which has a relief bano flat on the west side, east and north so that the area of Nature Reserve is a relatively safer place when compared with the surrounding area.

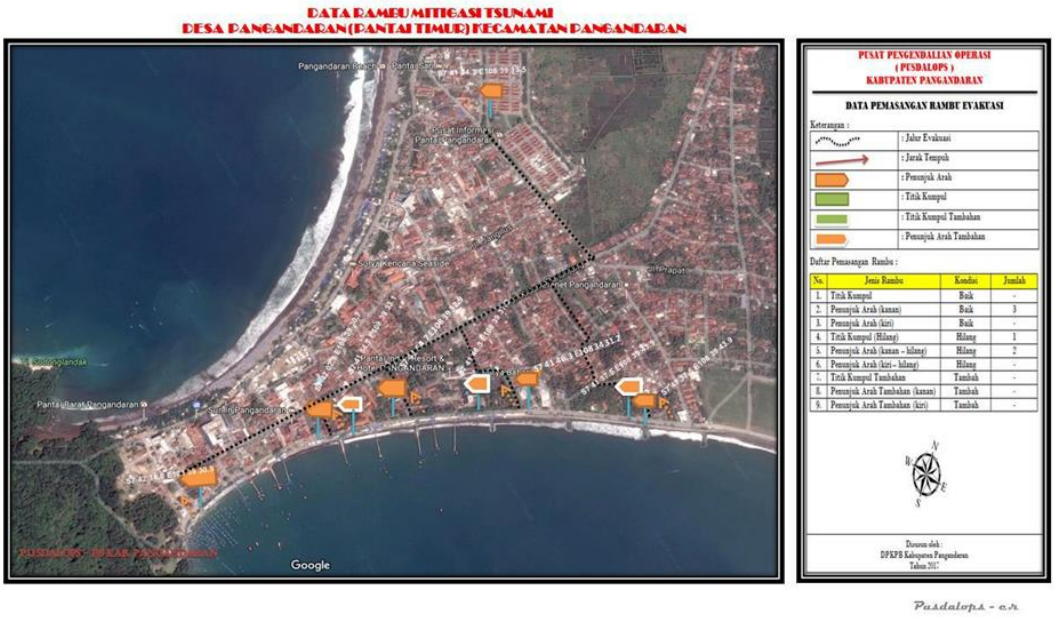

5.5 Disaster Mitigation Sign
Source: Fire and Disaster Prevention Agency of Pangandaran Regency

5. CONCLUSION AND DISCUSSION

1. The direct impact is on the physical parameters so that the physical vulnerability has the highest vulnerability value that is 0.66. While social vulnerability has a value of 0.19, followed by economic vulnerability 0.16. But this result is operator assumption to condition in field.
2. Pangandaran Village consists of 3 hamlets, that is West Pangandaran hamlet, east pangandaran hamlet, and prapat hamlet. Based on the physical, social, and economic parameters, west pangandaran hamlet is the highest vulnerability category because its parameters show high vulnerability value. east pangandaran hamlet belongs to medium vulnerability category, and Parapat hamlet belongs to low vulnerability category.

6. RECOMMENDATION

This work was suported by Digital Globe that provide high resolution imagery World View 2-A dgOrderNo 056633530. dgOrderItemNo = 056633530010.

REFERENCES

[1] Badan Nasional Penanggulangan Bencana. (2011). Indeks Rawan Bencana Indonesia. BNPB

[2] Bakornas Penanggulangan Bencana. 2007. Pengenalan Karakteristik Bencana dan Upaya Mitigasinya di Indonesia. Direktorat Mitigasi Lahar BAKORNAS PB: Jakarta

[3] Danianti, Rizsa Putrid an Sriffuddin. 2015. Tingkat Kerentanan Masyarakat Terhadap Bencana Banjir di Perumnas Tlogosari, Kota Semarang. *Jurnal Pengembangan Kota* (2015) Volume 3 No. 2 (90–99).

[4] Jaswadi, R. Rijanta, dan Pramono Hadi. 2012. "Tingkat Kerentanan dan Kapasitas Masyarakat dalam Menghadapi Risiko Banjir di Kecamatan Pasarkliwon Kota Surakarta". MGI Vol. 26, No. 1, Maret 2012 (119 - 148).

[5] Istiyanto, Dinar Catur. Sutikno, Pramono, Hadi (Ed.) 2003. Panduan Mitigasi Bencana Alam Tsunami. Yogyakarta: Badan Koordinasi Survey dan Pemetaan Nasional, Projek Penelitian dan Pengembangan Teknologi Survei dan Pemetaan dan Pusat Studi Bencana Universitas Gadjah mada.

[6] Teknomo, Kardi. 2010. Analytic Hierarchy Process (AHP) Tutorial. Revoledu

[7] Munda, G. (1995).Multicriteria evaluation in a fuzzy environment. Theory and applications in ecological economics, Physica-Verlag, Heidelberg.

[8] Munda, G. (2008). Social Multi-Criteria Evaluation for a Sustainable Economy, Berlin Heidelberg: Springer-Verlag

[9] Oswaldo, Mohammad Ibrahim; Ahmad Saikhu; Bilqis Amaliah. 2014. Implementasi Metode Piarwise Comparison pada Uji Kinerja Varian Metode Kecerdasan Buatan pada Penyelesaian Masalah TSP. Surabaya : JURNAL TEKNIK POMITS Vol. 2, No. 1, (2014) ISSN: 2337-3539

[10] Safiri, Mohammed and Restsios. 2004. Site Selection for wates disposal through spatial multiple criteria decision analysis. Enschede, Netherlands : Jurnal of Telecommunication and Information Technology.

[11] Shomat, Fazlurohman, et al. 2017. *ILWIS : Spatial Multi-Criteria Evaluation : Laboratory of Remote Sensing of Environment and Geographic Information System*. RoseGIS Laboratory.

[12] UNESCO-IOC, 2006, *Tsunami Glossary*, IOC Information Document No. 1221, Paris, UNESCO. Westen, C. v., Kingma, N., dan Montoya, L., 2009, Multi Hazard Risk Assessment, *Educational Guide Book Session 4: Elements at Risk*, edited by Cees van Westen, ITC, Enschede, The Netherlands.

[13] Usamah, M., Handmer, J., Mitchell, D., & Ahmed, I. (2014). "Can The Vulnerable Be Resilient? Coexistence Of Vulnerability And Disaster Resilience: Informal Settlements In The Philippines". International Journal of Disaster Risk Reduction, 10.

[14] Wibowo, Wahyu Totok. 2015. Evaluasi Multi-Kriteria Keruangan Untuk Pemetaan Kerentanan Terhadap Bahaya Tsunami di Pesisir Kabupaten Bantul. Solo : Prosiding Seminar Nasional Geografi UMS 2015

SPATIAL FACTORS AFFECTING THE LANDSLIDE VIA LOGISTIC REGRESSION MODEL IN NANGLAE NAI VILLAGE, CHIANG RAI PROVINCE

Piyanut Moonkhum[1]
Faculty of Science and Technology, Chiang Rai Rajabhat University, Chiang Rai province, Thailand, piyanut_293@hotmail.com
Pisit Sommoy[2]
Faculty of Science and Technology, Chiang Rai Rajabhat University, Chiang Rai province, Thailand, Pisit_ps@hotmail.com
Suruswadee Nanglae[3]
Faculty of Science and Technology, Chiang Rai Rajabhat University, Chiang Rai province, Thailand, SNanglae@gmail.com
krittawit Suk-ueng[4]
Faculty of Science and Technology, Chiang Rai Rajabhat University, Chiang Rai province, Thailand, nsukung@gmail.com

ABSTRACT

Landslide is a natural phenomenon caused by downslope movement of soil and rocks along the hillsides or anthropogenic activities, e.g. deforestation and agricultural practices in steep areas. Landslide risk mapping defined by the application of geographic information system and logistic regression model require the interaction between landslide areas and spatial factors. The study area is located at Nanglae Nai village, Mueang district, Chiang Rai province. The results of this study shown that the landslide areas appeared in 4 areas, including Doi Dang, Tad Hang waterfall, Baan Likai and Pha Lad Roy Wao. Based on the analysis of logistic regression model, it was found that the elevation (449-709 meters) and aspect (North and Northeast) were major spatial factors of landslide risk because they were possessed a high risk for landslides (> 80%) and the accuracy of the model was 71.8%.

Keywords: Landslide, Geographic information system, Logistic regression model, Chiang Rai province

1. INTRODUCTION

Landslide is a natural phenomenon caused by the movement of soil and rocks along the hillsides. This is due to natural disasters such as earthquakes, storms and heavy rain. Landslides, that caused deaths, injuries and missing person, occur throughout the world [1, 2], and economic losses of more than 0.9 billion USD. Therefore, the risk of landslide should be taken into consideration to reduce the damage [3, 4].

Environmental factors that cause landslides, such as rainfall, altitude, slope and aspect, etc., especially, the spatial factors, including slope (20% importance of landslide causal factors) and elevation (16% importance of landslide causal factors) involved with aspect

[5]. The risk of landslides is mostly identified by using a logistic regression model and environmental factors for landslide risk prediction [6].

Nanglae Nai village, Mueang district, Chiang Rai province, is selected as study area because it is an important village located along Nanglae Nai stream as well as upstream areas and famous tourist attraction in Nanglae District, such as Nanglae waterfall, Pha Lad Roi Wua and Doi Dang. However, forest areas have been destroyed by unsuitable highland agricultural landuse, such as paddy fields, lychee and pineapple farms [7] resulting in landslide in the area. The aim of this research was to predict landslide risk by using logistic regression model and spatial factors in Nanglae Nai village, Chiang Rai province.

2. OBJECTIVE

1) To predict landslide risk by using logistic regression model and spatial factors in Nanglae Nai village, Chiang Rai province.

3. METHODOLOGY

3.1. Study area

Study area was Nanglae Nai village, Mueang district, Chiang Rai province located from 2210000 to 2220000 degrees north latitude and 580000 to 590000 degrees east longitude (Fig. 1).

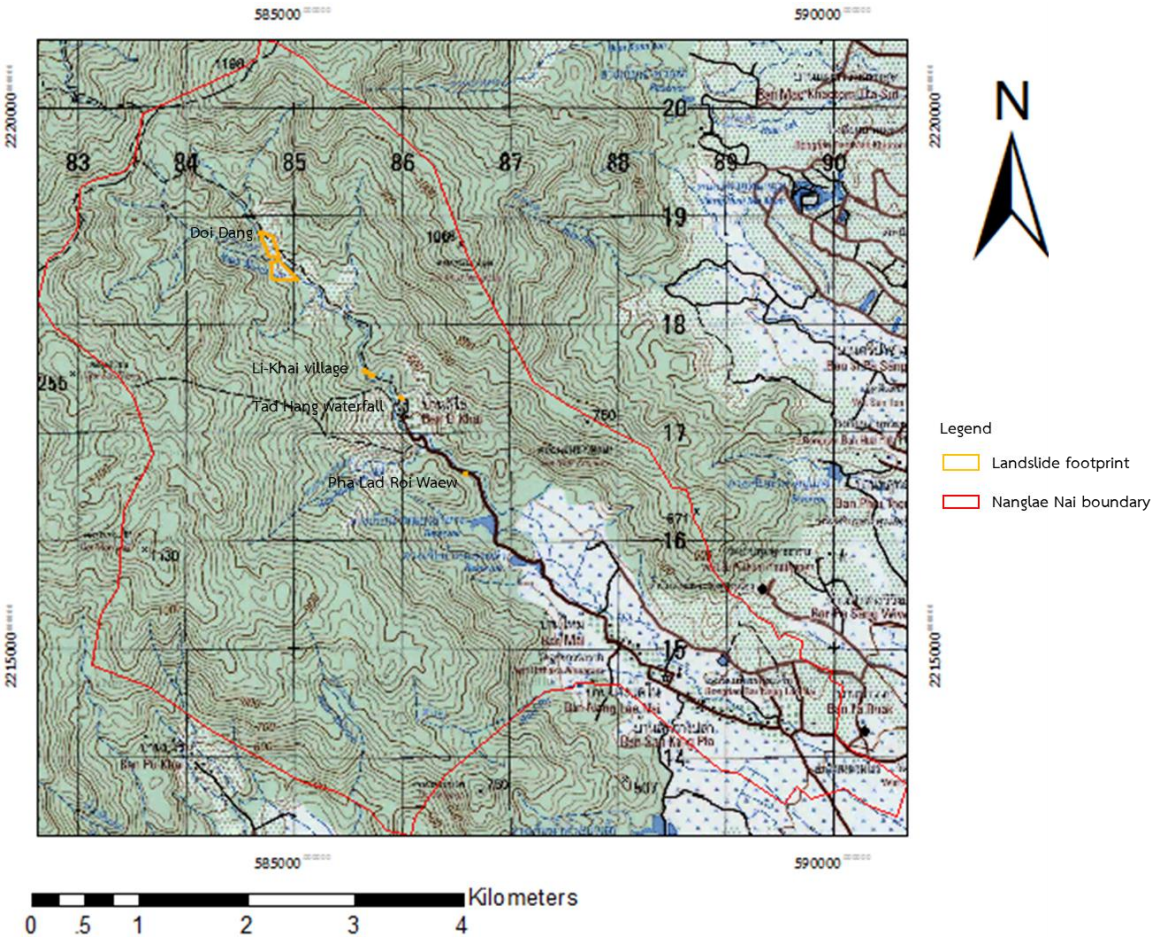

Figure 1 Study area and landslide footprint at Nanglae Nai village.

3.2. Data collection

1) Field survey

In this study, landslide footprint were conducted using walk-through survey along the stream, Li-Khai village to Doi Dang. Landslide footprint areas are also recorded x and y coordinates.

2) Logistic regression model

Landslide footprint areas are imported to determine areas of landslide occurrences. With the use of the statistical program R, points are randomly selected in the study area. Random points were separated into 2 groups. The first group was the points (each point being equal to 1) where landslide occurred. The second group was the points (each point being equal to 0) where landslide never occurred. Spatial factors, including DEM, slope, and aspect were used for the model. After random points establishment, dataset was applied with the use of logistic regression model and the number of dataset were divided into 2 groups. The first group was used for modelling in logistic regression model processing. The second group was used for validation of the model. Spatial factors were selected by stepwise method. As a result the best model was presented the lowest AIC (Akaike's Information Criterion) and the AUC (Area Under the ROC Curve) was used to verify the accuracy of the model.

4. RESULTS

4.1. Landslide footprint in Nanglae Nai village

There were 4 areas of landslide footprints, including Pha Lad Roy Wua, Li-Khai village, Tad Hang and Doi Dang (Fig. 1). Fifty-one points were randomly selected in areas where landslides occurred. As a result the average elevation of the landslides was 668.25 meters above mean sea level and aspect was 114.90 degrees (Southeast direction).

4.2. Landslide risk in Nanglae Nai village

With the use of logistic regression model with stepwise, P-values of DEM and aspect were statistically significant at the 0.10 and 0.05 levels, respectively (Table 1).

Table 1 Logistic regression model analysis

Variables	Coefficients	Std. Error	Z value	P-Value
(Intercept)	-16.91	9.890×10^{2}	-0.017	0.9864
DEM	-0.0016	8.411×10^{4}	-1.926	0.0541**
Slope	16.31	9.890×10^{2}	0.016	0.9868
Aspect	-0.0051	2.205×10^{-3}	-2.351	0.0187*
Pseudo-R^2 = 7.8 , AIC = 274.51				

*statistically significant at 0.05
**statistically significant at 0.10

The AIC value was 274.51. Pseudo-R^2 was 0.078 resulting in prediction model of 7.8%. Prediction equation is shown in the equations below, Equation 1.

$$Z = -16.91 - 0.0016DEM + 16.31Slope - 0.0051Aspect \quad \text{.....(1)}$$

A map of the risk of landslides in Nanglae Nai village (Fig. 2) is presented probability value from 0 to 0.22. The probability value was 0 (gray area), that there was no chance of landslide occurrence. The probability was 0.22 (green area), that there was high risk for landslide occurrence. An increased slope angle will increase the chance that a landslide will occur. Aspect direction that directly influences landslide occurrence in this area, was north (more than 337.5 to 22.5 degrees) and northeast (more than 22.5 to 67.5 degrees). The accuracy of the predictive model was 71.8% (AUC = 0.7179487).

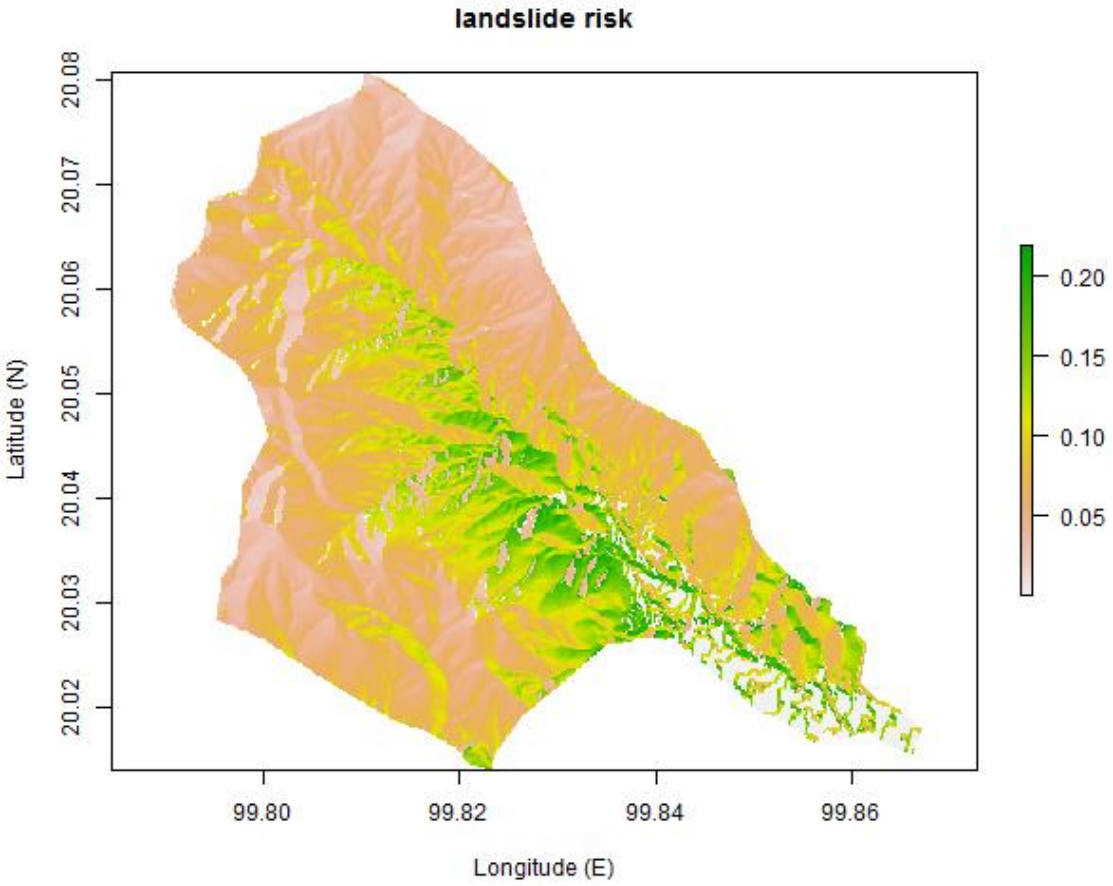

Figure 2 The risk map of landslides in Nanglae Nai village.

5. CONCLUSION AND DISCUSSION

5.1. Discussion

5.1.1. Landslide prediction by logistics regression model

Spatial factors related to landslides in Nanglae Nai were slope of more than 30 degrees, aspect directions, north (more than 337.5 to 22.5 degrees) and northeast (more than 22.5 to 67.5 degrees) and DEM. Although DEM was negative value, DEM and slope in the model were likely to occur landslide in the area [6]. The model was able to predict the risk of landslide in Nanglae Nai village about 7.8% resulting in insufficient spatial factors for prediction. The accuracy of the model was, however, 71.8% that is considered acceptable [5].

5.1.2. Preventing the landslide risk in Nanglae Nai village

People avoid living and farming in high risk zones with slope of more than 30 degrees and aspect directions (north and northeast). If they need for planting or cultivation, they must construct rice terraces for reducing the rate of soil erosion. Forests should be preserved for providing reinforcement and strengthening of soils. Vetiver grass (*Vetiveria Zizanioides* Nash) should be planted on steep slopes to prevent soil erosion [8, 9].

5.2. Conclusion

There were 4 areas of landslide footprints, including Pha Lad Roy Wua, Li-Khai village, Tad Hang and Doi Dang. Two important spatial factors were DEM and aspect. Aspect, that directly effects landslide occurrence in Nanglae Nai village, was north (more than 337.5 to 22.5 degrees) and northeast (more than 22.5 to 67.5 degrees). The accuracy of the predictive model was 71.8%.

6. RECOMMENDATION

The level of landslide risk should be studied to know the level of landslide risk of the area.

REFERENCES

[1] Highland, L.M. and P. Bobrowsky, The landslide handbook—A guide to understanding landslides, U.S. Geological Survey Circular 1325, Virginia, 2008.

[2] P. Salvati, O. Petrucci, M. Rossi, C. Bianchi, A.A. Pasqua, and F. Guzzetti, “Gender, age and circumstances analysis of flood and landslide fatalities in Italy,” Science of The Total Environment, 610-611, pp.876-879, 2018.

[3] N. Intarawichian, and S. Dasananda, “Analytical hierarchy process for landslide susceptibility mapping in lower Mae Chaem watershed, northern Thailand,” Suranaree Journal of Science and Technology, 17, pp. 1-16, 2010.

[4] Boongthong, B., An analysis of areas susceptible to landslide hazard in Changwat Chanthaburi, Master's thesis, Department of Geography, Faculty of Education, Ramkhamhaeng University, 2001. (in Thai)

[5] F. Mancini, C. Ceppi, and G. Ritrovato, "GIS and statistical analysis for landslide susceptibility mapping in the Daunia area, Italy." Natural hazards and earth system sciences, 10, pp. 1851-1864, 2010.

[6] Intarat. T., Assessment on landslide susceptibility in the Kitchakut range, Chanthaburi, Master's thesis, Department of Geographical Technology, Graduate School, Burapha University, 2007. (in Thai)

[7] Norkaew, S., (2016, July, 6), Nanglae Nai village's headman, Interview, 2016.

[8] Chalermpong, P., Guidelines for Community Management in Landslide Risk Areas of East - Coast Gulf Watershed, Master's thesis, Department of Geography, Graduate School, Kasetsart University, 2001. (in Thai)

[9] T. Jirathanathaworn, and R. Sarutirattanaworakun, "Effects of landslide disaster and problem resolution by limit equilibrium analysis using KU slope program: Maetaeng-to-Maehongsorn transmission project case study," Engineering Journal Kasetsart, 24(78), pp. 81-92, 2011. (in Thai)

IMPACTS OF LAND USE AND LAND COVER CHANGE ON RUNOFF AND SOIL EROSION IN SMALL WATERSHED

Komsan Kiriwongwattana
Spatial Research Unit, Geography Department, Faculty of Arts, Silpakorn University
Ratchamakkha Nai, Phra Pathom Chedi, Nakhonpathom, Thailand. 73000,
kiriwongwattana_k@su.ac.th

ABSTRACT

This study investigates the effects of land use and land cover change (LULCC) between 1999, 2009 and 2015 of Huai Ban Bo sub-watershed, Suanphueng district, Ratchaburi province, Thailand on runoff and sediment load for 1999, 2009 and 2015 years. A base map produced from Landsat 5 TM images and field visit/interview had been carried out for land use and land cover analysis. NRCS methods was used to evaluate the effect of LULCC on rainfall–runoff and RMMF model was used to evaluate the effect of LULCC on soil erosion rate relationships.

The result of the analysis indicated that mixed deciduous forest change from 1999 to 2015 was decreased from 69 % to 64 %. In contrast, agricultural was decreased by 2% in 2015 while built-up land change from 1999 to 2015 was increased from 7% to 12% and shrubs was increased by 1% in 2015. From the surface runoff estimation found that, in 1999 there was 243.2 mm out of total rainfall 1297.60 mm (18.74 %). In 2009, the total rainfall was 58 mm. and there was no runoff. In 2015, runoff was 164.77 mm out of rainfall total 560 mm (29.42%). The rates of soil erosion in 1999, 2009 and 2015 were 1.15, 0.002 and 0.65 kg/m^2 respectively. In the event of three years average rainfall (780.80 mm), the amount of surface runoff in 1999, 2009 and 2015 were found at 270.75, 289.77 and 330.82 mm (18%, 19% and 22%), whereas the soil erosion rate were 0.38, 0.68 and 0.98 kg/m^2 respectively. By compared the amount of surface runoff with land use and land cover found that, increased of built-up land and shrubs, increased the surface runoff (r = 0.957 and 0.948). Whereas there was highly positive correlation between built-up land and the shrubs and soil erosion rate. (r = 0.94 and 0.93) indicated that the transformation of forest areas to built-up land increased the rate of soil erosion.

Keywords: Land use/cover, Runoff, Soil erosion, Small watershed

1. INTRODUCTION

Land use and land cover (LULC) are one of the most important factors affecting runoff and soil erosion process. Many researchers found that decrease of plants cover are correlate with increase of runoff and soil loss [1] [2] [3]. Regarding to main objectives of watershed management are optimum use of land and resources, over use of that land and resources can cause runoff and soil loss increase rapidly [4] [5]. In the past decade human were modified land and resources to serves themselves. Thus, the effect of LULC on runoff and soil erosion in a watershed scale needs to be assessed. Conventional methods to assess effect of LULC on runoff and soil loss are costly, time consuming, and difficulty of inaccessible terrain in many of the watersheds [6]. Thus, the use of Geo-Informatics, to generate land based data for conserving soil and water resources in the watershed are very useful. In this study, Geo-Informatics were used to classified LULC type of 1999, 2009 and 2015 years from Landsat 5 TM images. Natural Resources Conservation service Curve Number (NRCS-CN) method [7] and Revised Morgan, Morgan and Finney (RMMF) model (Morgan 2001) were used to assess runoff and soil erosion rate of the study area.

2. OBJECTIVE

The main objectives of this study are (i) to study land use and land cover change (LULCC) and (ii) to study effect of LULCC on runoff and annual soil erosion rates in Huai Ban Bo sub-watershed, Suanphueng district, Ratchaburi province, Thailand.

3. METHODOLOGY

3.1 Materials

In the present study, LULC map of 1999, 2009 and 2015 years were derived from Landsat 5 TM satellite images. The hydrological soil group (HSG) was produced from soil group map of Land development department [8]. The slope data was classified from digital elevation model of Aster G-Dem 30x30 data. Rainfall data of Thai Meteorological Department [9] at Suan Phueng station lies within watershed was used.

3.2 Runoff estimation

Natural Resource Conservation Service Curve Number (NRCS-CN) method was used for runoff estimation as it simple and few requires prarameters [10] [11] [6].

$$F/S = OF / (P-I) \quad (1)$$

Where

F is actual retention (mm)
S is initial abstraction and maximum losses after overland flow begins (mm)
OF is the overland flow in a rainfall event or actual direct runoff (mm)
P is total rainfall (mm); and I initial abstraction (mm)
I is initial abstraction (mm)

Overland flow (*OF*) was computed by the following equation

$$OF = (P-0.2S)^2/(P+0.8S) \qquad (P>0.2S) \qquad (2)$$

Since overland flow (*OF*) will occur when *P* greater than 0.2*S*, the following equation was applied when this occurs. The parameter *S* was related to *CN* which is a dimensionless runoff index determined based on HSG, land use, precipitation and antecedent moisture condition (AMC)

$$S = (25400/CN)-254 \text{ (mm)} \qquad (3)$$

3.3 Soil erosion estimation

A revised Morgan, Morgan and Finney (RMMF) model was used to estimate the annual soil loss by sheet and rill erosion. This model is semi-physically based and estimates the rates of soil detachment by splash and runoff and compares the total rate of detachment with the runoff transport capacity to calculate the values of soil loss [12].

An estimation of rainfall energy and soil particle detachment by raindrop impact (*F*) can be done by using equation (4) to (10)

$$ER = R^*A \qquad (4)$$
$$LD = ER^*CC \qquad (5)$$
$$DT = ER-LD \qquad (6)$$
$$KE(DT) = DT^*(29.8-(127.5/I)) \qquad (7)$$
$$KE(LD) = (5.8^*PH0.5)-5.87 \qquad (8)$$
$$KE = KE(DT) + KE(LD) \qquad (9)$$
$$F = K^*KE^*10\text{-}3 \qquad (10)$$

Where

A	is rainfall intercepted by the vegetation or crop cover (between 0 and 1)
CC	is percentage canopy cover (between 0 and 1)
DT	is direct throughfall
ER	is effective rainfall (J/m^2)
F	is soil particle detachment by raindrop impact (kg/m^2)
I	is intensity of erosive rain (mm/h)
K	is soil detachability index (g/J)
KE	is total energy of the effective rainfall (J/m^2)
LD	is leaf drainage
R	is annual or mean annual rainfall (mm)

The annual runoff and the detachment of soil particles by runoff was estimated using equation (11) to (14)

$$Q = R^*exp(-Rc/Ro) \qquad (11)$$
$$Rc = 1000^*MS^*BD^*EHD^*Et/Eo \qquad (12)$$
$$H = Z^*Q1.5^*sinS(1-GC)^*10^{-3} \qquad (13)$$
$$Z = 1/(0.5^*COH) \qquad (14)$$

Where

BD	is bulk density of the top soil layer (Mg/m^3)
COH	is cohesion of the surface soil (kPa)
EHD	is effective hydrological depth of soil (m)
Et/E_0	is ratio of actual (E_t) to potential (E_0) evapotranspiration
H	is the detachment by runoff (kg/m^2)
MS	is soil moisture content at field capacity
Q	is annual runoff (mm)
R_c	is soil moisture storage capacity (mm)
R_o	is mean rain per rain day (mm)
S	is slop angle (°)
Z	is soil resistance to erosion

The method for estimating soil particles transport capacity by runoff was performed by equation (15)

$$TC = C*Q^2*sinS*10^{-3} \quad (15)$$

Where

C	is the crop or plant cover factor
Q	is annual runoff (mm)
TC	is transport capacity of the runoff (g/m^2)
S	is slope angle (°)

The estimates of soil particle detachment by raindrop impact and by runoff are added together to give a total annual detachment rate. This is then compared with the annual transport capacity and the lesser of the two values is the annual erosion rate [13] [14].

3.4 Land use and land cover classification

The cloud free Landsat 5 TM images acquired in January and February of years 1999, 2009 and 2015 were download from USGS website [15]. DN to top of atmosphere (TOA) reflectance conversion method was applied to all the images to obtained actual reflectance of the objects on the earth surface. The Iterative self-organizing data analysis technique (Iso Data) was used to classify LULC of the study area. The accuracy assessment at more than 70% was done to check the quality of LULC classification map.

4. RESULTS

4.1 Land use and land cover change

From the LULC map of 1999, 2009 and 2015 classified from Landsat images, the watershed has various type of land use and land cover. The results from Table 1 shown that there were a changes of LULC in the watershed from 1999 to 2015.

Table 1 Land use and land cover in 1999, 2009 and 2015

Categories	1999		2009		2015	
	Km^2	%	Km^2	%	Km^2	%
Dray Evergreen Forest	17355.94	2.54	17278.31	21.44	17279.44	21.45
Mixed Deciduous Forest	55819.69	69.28	53016.75	65.80	51176.81	63.52
Agricultural	1151.44	1.43	1054.69	1.31	1161.00	1.44
Built up Land	5693.06	7.07	8086.50	10.04	9594.56	11.91
Water	209.25	0.26	340.88	0.42	313.31	0.39
Shrubs	343.69	0.43	795.94	0.99	1047.94	1.30
Total	**80573.07**	**100.00**	**80573.06**	**100.00**	**80573.06**	**100.00**

The actual percentages covered by different land use and land cover types in the years 1999, 2009 and 2015 were presented in figure 1. The results show that mixed deciduous forest were decreased from 69% in 1999 to 64% in 2015. The Built up Land were rapidly increased from 7% in 1999 to 12% in 2015. Agricultural were slightly decreased from 2% in 1999 to 1% in 2015 and the Shrubs were slightly increased from 0.43% in 1999 to 1.30% in 2015.

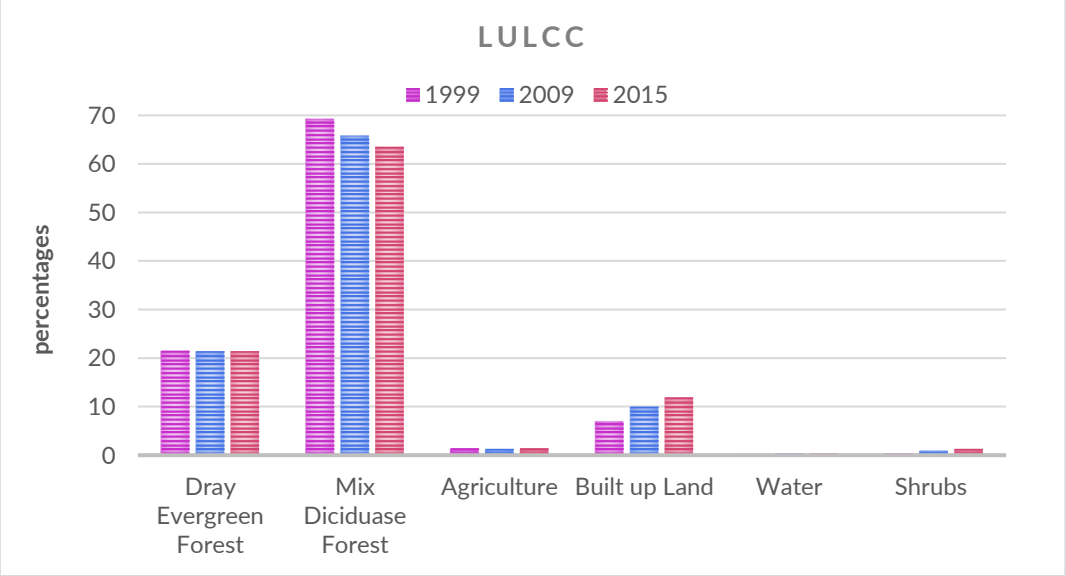

Figure 1. Percentage of LULC types for 1999, 2009 and 2015

4.2 Effect of LULC changes on runoff and soil erosion

The analysis of annual runoff in the watershed (Figure 2) indicated that in 1999 there was 243.2 mm out of total rainfall 1297.60 mm (18.74 %). In 2009, the total rainfall was 58 mm and there was no runoff. In 2015, runoff was 164.77 mm out of rainfall total 560 mm (29.42%).

The rates of soil erosion (Figure 3) in 1999, 2009 and 2015 were 1.15, 0.002 and 0.65 kg/m^2 respectively. In the event of three years average rainfall (780.80 mm), the amount of surface runoff in 1999, 2009, 2015 were found at 270.75, 289.77 and 330.82 mm (18%, 19% and 22%) whereas the soil erosion rate were 0.38, 0.68 and 0.98 kg/m^2 respectively.

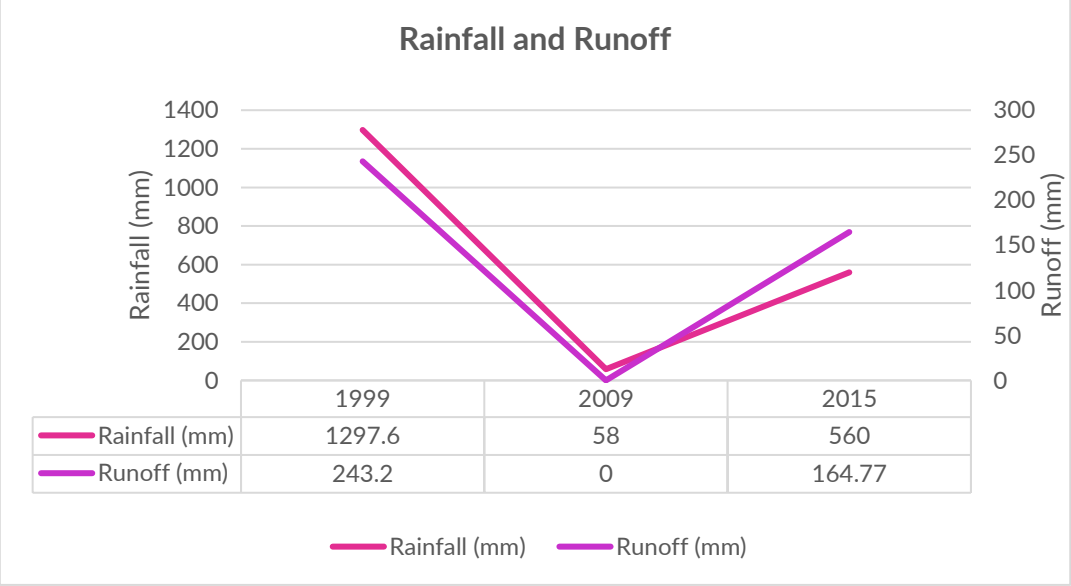

Figure 2 Rainfall and runoff of the watershed

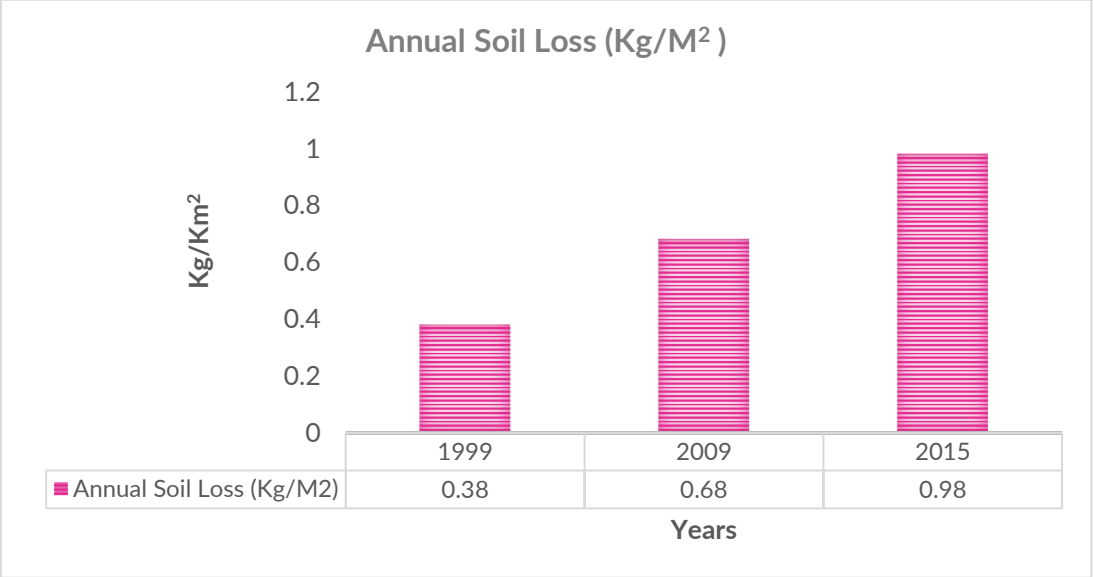

Figure 3 Rainfall and runoff of the watershed

5. CONCLUSION

The result of the analysis indicated that mixed deciduous forest change from 1999 to 2015 was decreased from 69 % to 64 %. In contrast, agricultural was decreased by 2% in 2015 while built-up land change from 1999 to 2015 was increased from 7% to 12% and shrubs was increased by 1% in 2015. From the surface runoff estimation found that, in 1999 there was 243.2 mm out of total rainfall 1297.60 mm (18.74 %). In 2009, the total rainfall was 58 mm. and there was no runoff. In 2015, runoff was 164.77 mm out of rainfall total 560 mm (29.42%). The rates of soil erosion in 1999, 2009 and 2015 were 1.15, 0.002 and 0.65 kg/m2 respectively. In the event of three years average rainfall (780.80 mm), the amount of surface runoff in 1999, 2009 and 2015 were found at 270.75, 289.77 and 330.82 mm (18%, 19% and 22%), whereas the soil erosion rate were 0.38, 0.68 and 0.98 kg/m2 respectively.

By compared the amount of surface runoff with land use and land cover found that, increased of built-up land and shrubs, increased the surface runoff (r = 0.957 and 0.948). Whereas there was highly positive correlation between built-up land and the shrubs and soil erosion rate. (r = 0.94 and 0.93) indicated that the transformation of forest areas to built-up land increased the rate of soil erosion.

REFERENCES

[1] García-Ruiz, J. M. “The effects of land uses on soil erosion in Spain: a review”. Catena, 81,1e11. 2010

[2] Kosmas, C., Danalatos, N., Cammeraat, L. H., Chabart, M., Diamantopoulos, J.,Farand, R., et al. “The effect of land use on runoff and soil erosion rates under Mediterranean conditions”.Catena, 29,45e59. 1997

[3] Mitchell, D. J. “The use of vegetation and land use parameters in modelling catchment sediment yields”. In J. B. Thornes (Ed.), Vegetation and erosion, processes and environments (pp. 289e314). Wiley & Chichester. 1990

[4] Oostwoud Wijdenes D.J., Poesen J., Vandekerckhove L. & Ghesquiere M. “Spatial distribution of gully head activity and sediment supply along an ephemeral channel in a Mediterranean environment”. Catena 39 (3): 147–167, DOI: 10.1016/S0341-8162(99)00092-2. 2000

[5] López-Vicente M. & Navas A. “Relating soil erosion and sediment yield to geomorphic features and erosion processes at the catchment scale in the Spanish Pre-Pyrenees.Environmental” Earth Sciences, DOI: 10.1007/s12665-009-0332-x. 2009

[6] Kiriwongwattana.K., Janimit.P. “Rainfall-Runoff Ratio of Small Watershed Study using NRCS-CN and Geo-informatics” 5th International Science, Social Science, Engineering and Energy Conference. 18th -20th December, 2013, Pavilion Rim Kwai Resor, Kanchanaburi, Thailand. 2013

[7] USDA-SCS. National Engineering Handbook Section 4, Hydrology. USDA-SCS, Washington DC, USA. 1972

[8] Soil Resources Survey and Research Division. Soil Group of Thailand 1:50,000. Land Development Department, Bangkok, Thailand. 2001

[9] Thai Meteorological Department. 2012

[10] Chow V. T., Maidment D. R., and Mays L.W. Applied Hydrology. McGraw-HillBook Co.,New York. 1988. 572 PP. 1988

[11] Mishra S K, Tyagi J V, Singh V P and Singh R. "SCS-CN-based modeling of sediment yield". Jurnal of Hydrology. Paper 324 page 301–322. 2006

[12] Juan F. M. M, Manuel L.V., Jean P., José D. R.S. "Modelling the effects of land use changes on runoff and soil erosion in two Mediterranean catchments with active gullies (South of Spain)" Landform Analysis, Vol. 17: 99–104. 2011

[13] Meyer, L D., Wischmeier,W.H. "Mathematical simulation of the process of soil erosion by water". Transactions of the American Society of Agricultural Engineers 12, 754-758 and 762. 1969

[14] Morgan R.P.C. "A simple approach to soil loss prediction: a revised Morgan–Morgan-Finney model".Catena44 (4): 305–322, DOI: 10.1016/S0341-8162(00)00171-5. 2001

[15] USGS Earth explorer [online]. https://earthexplorer.usgs.gov. Access: 10 may 2015.

CLIMATE CHANGE GIS-BASED MODELLING OF THAILAND MALARIA OUTBREAK

Chirakorn Seangprong[1]
Naresuan university, Chirakorn.ta@gmail.com
Pathana Rachavong[2]
Naresuan university, pathanar@gmail.com

ABSTRACT

The research aim of particular research is to construct a climate change model in order to find the factors related to the risk of malaria transmission by using the SimClim package and to provide Malaria Outbreak risk map based on climate change data. The data was extracted from the CMIP5 climate model using Representative Concentration Pathways: RCP of Thailand between 2016-2066. The climate change model was simulated over a period of 10 years by divided into three seasons which are summer, rainy and winter. The average temperature was classified into 9 classes. Malaria incidence information was analyzed in order to find the relationship between malaria outbreak and climate factors. The final output based on those approaches is a Malaria risk map which is classified into three classes including high, moderate and low risk levels.

Keywords: Climate scenario, Malaria outbreak

1. INTRODUCTION

Climate change is the world's important problem because it affects humans and environment both directly and indirectly in many respects namely: agriculture, urban development, tourism, public health, natural resources, and environment. The intergovernmental committee on climate change defined climate change whether from natural variance or human activities causing emission and accumulation of the greenhouse gas. The greenhouse gas has the property to absorb more heat that radiates from the atmosphere causing global warming and climate change activities. This research is interested in reproducing climate change driven by human by using the Representative Concentration Pathways (RCP) to display the climate scenarios under the scope of Coupled Model Intercomparison Project Phase 5 (CMIP5), using the climate change simulation software, SimClim 2013.

Currently, in 2017, Thailand hosted Malaria patients of 9,039 people. (6,236 Thais, 2,803 foreigners); the ratio of patients was 0.14 per 1,000 people; the amount of patients was reduced from 34.79% in 2016; most of them are farmers at 39.00%, military/police officers at 2.57%, children at 22.48% and others at 12.00%. The parasitic infection causing Malaria found in Thailand are in the kinds of P.vivax for 80.86% and

P.falciparum for 13.13% (Department of Disease Control, Ministry of Public Health, 2017). The important contagion is Malaria mosquitos in the kinds of An.minimus and An.dirus, the carriers of P.falciparum. That the life cycle of the mosquitos from being eggs to adult ones lasts for 7-14 days at the temperature of 31˚C; and at 28 ˚C for the life cycle of the mosquitos lasts for 10-12 days. After eating blood, mosquitos' egg take time to grow for 4-5 days at 28 ˚C, but at this temperature the mosquitos last for 7 days only [1]. At present, the climate changes have been evidently changed from time to times, it is found that Thailand has tended to have higher temperature then the previous time period. This climate change affects the outbreak of some important infectious diseases particularly those brought by insects. Although, the country is attempting attempts to get rid of Malaria out of Thailand, however, it has still been a deadly disease threatening the health and sanitation and destroying lives of Thai people. More importantly, some areas in Thailand are still in risk of Malaria incidence.

2. OBJECTIVE

The study aims to create the climate prediction model for designating the factors related to the risk level of Malaria incidence and create the map displaying the areas in risk of Malaria occurrence in Thailand.

3. METHODOLOGY

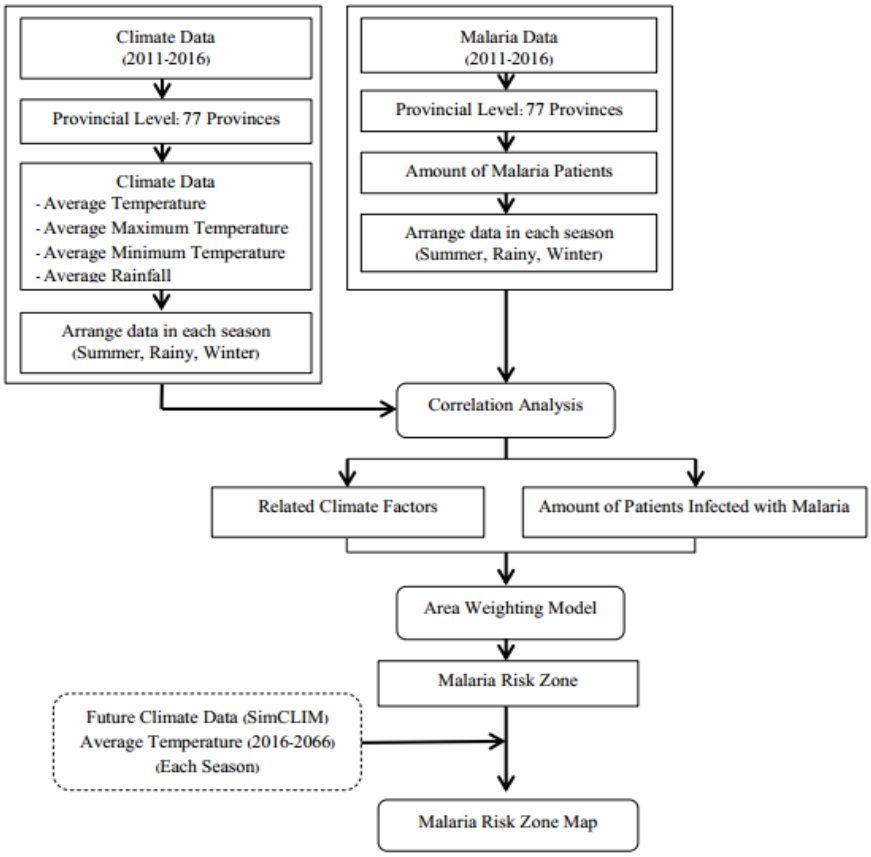

Figure 1: Studying Method

3.1 Data Used in this Study

Spatial Data

The preparation for database of spatial data, researcher requested map information that passed the authentication and verification then classified and assigned the reference point based on Geographic Coordinate (WGS84) before converting to a digital map database or Digital Maps as a result of the provincial scope data of Thailand.

Climate Data

Air Temperature and Rainfall Data in 2011-2016

The data obtained from the Department of Meteorology (both weather station and rainfall monitoring station) which is divided into summer: from March to June, rainy: from July to October and winter: from November to February. Incidentally, due to the monthly data limitation, it is not possible to divide the seasons following to the meteorological model. So, the mathematical estimation is used to obtain a result as the provincial scope data of Thailand.

Malaria Data in 2011-2016

Malaria data from Bureau of Vector Borne Disease (BVBD) which is the data of infected person in the districts. Then collected data for each province.

3.2 Data Analysis

3.2.1 Preparation of climate variables data which is the data of each station using a spatial analysis tool for surface estimation from 125 measurement stations as the provincial level.

3.2.2 Preparing the Malaria patients data of each district from Bureau of Vector Borne Disease (BVBD) for surface estimation as the provincial level of patient data.

3.2.3 Analysis of the relationship between data, average temperature and the number of Malaria patients. Then, using the result from factor analysis of climate that related in the same direction with the number of Malaria patients to analyze for finding the Malaria risk area by using the spatial weighting matrix tool.

3.2.4 The stimulation of climate change in Thailand between 2016 to 2066. The climate change model was simulated over a period of 10 years by divided into 3 seasons which are summer, rainy and winter. The analysis is divided into the following steps. Using temperature data to analyze the average by classified into 9 classes to describe the changing of temperature.

3.2.5 Using the Malaria risk area to compare with the future climate data generated from climate change model.

4. RESULTS

4.1 Relationships between Climate Data and Malaria Patients

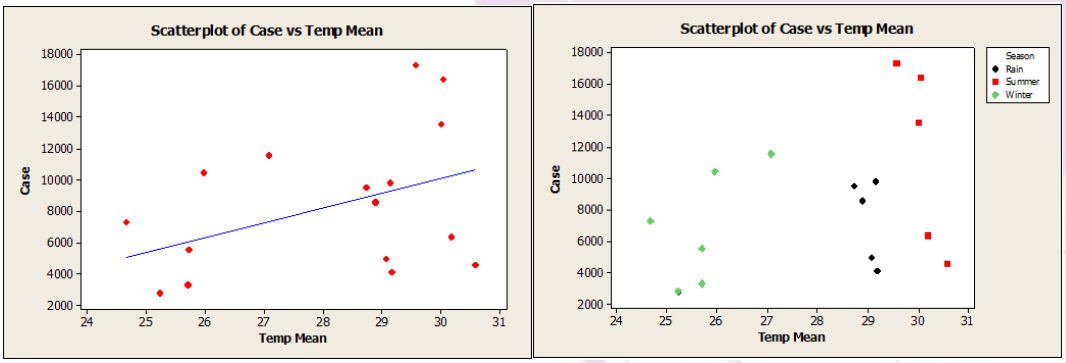

Figure 2: Relationships Between Average Temperature and Malaria Patients

Figure 2 shows the average temperature related to the amount of Malaria patients it implies that when the average temperature increases the amount of Malaria patients also increases. The results in indicate that the average temperature and the amount of malaria patients have a positive correlation (P-Value = 0.082) at the level of significance of 95 percent. Where P-Value = 0.082 showed the relationship went in the same direction at 43.4% or at a 0.05 level of significance.

Division of The Risk Level

The criterion of classifying the risk level of Malaria incidence in Thailand consisted of two criterions: Variables of climate and Variables of the amount of Malaria patients in previous 6 years.

Variables of climate used the average temperature of each season in previous 6 years between 2011-2016, giving the following risk values:

Average Temperature (Degree Celsius)	Risk Level (Weight Value)
< 26.3	Low (1)
26.4 - 28.6	Medium (2)
> 28.6	High (3)

Variables of the amount of Malaria patients used the data of patients in previous 6 years between 2011–2016, giving the following risk values:

Amount of Patients (Person)	Risk Level (Weight Value)
< 7	Low (1)
7 - 18	Medium (2)
> 18	High (3)

Next, calculating to find the risk areas using the following formula:

$$R_a = T_a \; x \; C_a$$

When R_a = Risk level of a area
T_a = Weight value of average temperature in each season of a area
C_a = Weight value of the amount of patients in each season of a area

4.2 The factors will then be analyzed of spatial weight with the amount of Malaria patients to find the risk level.

Season	2012	2013	2014	2015	2016
Summer	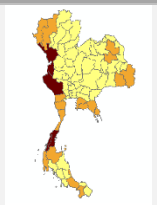	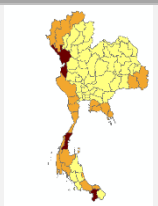	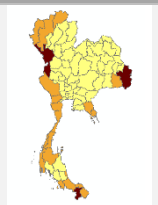	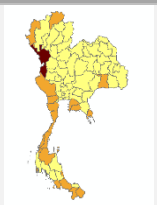	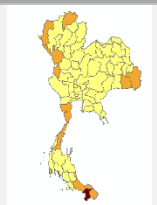
Winter	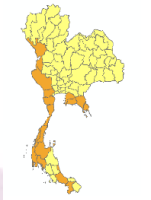			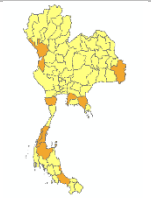	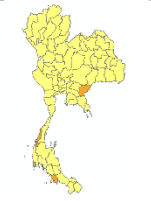
Rainny	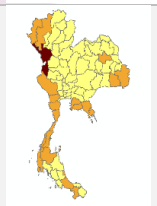	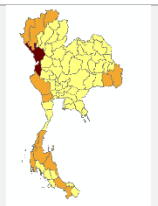	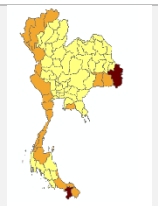	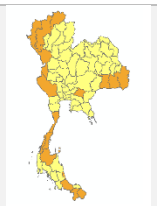	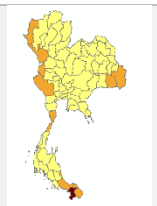

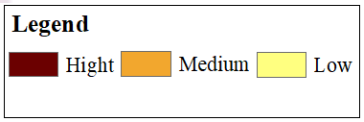

Figure 3: Relationships Between Average Temperature & Malaria Patients

The data obtained the spatial analysis and the weighted estimation between the average temperature and the amount of Malaria patients to estimate the Malaria risk could be divided into 3 levels: High, Medium, and Low risk areas.

4.3 The simulation of climate change in Thailand between 2026–2066

Season	2026	2036	2046	2056	2066
Summer	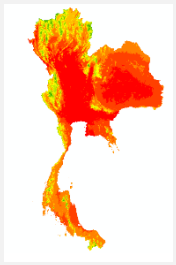	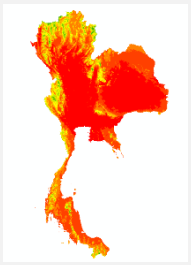	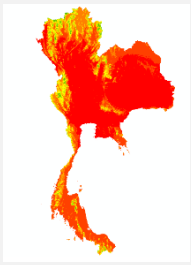		
Winter	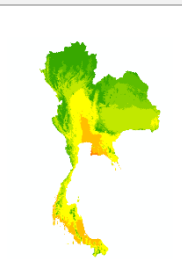	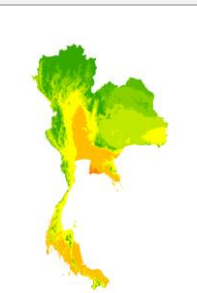	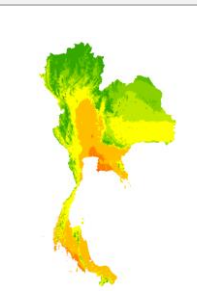	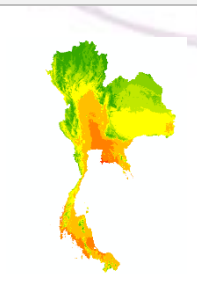	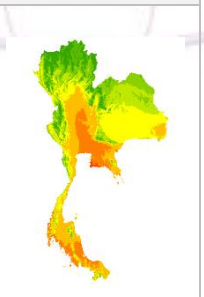
Rainy	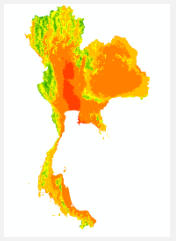	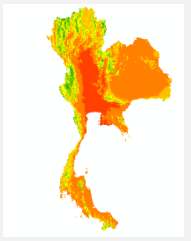		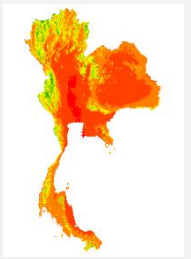	

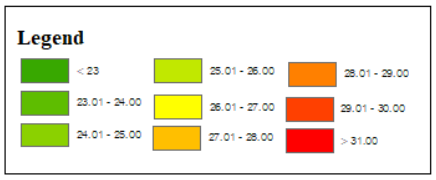

Figure 4: Map of Average Temperature Change Prediction of Thailand

The data obtained from prediction of average temperature change of Thailand showed increasing of temperature in each season clearly and continuously. In summer, rainy, and winter, the average temperature increased about 0.79 – 2.86˚C, 0.68 – 2.14 ˚C, 0.77 – 2.37 ˚C, respectively.

5. CONCLUSION AND DISCUSSION

The study found that the geographic factor related to the amount of Malaria patients was the average temperature with positive relationship which mean that. When the average temperature increases, the amount of Malaria patients also increases, where P-Value = 0.082 at a 0.05 level of significance. The related variables were analyzed by using spatial weighting method. The risk levels were divided into 3 levels which ware high, medium, and low levels of risk areas as shown in Figure 3. Apparently, in summer, the high risk areas were found in the west, the south, and the north east areas in 2014. The medium risk areas were the north, the south, and the north east partially. In the central part of Thailand were mostly the low risk areas. In rainy season, it is found that the high risk areas decreased located in the west region around the borders between 2012-2013, the north east in 2014, and the border area of the south in 2014 and 2016. It is found that the areas in the north, the east, and the south in some parts were medium risk areas. In winter, it is found that the medium risk areas were the western border along to the south area between 2012-2013; the east's area adjacent to the sea in 2014, and; the north east's border area in 2013 and 2015.

For the simulation of climate change in Thailand between 2026 to 2066, it is found that the average temperature in summer of Thailand in 2066 increased for 1.52 ˚C or 5.30% from 2026. The most changed area was the upper part of the northern region. In the southern region, the average temperature of the rainy season in 2066 increased for 1.30 ˚C or 4.78% from 2026; the most changed areas were the central region and the lower part of the northern region. The average temperature in winter of Thailand in 2066 increased 1.46˚C or counted as 5.95% from 2026; the most changed areas were the east and the south of Thailand.

For this study, we concluded that the more the average temperature increases the more the Malaria patients increase. The results were in accordance with Chamnan Apiwatanasorn (2012) [1] who studied the climate change and the mosquito vector. The study found that the life cycle of the mosquitos to grow from being eggs to be adult mosquitos takes 7-14 days at the temperature of 31˚C and at 28˚C for those have the life cycle of 10-12 days. After eating blood, eggs inside the mosquitos will take 4-5 days to grow; but at the temperature of 28˚C, the mosquitos take 7 days only. So, when the temperature is rising, the mosquitos will eat blood and lay eggs more frequently. Besides, this is related to Pornpan Sorncheua (2017) [2] who studied of the climate change and the infectious diseases. The results found the factors of temperature and climate are important factors that affect the epidemic brought by insects, which are contagious diseases like Malaria and Dengue Fever.

6. RECOMMENDATION

This model also has the limitations and the lack of some effective variables, for example, human behavior, human immune system. The statistics calculation showed vary low p – value due to the number of malaria patients collected from the Department of Disease Control were very small amount, which affects to the results of the study.

REFERENCES

[1] Chamnarn Apiwathnasorn. “Climate Change and Mosquito Vectors”,The Journal of tropical Medicine and Parasitology. 35(2),78-85, December 2012.

[2] Pornpan Sorncheua. “Climate change and Infectious disease”, Thammasat Medical Journal,17(3),440-447, July-September 2017.

AN ANALYSIS OF LAND USE CHANGE AT THE PERI-PROTECTED AREA: A CASE STUDY OF PHU KRADUENG NATIONAL PARK AND SURROUNDING AREAS DURING 1952 – 2016

Mayuree Nasa
PhD candidate in Geography section, School of Distance Education, Universiti Sains Malaysia, mn14_pjj013@student.usm.my

Fatimah Binti Hassan (Ph.D.)
Associate Professor in Geography section, School of Distance Education, Universiti Sains Malaysia, hfatimah@usm.my

ABSTRACT

Land use change reflects human's needs. Human gain materials for food, clothes, energy, and space for recreation or tourism. Changing land involved with the shift to a different use such as forest land to agricultural land or tourist destination or an intensification of the existing one such as in-season rice filed to off-season rice filed. Protected areas with the unique landscape are becoming tourist destinations. Protected areas often depend on surrounding area to maintain flows of organisms, water, nutrients, and energy. Hence, understanding in the pattern of land use change in the peri-protected area is crucial with regarding human activities and needs. Land use change in this studied were assessed by using Geographic Information System covering 1952, 2002, and 2016. The peri-protected area in this study covering Phu Kradueng National Park and surrounding areas. Among all land use type, forest land had been the most dominating land use type both in the first period (1952 - 2002) and the second period (2002 - 2016) of the study. However, the forest land decreasing in the first period due to the changing land to an agricultural land and water body. It is interesting that, during the second period, there was a decrease in agricultural land while an increase in forest land even though rising just a small percentage. Besides, the rate of change in land use was relatively slow.

Keywords: Land use change, Peri-Protected area, Phu Kradueng National Park

1. INTRODUCTION

Land use reflects human's needs. Human has the most severe potential impact on the ecosystems. Human can either destroy ecosystems or be able to build new ecosystems which are called cultural ecosystems or land utilization types. In the cultural ecosystem, the human gain materials for food, clothes, energy, and space for recreation or tourism. Other than the usability, the protection and conservation of natural ecosystems through nature reserves is seen as a popular kind of land use. It is reflecting not only human needs but also human responsibilities [1]. The term 'land-use' means the human occupied of the land which included settlement, cultivation, pasture, rangeland, recreation and land use for tourism purposes as well. Changing of land-used involved

with the shift to a different use or an intensification of the existing one [2]. Tourism industry as a driver of growth for the global economy, it is promoted at every geographical level. The expansion of tourism land coverage also includes the conversion of traditional land uses such as farming to mixed or entirely tourism-oriented uses [3]. Protected areas with unique landscape are becoming tourist destinations. Land use is also changing from the forest to recreation, tourism and, services purposes. Many National parks have faced the tension from the tourism activities and local communities near the parks. Moreover, not only the visitors interested in the National park but also the investors. Therefore, well understanding in the pattern of land use change in the peri-protected area is essential.

2. OBJECTIVE

Explore the land use patterns and land use change at the peri-protected area before and after the National park establishment and tourism destination had emerged.

3. METHODOLOGY

The effect of conservation policy and tourism policy on local land use pattern and change in place over a period of 60 years were evaluated to identify how land-use patterns changed. Phu Kradueng National Park (PKNP) and surrounding areas has been selected as study area to illustrate the understanding of the pattern of land use change. PKNP is located at 16o 49' to 16o 59' northern latitude and from 101o 41' to 101o 5' eastern longitude, at an elevation is between 400-1,200 metres with the summit point of 1,316 metres at Khok Moei. It is a part of Sritan Sub-district Phu Kradueng District Loei Province, which is in the northeast of Thailand [4]. PKNP is the second National Park in Thailand since 1961. It is becoming a nature-based tourist destination since the tourism policy emerges in the country due to the National Action Plan for Ecotourism in 2001. According to its high elevation and climatic condition, the weather on the mountaintop is cold all year round. Sometimes, in the winter season, the temperature may drop to freezing point. So, it is the most achievement to visitors who would like to be the PKNP conqueror at least once in their life due to the difficulty of the hiking trail up to the hilltop.

Data Sources and Analysis

Land use pattern and change in the peri-protected area were assessed by using Geographic Information System [5] covering 1952, 2002, and 2016. The present study used two software for digitization, analysis, and data entering. The first one is QGIS, which is the open source software, for digitization and analysis. The second one is MS Excel for data entering. The primary data source was the aerial map of 1952 from the Royal Thai Survey Department and the land utilization maps of 2002, 2016 from the Land Development Department.

An analysis of rate of land use change refers to the rate of annual change in land use amount in certain area at a certain time [6]. The rate of land use change in the Phu Kradueng National park and surrounding area (peri-protected area) is calculated as follows:

$$K = \frac{U_b - U_a}{U_a} \times \frac{1}{T} \times 100 \quad (1)$$

where K is the dynamic degree of a certain land use type in the study period; Ua and Ub are the amount of a certain land use type at the beginning and end of study, respectively; T is the length of study period, when T is year, the value of K is the rate of annual change in a certain land use type in the study area.

4. FINDINGS

Land use pattern 1952

Only two main categories of land use were seen in this period. Land use patterns included forest land and agricultural land (Table 1). Forest covered 428.40 km2 which was 98.87%. Agriculture land covered 4.92 km2 which was 1.13% of the total area.

Land use pattern 2002

Three main categories of land use were seen in the study area. Land use patterns included forest land, agricultural land, and built-up area (Table 1). In this period, forest land dominated the other land use types covering 375.24 km2 (86.93% of total area).

Land use pattern 2016

Four main categories of land use were seen in the study area. Land use patterns included forest land, agricultural land, built-up area, and water body. In this period, forest land was found to be the dominating land use types covering 376.76 km2 (86.95%).

Rate of change from 1952 – 2002 and 2002 – 2016

During 1952 – 2002, there was an increase in agricultural land while a decline in forest land in this period. For during 2002 – 2016, it is interesting that there was a decrease in agricultural land while an increase in forest land even though rising just a small percentage. Moreover, in 2002, there was an increase in built-up area 0.12 % of total area and 1.05 in 2016. The rate of change of the built-up area is 55.08% from 2002 – 2016. The data in 2016 also shown that there was a water body covering 3.91 km^2 which were 0.90% of total area. The detailed show in Table 1 and Figure 1.

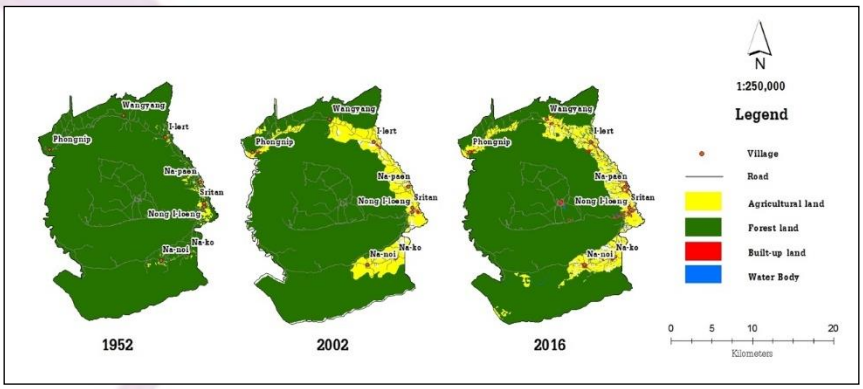

Figure 1. Land use change at the Phu Kradueng National park and surrounding areas

Table 1. The pattern of Land use change at the Phu Kradueng National park and surrounding areas

Land use type	1952		2002		2016		Rate of change (%)	
	Area (sq.Km.)	Proportion (%)	Area (sq.Km.)	Proportion (%)	Area (sq.Km.)	Proportion (%)	1952-2002	2002-2016
Forest land	428.40	**98.87**	375.24	**88.02**	376.76	**86.95**	- 0.25	0.03
Agriculture land	4.92	1.13	50.57	11.86	48.12	11.10	18.60	- 0.35
Built-up area	N/A	N/A	0.52	0.12	4.53	1.05	N/A	55.08
Water body	N/A	N/A	N/A	N/A	3.91	0.90	N/A	N/A
Grand total	**433.32**	**100.00**	**426.33**	**100.00**	**433.32**	**100.00**		

5. CONCLUSIONS

Land use pattern and change in the PKNP and surrounding areas are dynamic. It is classified into four categories, forest land, agricultural land, built-up area, and water body. There has been increasing in agricultural land in the first period and decreasing in the second period due to the changing land to the other type of land use such as built-up area. Among all land use type, forest land had been the most dominating land use type both in the first and second period of the study. However, the forest land decreasing in the first period due to the changing land to an agricultural land and water body. The understanding of the pattern and change in land use in the particular area, especially in the natural areas, may be useful in land use planning and management. It makes a clear picture for the planners and practitioners.

REFERENCES

[1] Vink, A.P.A., "Landschapsecologie en landgebruik", Davidson, D.A. (eds.) "Landscape ecology and land use", London and New york: Longman, 1983.

[2] Mayer, W.B. & Turner B.L. II. (Ed.), "Changes in Land Use and Land Cover: A Global Perspective", Cambridge: University Press, 1994.

[3] Terkenli, T.S. & Schistou, D.E., "Land use policy and tourism: The case of Greece", Paper presented at the 5th International Scientific Conference, Island of Rhodes, Greece, 2013, May 30th to June 2nd.

[4] Department of National park, Wildlife and Plant conservation (DNP), "Phu Kradueng National park", Retrieved from http://www.dnp.go.th/parkreserve/asp/style1/default.asp?npid=11&lg=2, 2015a.

[5] Baidya, N.G., Bhuju, D.R., & Kandel, P., "Land use change in Buffer zone of Chitwan National park, Nepal between 1978 and 1999", Journal of Ecological Society, 16, pp. 79-86, 2009.

[6] Yao, Y., Wu, D., Liu, Y., Chen, Q., Chen, H., Wu, J., & Zhong, J., "Land Use Change and Driving Forces in Guangzhou City during 1996-2012", Journal of Asian Agricultural Research, 7(9), pp. 33-40, 2015.

DETECTING THE EL NIÑO'S INDUCED CHANGES IN PHENOLOGY OF A SECONDARY DRY DIPTEROCARP FOREST BY USING REMOTE SENSING

Rungnapa Kaewthongrach[1], Phan Kieu Diem[2], Amnat Chidthaisong[3]*
The Joint Graduate School of Energy and Environment (JGSEE) and Center of Excellence on Energy Technology and Environment, KMUTT, Bangkok, Thailand
Rungnapa.kpp@gmail.com, pkdiem@ctu.edu.vn, amnat_c@jgsee.kmutt.ac.th

Tanita Suepa[4]
Geo-Informatics and Space Technology Development Agency, Bangkok, Thailand
tanita@gistda.or.th

Montri Sanwangsri[5]
School of Energy and Environment (SEEN), University of Phayao, Phayao, Thailand
montri.sa@up.ac.th

Phongthep Hanpattanakit[6]
Faculty of Environmental Culture and Ecotourism,Srinakharinwirot University, Bangkok, Thailand.
phongthep@g.swu.ac.th

Pariwate Varnkovida[7]
Geospatial Engineering and Innovation Center, Department of Mathematics, Faculty of Science, KMUTT, Bangkok, Thailand
pariwate@gmail.com

**Corresponding author: amnat_c@jgsee.kmutt.ac.th*

ABSTRACT

El Niño-Southern Oscillation (ENSO) is an important driver of climate variability on interannual time scale in Southeast Asia. Under future climate change, ENSO is expected to be intensified and its two opposite phases as warm El Niño and cool La Niña will be more frequent. Thus, negative impact of ENSO on the functions and services of terrestrial ecosystems is a foreseeable future. In tropical ecosystem, the secondary forestlands are increasing because of implementation of reforestation policy in many tropical countries. Therefore, the secondary forests are likely to have more roles on regional and global ecosystem function and services. In the present study, we investigated the response of the secondary dry dipterocarp forest phenology to El Niño events during 2009-2016. The forest phenology was evaluated by extracting the Normalized Difference Vegetation Index (NDVI) from Moderate Resolution Imaging Spectroradiometer (MODIS). The micro-meteorological data were collected at the study site in Ratchaburi Province that included rainfall, temperature and soil moisture. We found that El Niño in 2009/2010 and 2015/2016 led to a dramatic decline in NDVI. The impacts of these El Niño on forest phenology were characterized by the late start of growing season and shorter in the length of growing season when compared to other years.

Keywords: *Dry dipterocarp forest, El Niño, normalized vegetation indices, phenology*

1. INTRODUCTION

Forestland in Thailand accounts of 31.6% of total country area (102 million rai or 16.3 million hectare) in 2016. It has declined at 0.2% per year between 2008-2016 [1]. Forest logging has been banned in Thailand since 1989. Since then reforestation and afforestation policies have been implemented, leading to an increase of secondary forest. The dry deciduous dipterocarp forest is the most widespread forest in the continental Southeast Asia [2]. In Thailand, this forest covered about 21% of total natural forest area in 2005 [3]. A distinct seasonality is a dominant characteristic of this forest. Generally, the deciduous plants avoid the costs of maintaining leaves in unfavorable condition by shedding their leaves and carrying the costs of constructing new leaves during the onset of growing season [4]. The presence of leaves, which is the time between leaf-out and leaf senescence, affects various ecosystem function, including biogeochemical cycles and interspecific interaction. Moreover, this is a footprint of regional climate history that will reveal to forest response to climate change [5], [6]. Researches in the past have improved our understanding of the factors and mechanisms associated with phenological events at the start of growing season (SOS). However, the end of season (EOS) is still less understood especially in the timing and key driving factors. As a result, estimating the length of growing season (LOS) in dry dipterocarp forest is one of the least understood features of this forest ecosystem. The duration of growing season would indicate the capability of forest ecosystem to sequester carbon and to provide other ecosystem services. Thus, more work is needed to know how phenological events at the end of growing season are being affected by climate change [7]. This includes the fact that timing of leaf senescence might depend on local environmental conditions driven by climate variability, including temperature, soil moisture, frost and wind [8]. On interannual time scale, Asian-Pacific climate is driven by the El Niño-Southern Oscillation (ENSO). Future climate projection implies that the ENSO is expected to be intensified, leading to more frequent in extreme events [9], [10]. The intensification of the ENSO system is likely to pose a serious consequence on terrestrial ecosystem [11]. During El Niño, a shift in the walker circulation along with subsidence over Southeast Asia, a weakened monsoonal flow and reduction in moisture fluxes and rainfall location move away resulting in drought conditions in the region [12]–[14]. The impact of repetitive events is still far from being understood and how terrestrial ecosystems can adapt to more frequent severe drought events remains unknown [15].

The Moderate Resolution Imaging Spectroradiometer (MODIS) provides valuable data for long-term monitoring of vegetated phenology such as normalized difference vegetation index (NDVI) and Enhanced Vegetation Index (EVI) [16]–[18]. The time series of vegetated indices have been widely used to study the phenological characteristics under climate variability especially in extreme event as El Niño[19]–[21]. In the current study, the capacity of remote sensing to capture the phenological change affected by El Niño in secondary dry dipterocarp forest is evaluated. The relationship between phenological characteristics and climate variables are also investigated.

2. OBJECTIVE

To detect phenological characteristics of secondary dry dipterocarp forest those are influenced by El Niño by using remote sensing. Moreover, climate triggers affecting on phenology are also investigated; especially in the EOS.

3. METHODOLOGY

The study was conducted in a secondary dry dipterocarp forest, located in Ratchaburi province, western Thailand (13° 35' 13.3" N: 99° 30' 3.9" E, elevation of 118 m). The forest had been exploited by nearby communities for timber, charcoal or other products. This forest has been protected since 2005 and trees have naturally regenerated. The dominant species are *Dipterocarpus obtusifolius* Teijsm. Ex Miq, *Shorea siamensis*, Miq., *Shorea obtuse* Wall.ex Blume, *Shorea roxburghii* G.Don, and *Sindora siamensis* Teijsm. & Miq. In 2015, the trees were about 10 years with average height and diameter of 7.01 m and 6.80 cm, respectively. The soil texture for the top to 1 meter depth was loamy sand, with sand particle content of more than 70% and very small fraction of clay content [22].

3.1. Micro-climate measurement

The meteorological observation tower has been installed in the forest area since 2008 until now. Air temperature was measured by Vaisala senser (Vaisala Inc. Model HMP45C), and rainfall was collected by tipping bucket rain gauge (model TE525, Cambell Scientific, Inc.). These sensors were mounted on tower at 10 m above the ground. Soil moisture was measured at 5 cm below ground by water content reflectometers (CS615, Campbell Scientific, Inc.). All sensors were connected to data logger (CR1000, Cambell Scientific, Inc.) and recorded data for every 30 minutes.

3.2. Remote sensing process

Dataset: MODIS product in 8 days temporal resolution was used in this study. The two products consist of surface reflectance MOD09Q1, providing Bands 1 (Red) and Band 2 (NIR) at 250-meter resolution, and MOD09A1 at 500 meter resolution were used. The cloud contaminated pixels in MOD09Q1 were marked by using MOD09A1, then it was removed and replaced by using the method of [23]. After that, the NDVI were calculated between 2008-2016.

Phenological parameters include the start of growing of season (SOS), the end of growing season (EOS) and the length of growing season (LOS) were derived by TIMESAT program. In this step, the NDVI was implemented using a simple median filter to remove noise and then the Savitzky-Golay (SG) filter was applied to remove noise before dividing by the phenological parameters [24]. In this study, the SOS and EOS were calculated based on a threshold of 20% deviation from the amplitude of the minimum NDVI. The length of season is the duration between SOS and EOS.

3.3. Relationship between climate variables and phenological indices

The regression analysis was used to find the relationship between phenological parameters and climate variables.

4. RESULTS

4.1. Micro-climate

There was a remarkable extreme drought owing to less rainfall and low soil moisture in dry season 2009/2010 and 2015/2016 (Fig. 1a and Table 1). These periods corresponded to El Niño events as indicated by [25]. During that time, rainfall was only 59.1-71.4 mm, while the average rainfall was about 202.4±79.9 mm in other dry seasons. The soil moisture was lower than 5% VWC for five months during December to April for the El Niño years, while this was two-four months in other dry season, except dry season in 2011/2012. In contrast, the air temperature was not markedly different between the normal periods and El Niño events. The statistical descriptions of climate variables are illustrated in Table 2.

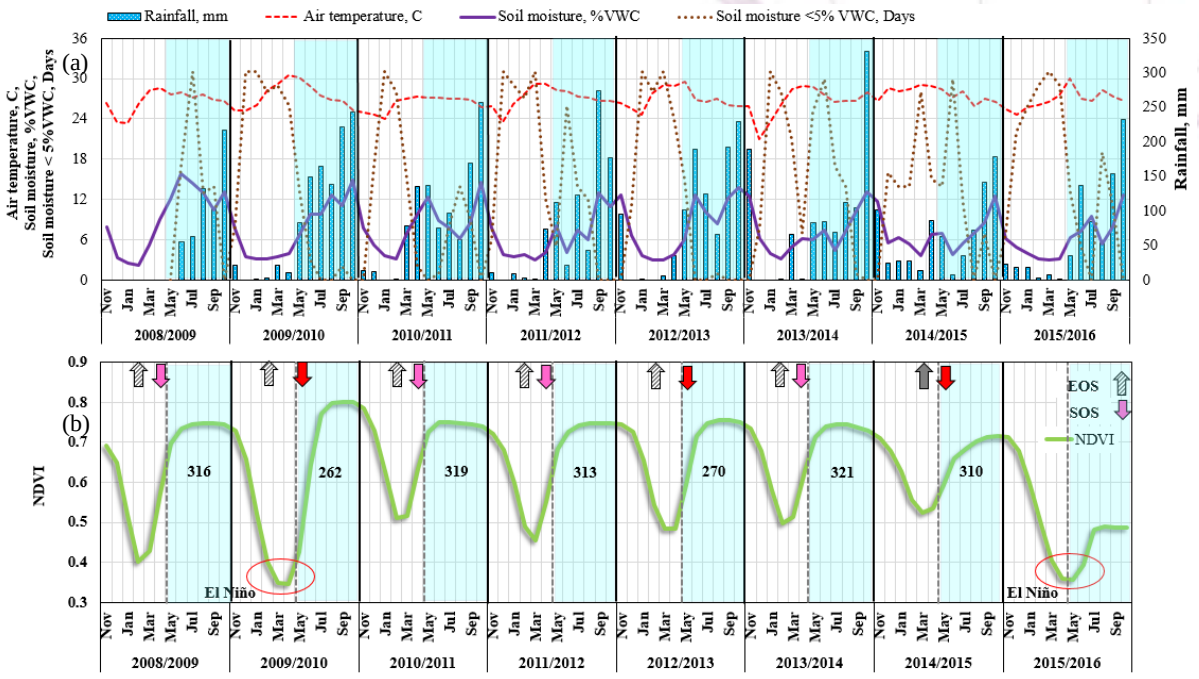

Fig. 1 a) Climate variables consisting of a) rainfall, air temperature, soil moisture and the number of days during which soil moisture was lower than 5%VWC, b) the NDVI value with the arrows indicating the start of growing season (SOS) and end of growing of season (EOS). The white areas are the dry season between November- April of the following year, and the blue areas are the wet season between May and October.

Table 1 Summary of climate variables (±SD) in dry season, wet season and annual period; including rainfall, air temperature, and soil moisture

Period	Season	Rainfall (mm)	Air temperature (°C)	Soil moisture (%VWC)
2008/2009	No complete data			
2009/2010	Annual	1058.3	27.5±1.9	7.5±4.1
	Dry	59.1	27.4±2.2	4.2±1.7
	Wet	999.2	27.5±1.7	10.9±2.8
2010/2011	Annual	1036.3	26.3±1.2	7.9±3.3
	Dry	240.7	25.8±1.5	6.1±2.6
	Wet	795.6	26.8±0.6	9.7±3.1
2011/2012	Annual	850	27.2±1.6	6.3±3.2
	Dry	98.3	27.0±2.2	4.3±1.7
	Wet	751.7	27.4±0.7	8.3±3.2
2012/2013	Annual	1040.4	27.0±1.5	8.0±4.2
	Dry	136.7	27.0±1.8	5.5±3.8
	Wet	903.7	27.0±1.3	10.5±3.0
2013/2014	Annual	1041.7	26.5±2.3	7.1±2.8
	Dry	257.0	25.7±2.9	6.1±3.3
	Wet	784.7	27.4±0.9	8.1±3.1
2014/2015	Annual	777.2	27.8±1.0	7.0±2.8
	Dry	279.4	28.3±0.9	6.6±2.8
	Wet	497.8	27.2±0.9	7.4±3.0
2015/2016	Annual	769.4	26.8±1.4	6.1±2.9
	Dry	71.4	26.0±1.0	4.0±1.3
	Wet	698.0	27.7±1.3	8.2±2.6

Table 2 Comparison of climate variables and NDVI between non- El Niño and El Niño period (dry season).

Variable	Non- El Niño	El Niño

	Rainfall (mm)	Temp (°C)	Soil moisture (%VWC)	NDVI	Rainfall mm	Temp (°C)	Soil moisture (%VWC)	NDVI
Mean	9.2	26.6	5.8	0.6	4.1	26.8	5.1	0.5
Median	0.0	26.7	4.1	0.5	0.0	26.3	3.5	0.5
Variance	472.9	5.2	12.0	0.0	76.3	4.8	9.9	0.0
SD	21.7	2.3	3.5	0.1	8.7	2.2	3.1	0.2
Minimum	0.0	19.4	2.8	0.4	0.0	22.8	2.8	0.3
Maximum	164.8	31.1	15.3	0.7	41.1	31.4	14.4	0.8
Range	164.8	11.7	12.5	0.3	41.1	8.6	11.6	0.5
Skewness	4.1	-0.7	1.3	0.1	2.5	0.5	1.8	0.1
Kurtosis	25.2	3.5	3.5	1.9	8.8	2.3	5.1	1.8

4.2. Phenological change

During the two El Niño events, NDVI dropped to the lowest annual minimum (Fig. 2). The phenological parameters were extracted only for the events in 2009/2010 due to incomplete NDVI curve in 2015/2016. In addition, in 2015/2016 the young leaves were damaged by forest fire in some areas during the EOS and by heavy insect outbreaks during the onset of season. Results revealed the SOS was significant late, while the length of growing season was the shortest during this El Niño. The EOS showed a slightly earlier in 2009/2010 but it seems not different from the other periods. In addition, we found the strong relationship between the SOS and LOS which indicates that the SOS had high impact on LOS. So, we assumed that the shorter LOS detected in the current study was due to SOS rather than EOS.

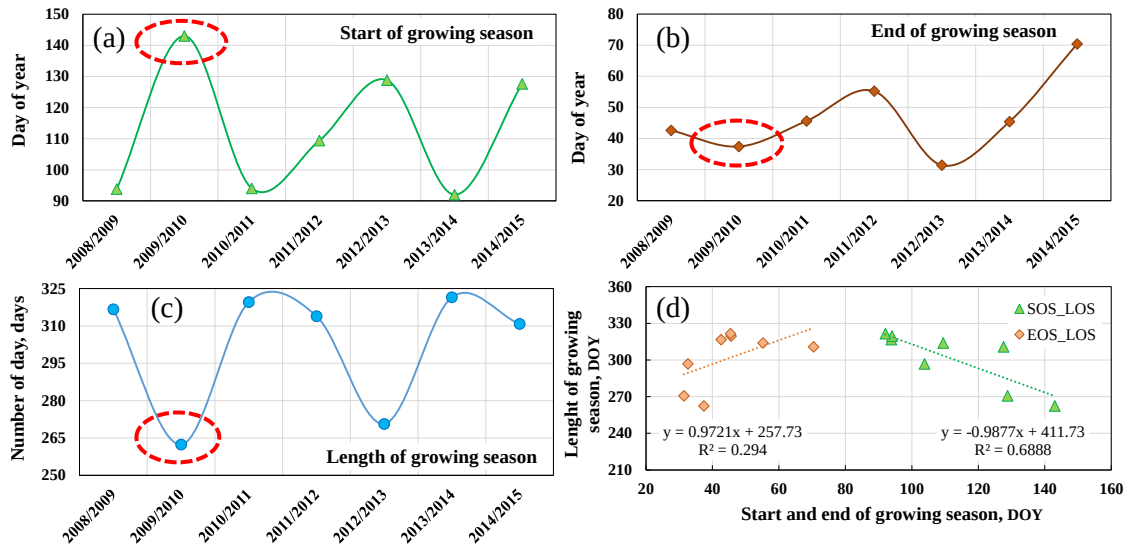

Fig. 2 The phenological parameters, including a) the start of growing season (SOS), b) end of growing season (EOS), c) length of growing season (LOS), and d) the relationship between start and end of growing season with length of growing season (DOY = day of year)

4.3. Effect of El Niño and micro-climate on phenological change of secondary dry dipterocarp forest

To find the impact of El Niño on climate variables and forest phenology, the anomaly characteristic in dry season were analyzed. Results show both rainfall and soil moisture anomalies in 2009/2010 and 2015/2016 were significantly lower compared to other years, corresponding to a significant drop of NDVI. Meanwhile, the air temperature did not show a significant deviation from the other years (Fig. 3). The significantly high correlation between the SOS and start of raining season (SRS) was observed (Fig.4). In this study, the SRS defined as the time during which rainfall is detected for at least four days within five days and the amount of cumulative rainfall is higher than 10 mm, or the amount of rainfall at less 30 mm within 1-2 days. The end of rainy season (ERS) is defined at the time when the cumulative rainfall is lower than 10 mm for at least four days within five days or rainfall is lower than 30 mm within 1-2 days. The SRS were occurred between March-May at this forest site. This means that the coming of rainfall was very important to new leaves expose. However, there was a low relationship between EOS and ERS, consisting with other reports that EOS is current difficult to clearly define. At this forest site, soil moisture or water stored in the deep soil, which may be highly variables, may be a factor that make the end of season difficult to detect. Soil moisture was found to correlate to the NDVI only during the declining curve (it is defined at point that the NDVI begins to permanent drop at the end of growing season), about September to March) (Fig.1b). In addition, it seems that the soil moisture at lower than 5%VWC was a limiting factor for remaining of leaves (Fig.5). The higher number of days with soil moisture less than 5% VWC were found during El Niño 2009/2010 and 2015/2016 (Fig. 1a), compared to other periods. The number of days in dry season with the soil moisture lower than 5%VWC were 24.8±1.1 and 18.7±3.6 days in normal and El Niño, respectively. From the relationship in Fig. 5, we notice that the minimum soil moisture was not different between non-El Niño and El Niño but the NDVI was significantly decreased during the El Niño. Thus, low soil moisture coupled with prolonged duration had the additional impact on NDVI.

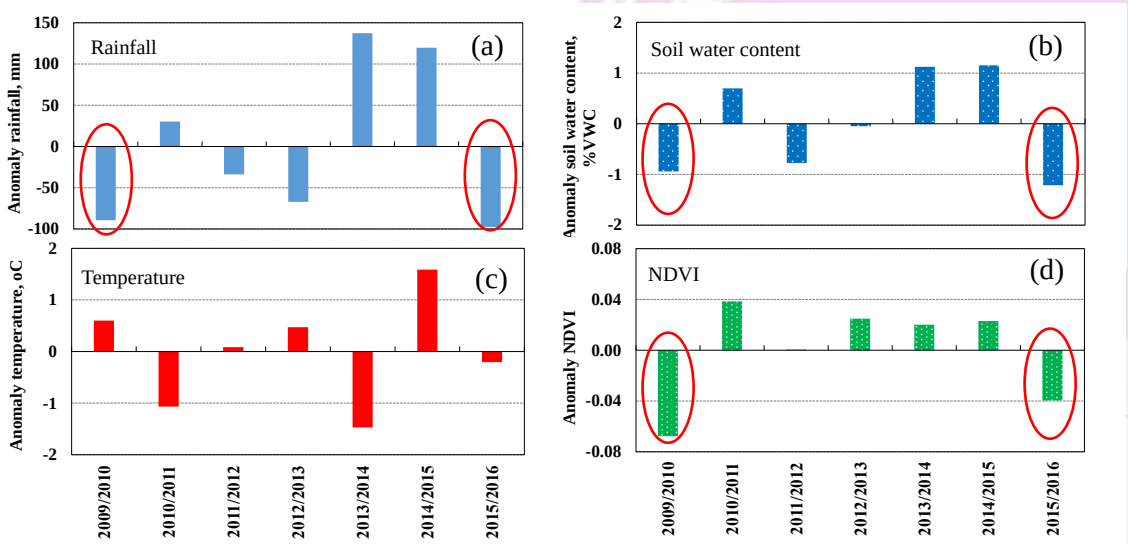

Fig. 3 The anomaly characteristics of a) rainfall, b) soil moisture, c) temperature, and d) the NDVI in dry season for seven periods.

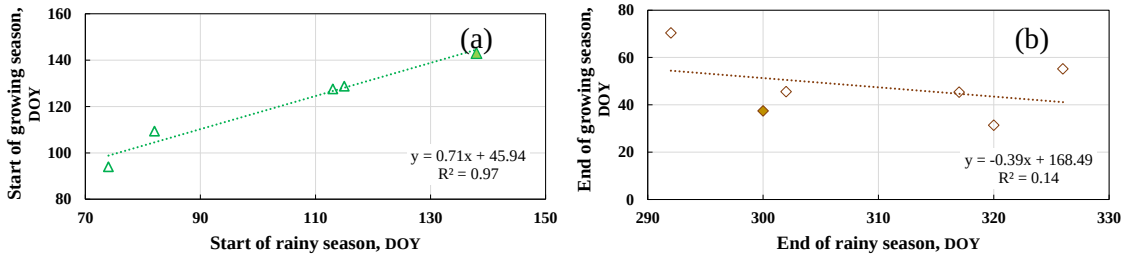

Fig. 4 Relationship between a) start of rainy season and start of growing season, b) end of rainy season and end of growing season.

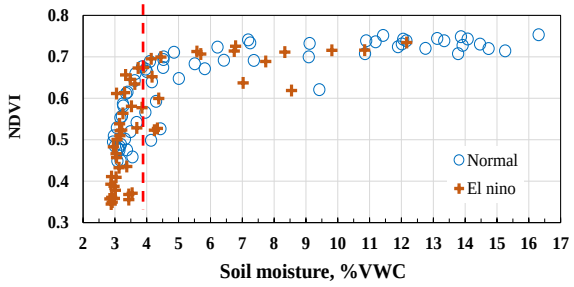

Fig. 5 Relationship between soil moisture and NDVI during its reducing phase; September to March of the following year.

5. CONCLUSION AND DISCUSSION

The markedly low rainfall and late shifting of SRS are the main characteristics detected during the El Niño periods at this forest site. This event was also consistent with a period with water

deficit due to decreased soil moisture. Thus, the prolonged drought was occurred in secondary dry dipterocarp forest during El Niño events.

The significant drop in NDVI during the dry season is a common characteristic of this dry dipterocarp forest. However, in the current study we show that the extended dry periods induced by El Niño could further reduce NDVI when compared to the non- El Niño year. The minimum point of NDVI was 0.40-0.52 during non- El Niño while it dropped to 0.35-0.36 during El Niño. The cause of relatively high NDVI during non-El Niño may be due to of the incomplete deciduousness owing to the overlap between leaf fall and leaf flushing of some dipterocarp species. During El Niño, the significant reduction of the NDVI occurred because of leaflessness before leaf flushing as an adaptive mechanism to reduce water loss in transpiration. Singh and Kushwaha reported that the leaf phenology of *Shorea robusta* species, which is in the same genus of the dominant species in this studied forest, had various leaf phenological characteristics including a) leaf fall completely before flushing, b) overlap between leaf fall and flushing, c) leaf fall completed but leaf flush delayed, and d) leaf fall incomplete (old leaves persist) and leaf flush delayed. The appearance of these characteristics was depended on the degree of drought [26]. Thus, El Niño might force some species or some trees to be a leaflessness. That would be one possible reason why the NDVI dropped significantly during El Niño.

The remarkable less rainfall and the shifting of SOS during El Niño, and the strong correlation between the SOS and SRS, were consistent with a large scale investigation in vegetation phenological change of naturally area in Monsoon Southeast Asia [20]. The shift of rainfall closely related to late starting of growing season and shorter length of growing season. Similar results were reported for tropical dry forest in Hawaii. The NDVI was more closely related with precipitation and the spatial pattern of NDVI responding to El Niño 2002-2003. The mechanisms controlling dry forest leaf phenology were related to water- limitation, whereas rainforests were more light-limited [27]. In contrast, El Niño events were correlated with an earlier start of growing season (SOS) than La Niña events in western U.S. However, there was difference in timing of the end of growing season (EOS). The length of growing season was mostly positive in El Niño years. The El Niño was found to associate with significantly higher net primary production (NPP) due to longer growing season in the northern hemisphere (by up to 52 days) [11]. Interestingly, this secondary dry dipterocarp forest seems to effectively adapt to El Niño because the net ecosystem production (NEP) at this site for the normal year (12.06 ton C ha^{-1} yr^{-1}) and El Niño year (12.26 ton C ha^{-1} yr^{-1}) was not significantly differentially. Although, this secondary forest released more carbon for longer period during the El Niño compared to normal year, but the higher rate of carbon uptake in rainy season could compensate for the released carbon during dry period [28], [29]. Consequently, the El Niño effects on shift and shorter length growing of season in secondary dry dipterocarp forest, but it was less impact on annual carbon uptake. Thus, it is probable that the secondary has high efficiency to adapt to increased intensity and frequency of extreme climate in the future.

REFERENCES

[1] Royal Forest Department, “Forestry statistics,” 2017. [Online]. Available: http://forestinfo.forest.go.th/Content.aspx?id=9. [Accessed: 29-Dec-2017].

[2] T. T. Nguyen and P. J. Baker, "Structure and composition of deciduous dipterocarp forests in Central Vietnam: patterns of species' dominance and regeneration failure," *Plant Ecol. Divers.*, vol. 9, pp. 589–601, 2016.

[3] Royal Forest Department, "Forestry statistics," 2005. [Online]. Available: http://forestinfo.forest.go.th/.

[4] E. February, E. C. February, and S. I. Higgins, "Rapid leaf deployment strategies in a deciduous savanna rapid leaf deployment strategies in a deciduous savanna," *PLoS One*, pp. 1–11.

[5] K. M. Dahlin, R. A. Fisher, and P. J. Lawrence, "Environmental drivers of drought deciduous phenology in the," *Biogeosciences*, vol. 12, pp. 5061–5074, 2015.

[6] C. M. Zohner and S. S. Renner, "Innately shorter vegetation periods in North American species explain native–non-native phenological asymmetries," *Nat. Ecol. Evol.*, pp. 1–6, 2017.

[7] A. D. Richardson, T. F. Keenan, M. Migliavacca, Y. Ryu, O. Sonnentag, and M. Toomey, "Climate change, phenology, and phenological control of vegetation feedbacks to the climate system," *Agric. For. Meteorol.*, vol. 169, pp. 156–173, Feb. 2013.

[8] Z. A. Panchen, R. B. Primack, A. S. Gallinat, B. Nordt, A. Stevens, Y. Du, and R. Fahey, "Substantial variation in leaf senescence times among 1360 temperate woody plant species : implications for phenology and ecosystem processes," *Ann. Bot.*, pp. 1–9, 2015.

[9] W. Cai, G. Wang, A. Santoso, M. J. McPhaden, L. Wu, F.-F. Jin, A. Timmermann, M. Collins, G. Vecchi, M. Lengaigne, M. H. England, D. Dommenget, K. Takahashi, and E. Guilyardi, "Increased frequency of extreme La Niña events under greenhouse warming," *Nat. Clim. Chang.*, vol. 5, no. 2, pp. 132–137, 2015.

[10] T. Zhou, B. Wu, and L. Dong, "Advances in research of ENSO changes and the associated impacts on Asian-Pacific climate," *Asia-Pacific J. Atmos. Sci.*, vol. 50, no. 4, pp. 405–422, 2014.

[11] M. P. Dannenberg, C. Song, T. Hwang, and E. K. Wise, "Empirical evidence of El Niño-Southern Oscillation influence on land surface phenology and productivity in the western United States," *Remote Sens. Environ.*, vol. 159, pp. 167–180, 2015.

[12] S. B. Ratna, J. V Ratnam, S. K. Behera, F. T. Tangang, and T. Yamagata, "Validation of the WRF regional climate model over the subregions of Southeast Asia : climatology and interannual variability," *Clim. Res.*, vol. 71, pp. 263–280, 2017.

[13] C. Ummenhofer, R. D. Arrigo, K. Anchukaitis, M. Hernandez, and E. Cook, "Asian monsoon variability from the monsoon Asia drought atlas (MADA) and Links to Indo-Pacific Climate," vol. 16, p. 13249, 2014.

[14] K. E. Trenberth, "El Niño southern oscillation (ENSO)," *J Climate*, vol. 23, pp. 1-11, 2010.

[15] D. Bonal, B. Burban, C. Stahl, F. Wagner, B. Hérault, and F. Wagner, "The response of tropical rainforests to drought — lessons from recent research and future prospects," *Annu. For. Sci.*, vol. 73, pp. 27–44, 2016.

[16] O. Dubovyk, T. Landmann, B. F. N. Erasmus, A. Tewes, and J. Schellberg, "Monitoring vegetation dynamics with medium resolution MODIS-EVI time series at sub-regional scale in southern Africa," *Int. J. Appl. Earth Obs. Geoinf.*, vol. 38, no. 1, pp. 175–183,

2015.

[17] T. Hwang, L. E. Band, C. F. Miniat, C. Song, P. V. Bolstad, J. M. Vose, and J. P. Love, "Divergent phenological response to hydroclimate variability in forested mountain watersheds," *Glob. Chang. Biol.*, vol. 20, no. 8, pp. 2580–2595, 2014.

[18] J. Peñuelas, I. Filella, X. Zhang, L. Llorens, R. Ogaya, F. Lloret, P. Comas, M. Estiarte, and J. Terradas, "Complex spatiotemporal phenological shifts as a response to rainfall changes," *N. Biotechnol.*, vol. 161, pp. 837–846, 2004.

[19] P. K. Diem, U. Pimple, A. Sitthi, P. Varnakovida, R. Kaewthongrach, and A. Chidthaisong, "Responses of tropical deciduous forest phenology to climate variation in Northern Thailand," in *International Conference on Environmental Research and Technology (ICERT 2017)*, 2017, pp. 340–345.

[20] T. Suepa, J. Qi, S. Lawawirojwong, and J. P. Messina, "Understanding spatio-temporal variation of vegetation phenology and rainfall seasonality in the monsoon Southeast Asia," *Environ. Res.*, vol. 147, pp. 621–629, 2016.

[21] C. Prabakaran, C. P. Singh, S. Panigrahy, and J. S. Parihar, "Retrieval of forest phenological parameters from remote sensing-based NDVI time-series data Retrieval of forest phenological parameters from remote sensing-based NDVI time-series data," *Curr. Sci.*, vol. 105, no. 6, pp. 795–802, 2013.

[22] P. Hanpattanakit, "Temporal variations of soil respiration in a dry dipterocarp forest," King Mongkut's University of Technology Thonburi, Bangkok, Thailand, 2013.

[23] N. T. Hoan and R. Tateishi, *Global MODIS 250 m dataset for 10 years (2003-2012) User ' s Manual*. Center for Environmental Remote Sensing (CEReS) Chiba University, 2013.

[24] L. Eklundha and P. Jönssonb, "TIMESAT 3.1 software manual," *Lund Univ. Sweden*, pp. 1–82, 2012.

[25] NOAA, "Cold and warm episodes by season," 2017. [Online]. Available: http://origin.cpc.ncep.noaa.gov/products/analysis_monitoring/ensostuff/ONI_v5.php. [Accessed: 31-Dec-2017].

[26] K. P. Singh and C. P. Kushwaha, "Paradox of leaf phenology : *Shorea robusta* is a semi-evergreen species in tropical dry deciduous forests in India," *Curr. Sci.*, vol. 88, no. 10, pp. 1820–1824, 2005.

[27] S. Pau, G. S. Okin, and T. W. Gillespie, "Asynchronous response of tropical forest leaf phenology to seasonal and el niño -driven drought," *PLoS One*, vol. 5, no. 6, 2010.

[28] M. Sanwangsri, A. Chidthaisong, and P. Hanpattanakit, "Responses of CO_2 exchange to drought in dry dipterocarp forest , Western Thailand," in *3rd iLEAPS International Science Conference*, 2011.

[29] M. Sanwangsri, *Seasonal dynamics of CO_2 and energy exchange in dry dipterocarp forest of western Thailand*. King Mongkut's University of Technology Thonburi, Bangkok, Thailand, 2017.

TOWARDS AN AUTOMATIC CHANGE DETECTION SYSTEM FOR LAND USE LAND COVER

Cheng-Chien Liu
Global Earth Observation and Data Analysis Centre, National Cheng Kung University
No 1, Ta-Hsueh Road, Tainan, Taiwan
ccliu88@mail.ncku.edu.tw

ABSTRACT

Detecting the changes of land use and land cover (LULC) from space has long been a main goal of satellite remote sensing. Although various reliable approaches and tools were proposed and developed, and the potential of time series observations was clearly demonstrated, there is no such a system to provide the near-real time changes of LULC to the general publics in a fully automated fashion. This paper reports the efforts to develop an automatic change detection system for land use land cover in Taiwan. Thanks to the success of Sentinel-2 mission and the Copernicus programme that adopt the free and open data policy, all Sentinel-2 high-temporal (5 days), -spatial (10m), -spectral (13 bands), and -radiometric (12 bits) data are made available systematically and freely to all registered users. They serve as an ideal and cost-effective data source for change detection of LULC. The cloud and its cast shadow are both very strong signals that would represent a large fraction of changes by simply comparing two images. In this work, the cloud mask is calculated by the atmospheric correction algorithm (Sen2cor), and its cast shadow is determined by the similarity measurements, following the same approach of functional mask developed for Landsat. After excluding the union mask of cloud and cloud shadow, the subtle and crucial signals of changes can be successfully retrieved from the image pair. They serve as a reliable information for change detection of LULC. Based on the automatic image processing systems developed for Formosat-2 and Landsat-8 imagery, the capacity has been expanded to process and detect the changes for each pair of Sentinel-2 images. All results are provided as browsable image and vector tiles to the general public through the internet in near real-time. The same system and service can be provided to the other countries as well.

Keywords: *Land use Land Cover, Change Detection, Sentinel-2, Cloud, Shadow*

MEDIAN GROUND MODELS FOR DRONE LIDAR FROM VELODYNE PUCK SYSTEMS

Martin Isenburg
Chief Scientist, rapidlasso GmbH
Caspariagasse 16, 97286 Sommerhausen, Germany
martin@rapidlasso.com

ABSTRACT

Points clouds from UAVs have become a common sight. Cheap consumer drones equipped with cameras produce points from images with increasing quality as photogrammetry software is improving. But vegetation is always a show stopper for point clouds generated from imagery data. Only an active sensing technique such as laser scanning can penetrate through the vegetation and generate points on the ground under the canopy of a forested area. Advances in UAV technology and the miniaturization of LiDAR systems have allowed lasers-scanning solutions for drones to enter the market. One such system is the "YellowScan Surveyor" built around the Velodyne VLP-16 Puck LiDAR scanner and the Applanix APX15 single board GNSS-Inertial solution.

A common challenge observed in LiDAR data generated by the Velodyne Puck is that surfaces are not as "crisp" as those generated by other laser scanners. Flat and open terrain surfaces are described by a layer of points with a "thickness" of a few centimeter. Standard ground classification routines will "latch onto" the lowermost envelope of these thick point layers and therefore produce a sub-optimal Digital Terrain Model (DTM).

We show how to deal with "thickness" in a layer of points describing a ground surface. We first produce a "lowest ground" which we then widen into a "thick ground" from which we then derive "median ground" points that create a plausible terrain representation when interpolated by a Delaunay triangulation and rasterized onto a DTM. We present how to process an example scan of the Château de Flaugergues in Montpellier, France. We will make this data set available to the audience so they will be able reproduce the presented results on their own.

Keywords: LiDAR, ground classification, median DTM, Velodyne Puck, drone survey

1. INTRODUCTION

Points clouds from UAVs have become a common sight. Cheap consumer drones equipped with cameras produce points from images with increasing quality as photogrammetry software is improving. But vegetation is always a show stopper for point clouds generated from imagery data. Only an active sensing technique such as laser scanning can penetrate through the vegetation and generate points on the ground under the canopy of a forested area. Advances in UAV technology and the miniaturization of LiDAR systems have allowed lasers-scanning solutions for drones to enter the market.

Last summer we attended the LiDAR for Drone 2017 Conference by YellowScan and processed some data sets flown with their Surveyor system that is built around the Velodyne VLP-16 Puck LiDAR scanner and the Applanix APX15 single board GNSS-Inertial solution. One common challenge observed in LiDAR data generated by the Velodyne Puck is that surfaces are not as “crisp” as those generated by other laser scanners. Flat and open terrain surfaces are described by a layer of points with a “thickness” of a few centimeter as you can see in Figure 1 and Figure 2 below. These visualizations uses a 10 meter by 5 meter cut-out of from this data set with the coordinate range [774280,774290) in x and [6279463,6279468) in y. Standard ground classification routines will “latch onto” the lowermost envelope of these thick point layers and therefore produce a sub-optimal Digital Terrain Model (DTM).

Figure 1. Left: Triangulation of all last returns of mostly flat 10 meter by 5 meter area. Points are colored by flightline ID. Middle: Zooming shows the vertical spread of the points. Points are colored by flightline ID. Right: Zooming further in and pink like with length of 8 cm for scale. Points are colored by flightline ID.

2. METHODOLOGY

Once you decompress the RAR file (e.g. with the UnRar.exe freeware) you will find six raw flight strips in LAS format and the trajectory of the UAV in ASCII text format as it was provided by YellowScan.

```
E:\LAStools\bin>dir Flaugergues
06/27/2017 08:03 PM 146,503,985 Flaugergues_test_demo_ppk_L1.las
06/27/2017 08:02 PM  91,503,103 Flaugergues_test_demo_ppk_L2.las
06/27/2017 08:03 PM 131,917,917 Flaugergues_test_demo_ppk_L3.las
06/27/2017 08:03 PM 219,736,585 Flaugergues_test_demo_ppk_L4.las
06/27/2017 08:02 PM 107,705,667 Flaugergues_test_demo_ppk_L5.las
06/27/2017 08:02 PM  74,373,053 Flaugergues_test_demo_ppk_L6.las
06/27/2017 08:03 PM   7,263,670 Flaugergues_test_demo_ppk_traj.txt
```

As usually we start with quality checking by visual inspection with 'lasview' and by creating a textual report with 'lasinfo'. See Appendix A for the resulting report.

```
E:\LAStools\bin>lasview -i Flaugergues_test_demo_ppk_L1.las

E:\LAStools\bin>lasinfo -i Flaugergues_test_demo_ppk_L1.las
```

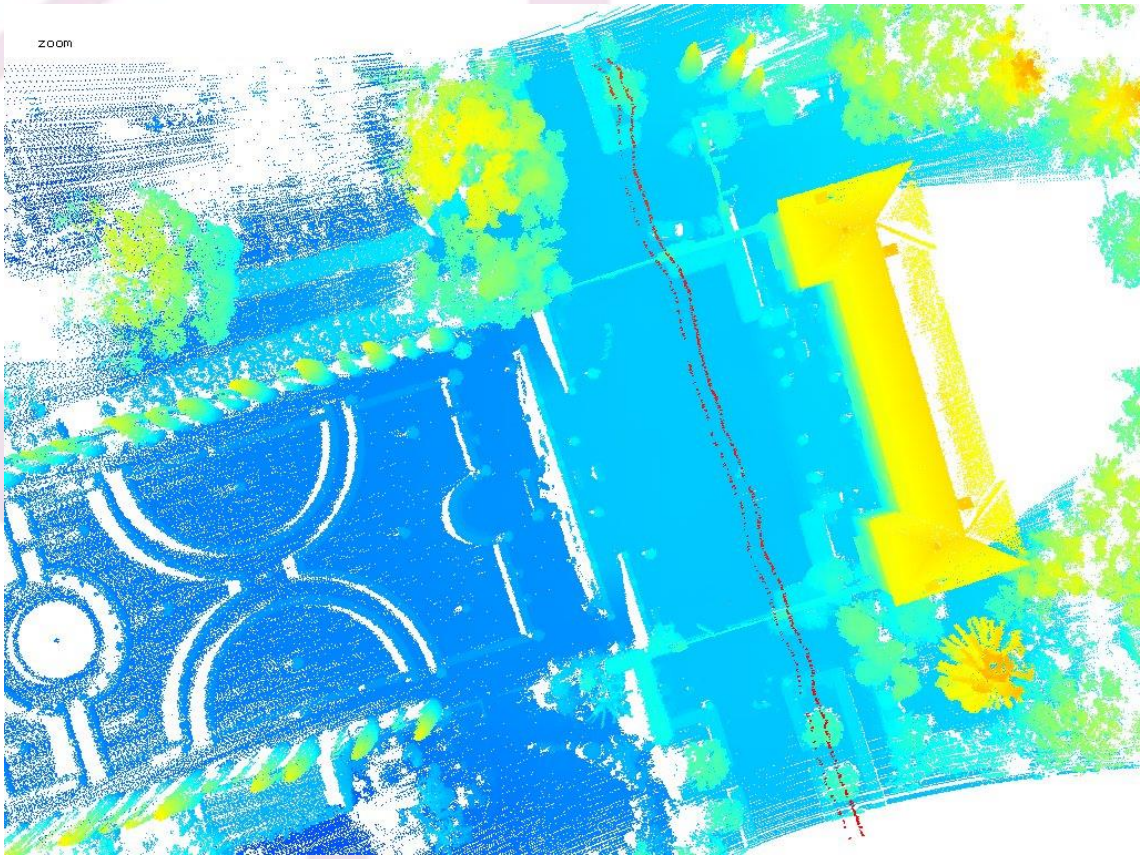

Figure 4. The raw LAS file "Flaugergues_test_demo_ppk_L1.las" colored by elevation.

Nicely visible are the circular scanning patterns of the Velodyne VLP-16 Puck. We also notice that the trajectory of the UAV can be seen in the lasview visualization because the Puck was scanning the drone's own landing gear. The lasinfo report (see Appendix

A) tells us that point coordinates are stored with too much resolution (mm) and that points do not need to be stored using point type 3 (with RGB colors) because all RGB values are zero. We fix this with an initial run of 'las2las' and also compress the raw strips to the LAZ format on 4 CPUs in parallel.

```
las2las -i Flaugergues\*.las ^
        -rescale 0.01 0.01 0.01 ^
        -auto_reoffset ^
        -set_point_type 1 ^
        -odir Flaugergues\strips_raw -olaz ^
        -cores 4
```

Next we do the usual check for flightline alignment with 'lasoverlap' which we consider to be by far the most important quality check. We compare the lowest elevation from different flightline per 25 cm by 25cm cell in all overlap areas. We consider a vertical difference of up to 5 cm as acceptable (color coded as white) and mark differences of over 30 cm (color coded as saturated red or blue).

```
lasoverlap -i Flaugergues\strips_raw\*.laz -faf ^
           -step 0.25 ^
           -min_diff 0.05 -max_diff 0.3 ^
           -odir Flaugergues\quality -o overlap.png
```

The vertical difference in open areas between the flightlines is slightly above 5 cm which we consider acceptable in this example. Depending on the application we recommend to investigate further where these differences come from and what consequences they may have for post processing. We also create a color-coded visualization of the last return density per 25 cm by 25 cm cell using 'lasgrid' with blue meaning less than 100 returns per square meter and red meaning more than 4000 returns per square meter.

```
lasgrid -i Flaugergues\strips_raw\*.laz -merged ^
        -keep_last ^
        -step 0.25 ^
        -point_density ^
        -false -set_min_max 100 4000 ^
        -odir Flaugergues\quality -o density_100_4000.png
```

Figure 5. Color codes number of overlapping flightlines. Color codes vertical difference between flightlines. Color coded density of last returns per square meter for each 25 cm by 25 cm cell. Blue means 100 or less last returns per square meter. Red means 4000 or more last returns per square meter

As usual we start the LiDAR processing by reorganizing the flightlines into square tiles. Because of the variability in the density that is evident in the visualization above we use 'lastile' to create an adaptive tiling that starts with 200 m by 200 m tiles and then iterate to refine those tiles with over 10 million points down to smaller 25 m by 25 m tiles.

```
lastile -i Flaugergues\strips_raw\*.laz ^
        -apply_file_source_ID ^
```

```
        -tile_size 200 -buffer 8 -flag_as_withheld ^
        -refine_tiling 10000000 ^
        -odir Flaugergues\tiles_raw -o flauge.laz

lastile -i Flaugergues\tiles_raw\flauge*_200.laz ^
        -refine_tiles 10000000 ^
        -olaz ^
        -cores 4

lastile -i Flaugergues\tiles_raw\flauge*_100.laz ^
        -refine_tiles 10000000 ^
        -olaz ^
        -cores 4

lastile -i Flaugergues\tiles_raw\flauge*_50.laz ^
        -refine_tiles 10000000 ^
        -olaz ^
        -cores 4
```

Subsequent processing is faster when the points have a spatially coherent order. Therefore we rearrange the points into standard space-filling z-order using a call to 'lassort'. We run this in parallel on as many cores as it makes sense (i.e. not using more cores than there are physical CPUs).

```
lassort -i Flaugergues\tiles_raw\flauge*.laz ^
        -odir Flaugergues\tiles_sorted -olaz ^
        -cores 4
```

Next we classify those points as noise that are isolated on a 3D grid of 1 meter cell size using 'lasnoise' as classification 7. See the README file of 'lasnoise' for a description on the exact manner in which the isolated points are classified. We do this to eliminate low noise points that would otherwise cause trouble in the subsequent processing.

```
lasnoise -i Flaugergues\tiles_sorted\flauge*.laz ^
         -step 1 -isolated 5 ^
         -odir Flaugergues\tiles_denoised -olaz ^
         -cores 4
```

Next we mark a subset of lowest points on a 2D grid of 10 cm cell size with a different classification code 8 using 'lasthin' while ignoring the noise points with classification code 7 that were marked as noise in the previous step.

```
lasthin -i Flaugergues\tiles_denoised\flauge*.laz ^
        -ignore_class 7 ^
        -step 0.1 -lowest ^
        -classify_as 8 ^
        -odir Flaugergues\tiles_lowest -olaz ^
        -cores 4
```

Considering only the resulting points marked with classification 8 we then create a temporary ground classification that we refer to as the "lowest ground". For this we

run 'lasground' with a set of suitable parameters that were found by experimentation on two of the most complex tiles from the center of the survey.

```
lasground -i Flaugergues\tiles_lowest\flauge*.laz ^
          -ignore_class 0 7 ^
          -step 5 -hyper_fine -bulge 1.5 -spike 0.5 ^
          -odir Flaugergues\tiles_lowest_ground -olaz ^
          -cores 4
```

We then "thicken" this "lowest ground" by classifying all points that are between 2 cm below and 15 cm above the lowest ground to a temporary classification code 6 using the 'lasheight' tool. Depending on the spread of points in your data set you may want to tighten this range accordingly, for example when processing the flightlines acquired by the Velodyne Puck individually. We picked our range based on the visual experiments with "drop lines" and "rise lines" in the 'lasview' viewer shown in earlier images. The results for "lowest ground" and the generated "thick ground" are shown in Figure 5.

```
lasheight -i Flaugergues\tiles_lowest_ground\flauge*.laz ^
          -do_not_store_in_user_data ^
          -classify_between -0.02 0.15 6 ^
          -odir Flaugergues\tiles_thick_ground -olaz ^
          -cores 4
```

The final ground classification is obtained by creating the "median ground" from the "thick ground". This uses a relatively new option in the 'lasthin' tool of LAStools. The new '-percentile 50 10' option selects the point that is closest to the specified percentile of 50 of all point elevations within a grid cell of a specified size given there are at least 10 points in that cell. The selected point either survives the thinning operation or gets marked with a specified classification code or flag.

```
lasthin -i Flaugergues\tiles_thick_ground\flauge*.laz ^
        -ignore_class 0 1 7 ^
        -step 0.1 -percentile 50 10 ^
        -classify_as 8 ^
        -odir Flaugergues\tiles_median_ground_10_10cm -olaz ^
        -cores 4
```

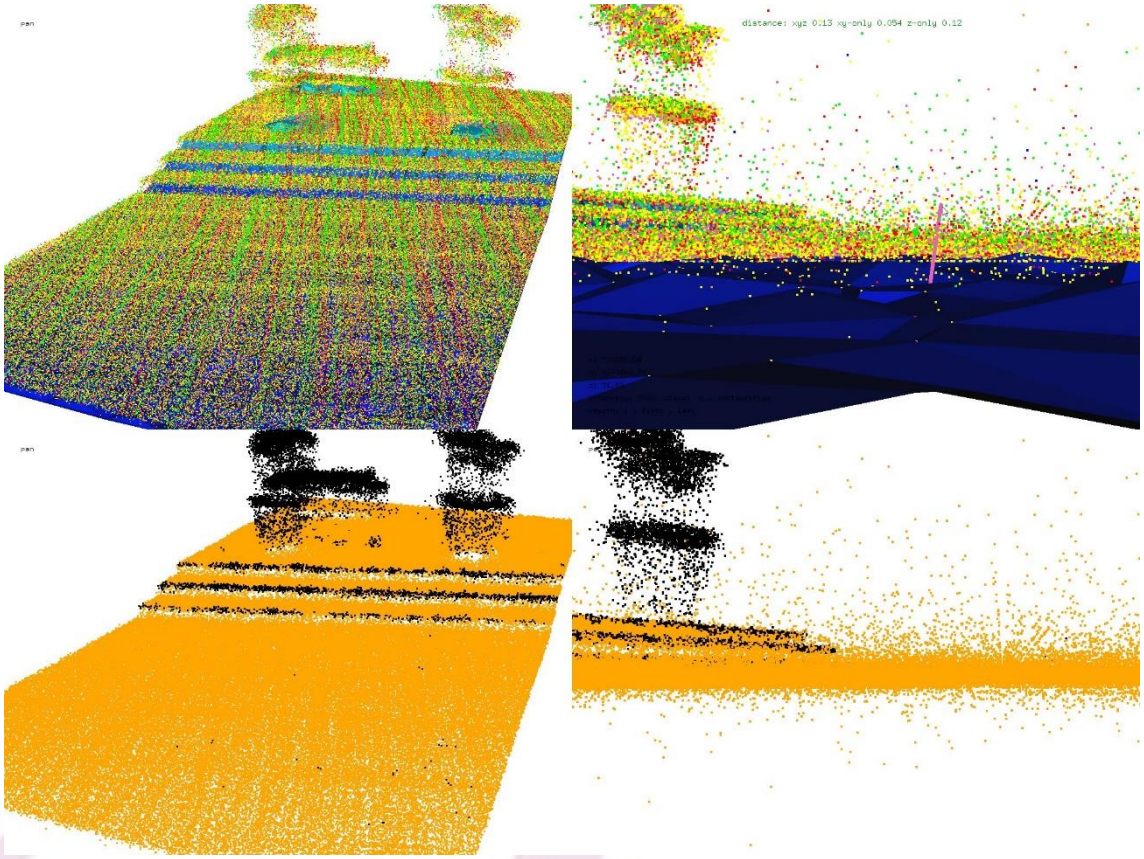

Figure 5. Top: lowest ground points triangulated, other points colored by flightline ID. Bottom: Thickened ground points in orange. Left: full view. Right: zoomed-in view.

```
lasthin -i Flaugergues\tiles_median_ground_10_10cm\%NAME%*.laz ^
        -ignore_class 0 1 7 ^
        -step 0.2 -percentile 50 10 ^
        -classify_as 8 ^
        -odir Flaugergues\tiles_median_ground_10_20cm -olaz ^
        -cores 4

lasthin -i Flaugergues\tiles_median_ground_10_20cm\%NAME%*.laz ^
        -ignore_class 0 1 7 ^
        -step 0.4 -percentile 50 10 ^
        -classify_as 8 ^
        -odir Flaugergues\tiles_median_ground_10_40cm -olaz ^
        -cores 4

lasthin -i Flaugergues\tiles_median_ground_10_40cm\flauge*.laz ^
        -ignore_class 0 1 7 ^
        -step 0.8 -percentile 50 10 ^
        -classify_as 8 ^
        -odir Flaugergues\tiles_median_ground_10_80cm -olaz ^
        -cores 4
```

3. RESULTS

The images shown in Figure 6 compare a triangulation of the median ground points with a triangulation of the highest and the lowest points per 10 cm by 10 cm cell. This visually demonstrate that – at least in open areas – we really have computed a median ground surface that serves as a plausible DTM for point clouds exhibiting the typical "thickness" or "fluffiness" found in the scans of the Velodyne Puck scanning system.

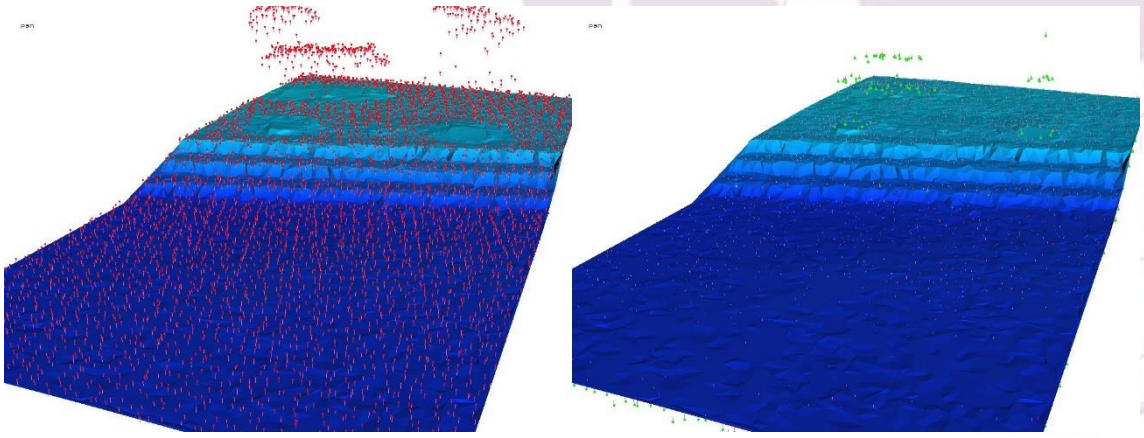

Figure 6. Comparing triangulation of median ground points to lowest returns on a 10 cm by 10 cm grid with 5 cm rise lines. Comparing triangulation of median ground points to highest returns on a 10 cm by 10 cm grid with 5 cm drop lines.

Finally we raster the tiles with the 'las2dem' tool onto binary elevation grids in BIL format. Here we make the resolution dependent on the tile size, giving the 25 meter and 50 meter tiles the highest resolution of 10 cm and rasterize the 100 meter and 200 meter tiles at 20 cm and 40 cm respectively.

```
las2dem -i Flaugergues\tiles_median_ground_10_80cm\*_25.laz ^
        -i Flaugergues\tiles_median_ground_10_80cm\*_50.laz ^
        -keep_class 8 ^
        -step 0.1 -use_tile_bb ^
        -odir Flaugergues\tiles_dtm -obil ^
        -cores 4

las2dem -i Flaugergues\tiles_median_ground_10_80cm\*_100.laz ^
        -keep_class 8 ^
        -step 0.2 -use_tile_bb ^
        -odir Flaugergues\tiles_dtm -obil ^
        -cores 4

las2dem -i Flaugergues\tiles_median_ground_10_80cm\*_200.laz ^
        -keep_class 8 ^
        -step 0.4 -use_tile_bb ^
        -odir Flaugergues\tiles_dtm -obil ^
        -cores 4
```

Because all LAStools can read BIL files via on the fly conversion from rasters to points we can visually inspect the resulting elevation rasters with the 'lasview' tool. By adding the '-faf' or 'files_are_flightlines' argument we treat the BIL files as if they were

different flightlines which allows us to assign different color to points from different files to better inspect the transitions between tiles. The '-points 10000000' argument instructs 'lasview' to load up to 10 million points into memory instead of the default 5 million. The resulting DTM composited of these tiles is shown in Figure 7.

```
lasview -i Flaugergues\tiles_dtm\*.bil -faf -points 10000000
```

For visual comparison we also produce a DSM and create hillshades. Note that the workflow for DSM creation shown below produces a "highest DSM" that will always be a few centimeter above the "median DTM". This will be noticeable only in open areas of the terrain where the DSM and the DTM should coincide and their elevation should be identical.

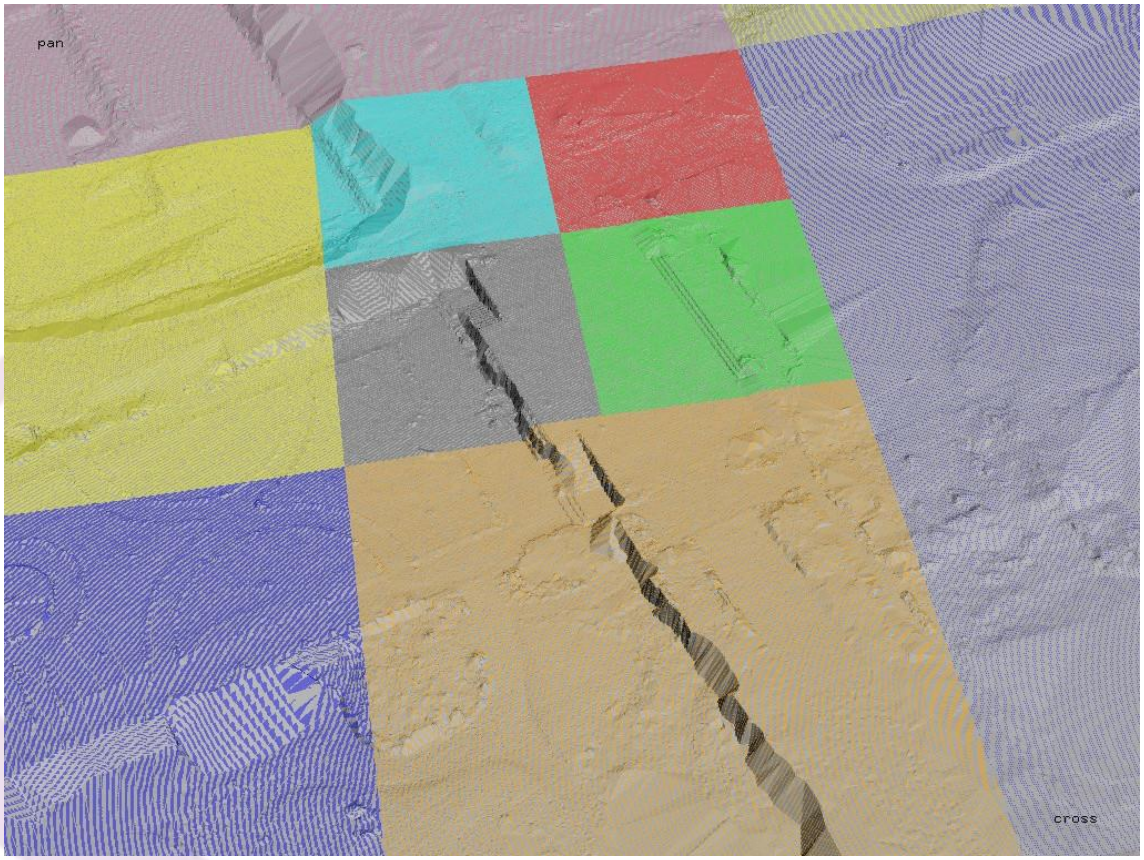

Figure 7. Final raster tiles in BIL format of three different sizes form seamless DTM.

```
lasthin -i Flaugergues\tiles_denoised\flauge*.laz ^
        -keep_z_above 110 ^
        -filtered_transform ^
        -set_classification 18 ^
        -ignore_class 7 18 ^
        -step 0.1 -highest ^
        -classify_as 5 ^
        -odir Flaugergues\tiles_highest -olaz ^
        -cores 4

las2dem -i Flaugergues\tiles_highest\*_25.laz ^
        -i Flaugergues\tiles_highest\*_50.laz ^
```

```
        -keep_class 5 ^
        -step 0.1 -use_tile_bb ^
        -odir Flaugergues\tiles_dsm -obil ^
        -cores 4

las2dem -i Flaugergues\tiles_highest\*_100.laz ^
        -keep_class 5 ^
        -step 0.2 -use_tile_bb ^
        -odir Flaugergues\tiles_dsm -obil ^
        -cores 4

las2dem -i Flaugergues\tiles_highest\*_200.laz ^
        -keep_class 5 ^
        -step 0.4 -use_tile_bb ^
        -odir Flaugergues\tiles_dsm -obil ^
        -cores 4
```

We thank YellowScan for challenging us to process their drone LiDAR with LAStools in order to present results at their LiDAR for Drone 2017 Conference and for sharing several example data sets with us, including the one used here.

APPENDIX A

```
lasinfo (171011) report for Flaugergues_test_demo_ppk_L1.las
reporting all LAS header entries:
 file signature: 'LASF'
 file source ID: 1
 global_encoding: 1
 project ID GUID data 1-4: 00000000-0000-0000-0000-000000000000
 version major.minor: 1.2
 system identifier: 'YellowScan Surveyor'
 generating software: 'YellowReader by YellowScan'
 file creation day/year: 178/2017
 header size: 227
 offset to point data: 297
 number var. length records: 1
 point data format: 3
 point data record length: 34
 number of point records: 4308932
 number of points by return: 4142444 166488 0 0 0
 scale factor x y z: 0.001 0.001 0.001
 offset x y z: 774282 6279505 92
 min x y z: 774152.637 6279377.623 82.673
 max x y z: 774408.344 6279541.646 116.656
variable length header record 1 of 1:
 reserved 0
 user ID 'LASF_Projection'
 record ID 34735
 length after header 16
 description ''
 GeoKeyDirectoryTag version 1.1.0 number of keys 1
 key 3072 tiff_tag_location 0 count 1 value_offset 2154 - RGF93 /
```

```
Lambert-93
reporting minimum and maximum for all LAS point record entries …
 X -129363 126344
 Y -127377 36646
 Z -9327 24656
 intensity 0 65278
 return_number 1 2
 number_of_returns 1 2
 edge_of_flight_line 0 0
 scan_direction_flag 0 0
 classification 0 0
 scan_angle_rank -120 120
 user_data 75 105
 point_source_ID 1 1
 gps_time 219873.160527 219908.550379
 Color R 0 0
 G 0 0
 B 0 0
number of first returns: 4142444
number of intermediate returns: 0
number of last returns: 4142444
number of single returns: 3975956
overview over number of returns of given pulse: 3975956 332976 0 0 0
0 0
histogram of classification of points:
 4308932 never classified (0)
```

REFERENCES

[1] http://rapidlasso.com/2017/10/29/processing-drone-lidar-from-yellowscans-surveyor-a-velodyne-puck-based-system/

S – 5 – 2 SCGI022

A CROSS-ANCHOR UWB LOCATING SCHEME IN TDOA MODE FOR WIDE AREA UWB NETWORK

Zhang Xiaoguang[1], Liu Zhenyao[2]., Gong Yingkui[3], Deng Pingke[4]
[1-5] *(Academy of Opto-Electronics,Chinese Academy of sciences,Beijing 100080)*
1. *zxg@aoe.ac.cn, 2. lzyao@aoe.ac.cn,3.ykgong@aoe.ac.cn,4.pkdeng@aoe.ac.cn,5*

ABSTRACT

For indoor or GNSS signal destroyed environments, too many locating methods have been proposed and applied, wifi, blue tooth, SLAM ,etc.

And UWB (ultra-wide band) is one of the attractive methods with its inhibition of multipath interference (with narrow pulse character, UWB receiver can accurately get the first path signal arriving time). Smartly deploying UWB signal transmitters (anchors) based on the spatial structure, under the TDOA algorithm, can ensure that enough anchor points get the UWB transmitter signal (Tag) in the direct link. Then the accurate location information can be obtained by calculating the hyperbola focus point based on four anchors. But its application for wide areas is limited by various technical issues, Non-simultaneous signal measurement in TWR (two-way ranging) mode, anchor synchronization in TDOA mode, and cross-anchor locating service problem, etc.

In this paper, it mainly focuses on the last problem. Under TDOA mode, UWB-locating network constructing problem (*wireless synchronization*) in wide area is discussed, a related cross-anchor UWB locating scheme for wide area is proposed, and the UWB Test board system structure and its test result are deployed.

Keywords: *TDOA, wireless synchronization, UWB-locating network*

1. UWB-TDOA PRINCIPLE

The localization system architecture developed is shown in Fig. 1. Anchor nodes measure time of arrival of packets transmitted by tags and the reference node. Results are send to the System controller over WiFi/wired interface. The controller evaluates tag's position. The system implements TDOA positioning technique so the anchors synchronization is needed. In this paper the synchronization problem is not discussed, the method can be find in [10].

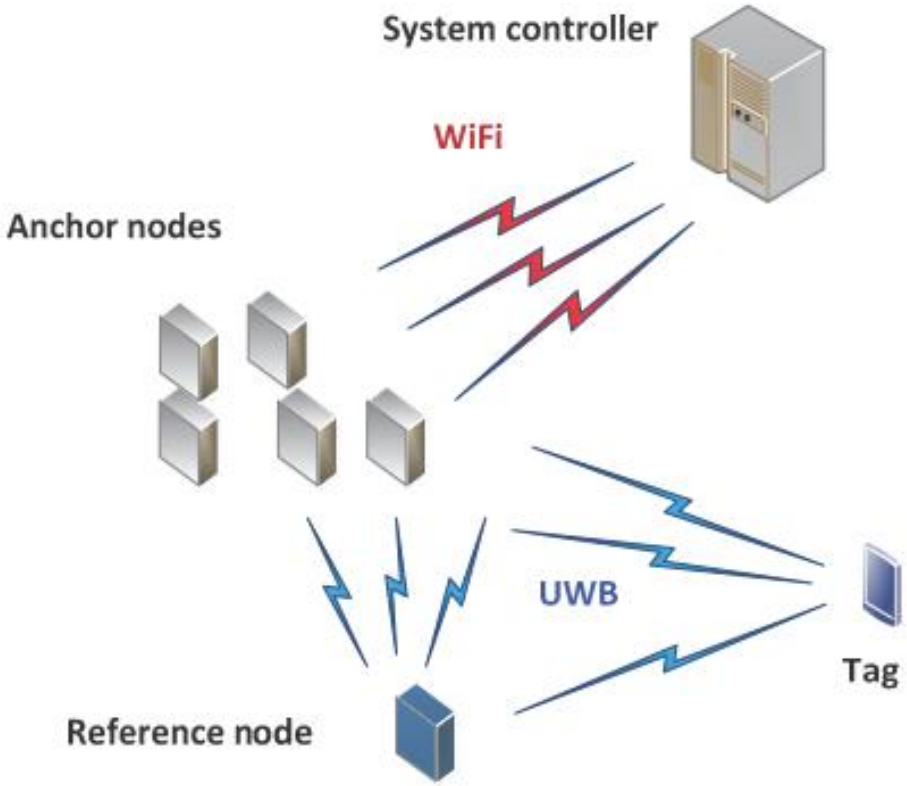

fig 1 UWB-TDOA system

2. CORSS ANCHOR MODELING

This paper mainly focus on tag moving from one anchor domain to another. The basic struct of cross TDOA-system is demonstrated in **Error! Reference source not found.**, we call locating crossing one cell to its neighbor cell "cross-anchor UWB locating".

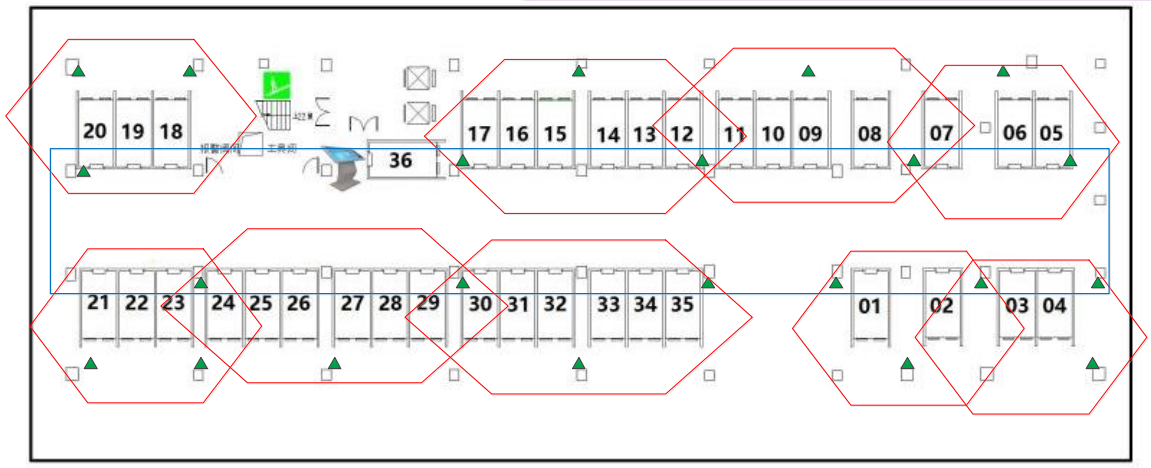

fig 2 cross UWB-TDOA system

For multi-system co-location, state transition model and multi-system parallel observing model can be expressed as:

$$\mathbf{x}(k+1)=\mathbf{F}(k)\mathbf{x}(k)+\mathbf{G}\mathbf{w}(k) \tag{1}$$

$$\mathbf{z}_i(k+1)=\mathbf{H}_i(k+1)\mathbf{x}(k+1)+\mathbf{v}_i(k+1) \tag{2}$$

Where $\mathbf{x}(k)$ is state vector, $\mathbf{z}_i(k+1)$ is observing vector for system I in time $k+1$, $\mathbf{H}_i(k+1)$ is observing matrix, $\mathbf{F}(k)$ is state trainsition matrix, $\mathbf{G}$ is noise trainsition matrix and is invariable, and $\mathbf{w}(k)$、$\mathbf{v}_i(k+1)$ is process noise and observing noise, which are WGN (white gauss noise).

In this paper, considering location character performance changing in the process of corss-cell and the cells weight changing in the whole fusing system, a one-step Markov chain is used to describe the process:

$$T_{ij}=P\{\varepsilon_j(k+1)\,|\,\varepsilon_i(k),X^k\} \tag{3}$$

Where $\varepsilon_j(k+1)$ denote system j is effective in time $k+1$, $X^k=\{\mathbf{x}(j)\}_{j=1}^{k}$ denote the state vector set, and $\sum_{j=1}^{n}T_{ij}=1$.

3. BAYESIAN THEORY BASED CROSS-ANCHOR LOCATION

3.1 One-Step Markov Chain Based Cross-Cell Location

Before filtering, based on system priori probability and cross-cell conditional probability, the corss-cell locationing interacting is finished:

$$\begin{aligned}&\beta_{i|j}(k\,|\,k+1)\\&=P\left\{\varepsilon_i(k)\,|\,\varepsilon_j(k+1),X^k\right\}\\&=\frac{1}{\bar{b}_j}T_{ij}\beta_i(k)\end{aligned}\tag{4}$$

Where $\beta_i(k)=P\left\{\varepsilon_i(k)\,|\,X^k\right\}$ is priori probability of UWB cell i in time k, and based on Chapman-Kolmogorov theorem, the normalization factor is:

$$\begin{aligned}\bar{b}_j&=P\left\{\varepsilon_j(k+1)\,|\,X^k\right\}\\&=\sum_{i=1}^{n}P\left\{\varepsilon_j(k+1)\,|\,\varepsilon_i(k),X^k\right\}\\&\times P\left\{\varepsilon_i(k)\,|\,X^k\right\}\\&=\sum_{i=1}^{n}T_{ij}\beta_i(k)\end{aligned}\tag{5}$$

The location information and noise variance mixing can be got in time $k+1$:

$$\hat{\mathbf{z}}^{oj}(k+1\,|\,k+1)=\sum_{i=1}^{n}\mathbf{z}_i(k+1)\beta_{i|j}(k\,|\,k+1)\tag{6}$$

$$\begin{aligned}&\mathbf{R}^{oj}(k+1\,|\,k+1)\\&=\sum_{i=1}^{n}\beta_{i|j}(k\,|\,k+1)\{\mathbf{R}_i(k+1)\\&+\left[\mathbf{z}_i(k+1)-\hat{\mathbf{z}}^{oj}(k+1\,|\,k+1)\right]\\&\times\left[\mathbf{z}_i(k+1)-\hat{\mathbf{z}}^{oj}(k+1\,|\,k+1)\right]^T\}\end{aligned}\tag{7}$$

3.2 PARALLEL FILTERING

Multi-system location and noise variance are used as input for parallel filtering. Here for simplicity, expressed kalman filter is used:

Prediction value can be calculated as:

$$\mathbf{x}(k+1\,|\,k)=\mathbf{F}(k)\mathbf{x}(k\,|\,k)\tag{8}$$

$$\mathbf{P}(k+1\,|\,k)=\mathbf{F}(k)\mathbf{P}(k\,|\,k)\mathbf{F}^T(k)+\mathbf{GQG}^T\tag{9}$$

Where $\mathbf{G}$ is noise trainsition matrix, and the innovation and noise variance of system j can be calculated:

$$\begin{aligned}&\mathbf{v}_j(k+1)\\&=\hat{\mathbf{z}}^{oj}(k+1\,|\,k+1)\\&-\mathbf{H}_i(k+1)\mathbf{x}(k+1\,|\,k)\end{aligned}\tag{10}$$

$$\begin{aligned}&S_j(k+1)\\&=\mathbf{H}_j(k+1)\mathbf{P}(k+1\,|\,k)\mathbf{H}_j^T(k+1)\\&+\mathbf{R}^{oj}(k+1\,|\,k+1)\end{aligned}\tag{11}$$

Gaining factor can be calculated as :

$$K_j(k+1) = \mathbf{P}(k+1|k)\mathbf{H}_j^T(k+1)S_j^{-1}(k+1) \tag{12}$$

The state and variance are：

$$\begin{aligned} &\mathbf{x}_j(k+1|k+1) \\ &= \mathbf{x}(k+1|k) + K_j(k+1)\mathbf{v}_j(k+1) \end{aligned} \tag{13}$$

$$\begin{aligned} &\mathbf{P}_j(k+1|k+1) \\ &= \mathbf{P}(k+1|k) \\ &-K_j(k+1)S_j(k+1)K_j(k+1)^T \end{aligned} \tag{14}$$

3.3 The Updated Probability

The innovation variance and updated cell probability can be calculated as:

$$\begin{aligned} &\beta_j(k+1) \\ &= P\left\{\varepsilon_j(k+1)\,|\,X^{k+1}\right\} \\ &= P\left\{\varepsilon_j(k+1)\,|\,X^k, \left\{\mathbf{z}_j(k+1)\right\}_{j=1}^n\right\} \\ &= \frac{1}{b} \times P\left\{\left\{\mathbf{z}_j(k+1)\right\}_{j=1}^n \,|\, \varepsilon_j(k+1), X^k\right\} \\ &\times P\left\{\varepsilon_j(k+1)\,|\,X^k\right\} \\ &= \frac{1}{b} \times P\left\{\mathbf{z}_j(k+1)\,|\,\varepsilon_j(k+1), X^k\right\} \times \bar{b}_j \end{aligned} \tag{15}$$

Where $\left\{\mathbf{z}_j(k+1)\right\}_{j=1}^n$ donotes multi-cell observation vector set in time $k+1$

$$\begin{aligned} b &= P\left\{\mathbf{z}_j(k+1)\,|\,X^k\right\} \\ &= \sum_{j=1}^n P\left\{\mathbf{z}_j(k+1)\,|\,\varepsilon_j(k+1), X^k\right\} \times \bar{b}_j \end{aligned} \tag{16}$$

$$\begin{aligned} &P\left\{\mathbf{z}_j(k+1)\,|\,\varepsilon_j(k+1), X^k\right\} \\ &= N\left[\mathbf{v}_j(k+1) : 0, S_j(k+1)\right] \end{aligned} \tag{17}$$

3.4 Two Cross-Cell Based Locating

Based on the cell priori probability, the final locating estimation $\mathbf{x}(k+1|k+1)$ and covariance $P(k+1|k+1)$ can be calculated:

$$\begin{aligned}&\mathbf{x}(k+1|k+1)\\&=\sum_{j=1}^{n}\mathbf{x}_j(k+1|k+1)\\&\times P\left\{\varepsilon_j(k+1)|X^k,\left\{\mathbf{z}_j(k+1)\right\}_{j=1}^{n}\right\}\\&=\sum_{j=1}^{n}\mathbf{x}_j(k+1|k+1)\beta_j(k+1)\end{aligned}\tag{18}$$

$$\begin{aligned}&P(k+1|k+1)\\&=\sum_{j=1}^{n}\beta_j(k+1)\{P_j(k+1|k+1)\\&+\left[\mathbf{x}_j(k+1|k+1)-\mathbf{x}(k+1|k+1)\right]\\&\times\left[\mathbf{x}_j(k+1|k+1)-\mathbf{x}(k+1|k+1)\right]^T\}\end{aligned}\tag{19}$$

4. SIMULATION ANALYSIS

In this section, the comparative analysis simulation of the proposed algorithm [9][11] are given. In this simulation, the initial position and velocity of the object are $(-10^4 m,-10^4 m)$ and $(30m/s,0m/s)$. In the first 1,500s, the object obeys uniform motion, then in the next 1,500s it obeys uniform acceleration motion with an acceleration $(0.1m/s^2,0.1m/s^2)$. There are three UWB-cells with the observation matrix $H_j=\begin{bmatrix}1&0&0&0&0&0\\0&0&0&1&0&0\end{bmatrix}(j=1,2,3)$ with sampling interval 1s. Their observation variance are listed in Table 1:

Table 1 the variance of three location cells (m)

Sampling time	System I	System II	System III
1~1000s	7	10	10
1000~2000s	10	7	10
2000~3000s	10	10	7

The one-step Markov transition probability matrix of corss-cell is:

$$T_{ij}=\begin{bmatrix}0.98&0.01&0.01\\0.01&0.98&0.01\\0.01&0.01&0.98\end{bmatrix}$$

The initial cell probabilities are $\beta_i=1/3\ \ (i=1,2,3)$. The motion model is uniform motion, and the state transformation matrix is $F=diag([A,A])$

$$A=\begin{bmatrix} 1 & T & \frac{1}{2}T^2 \\ 0 & 1 & T \\ 0 & 0 & 1 \end{bmatrix}$$

The error transformation matrix is:

$$G=\begin{bmatrix} \frac{1}{2}T^2 & T & 1 & 0 & 0 & 0 \\ 0 & 0 & 0 & \frac{1}{2}T^2 & T & 1 \end{bmatrix}^T$$

The acceleration noise standard variance are $w_x = w_y = 0.16m/s^2$, and the corresponding covariance matrix is $Q = diag\left(\left[w_x^2, w_y^2\right]\right)$. The RMSE of position error and velocity error based on 50 sampling in 3,000 sampling in Monte carlo simulation are shown in fig 2 and fig 3. From the simulation, the better performance can be got from the proposed algorithm.

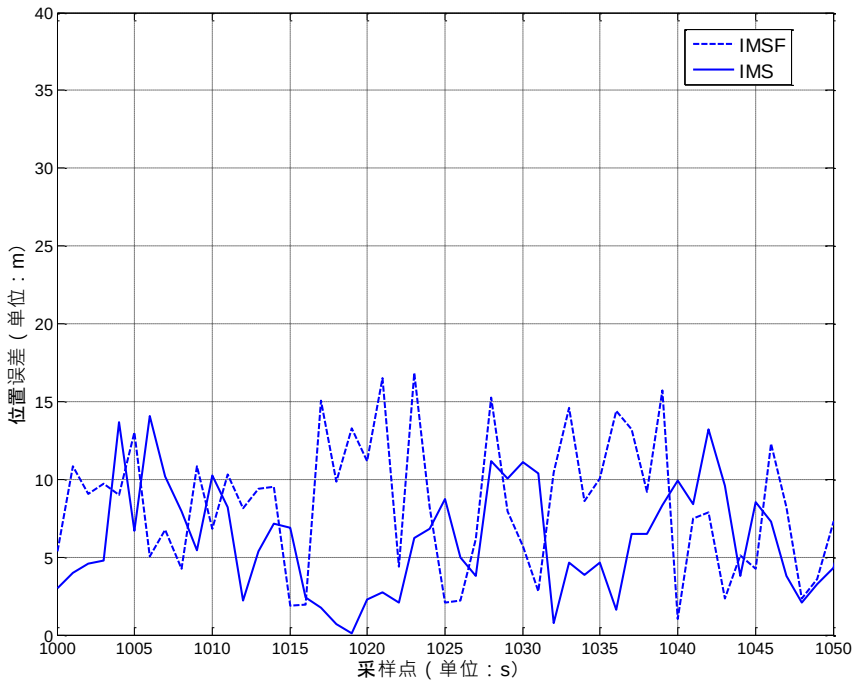

fig 2 RMSE of position error

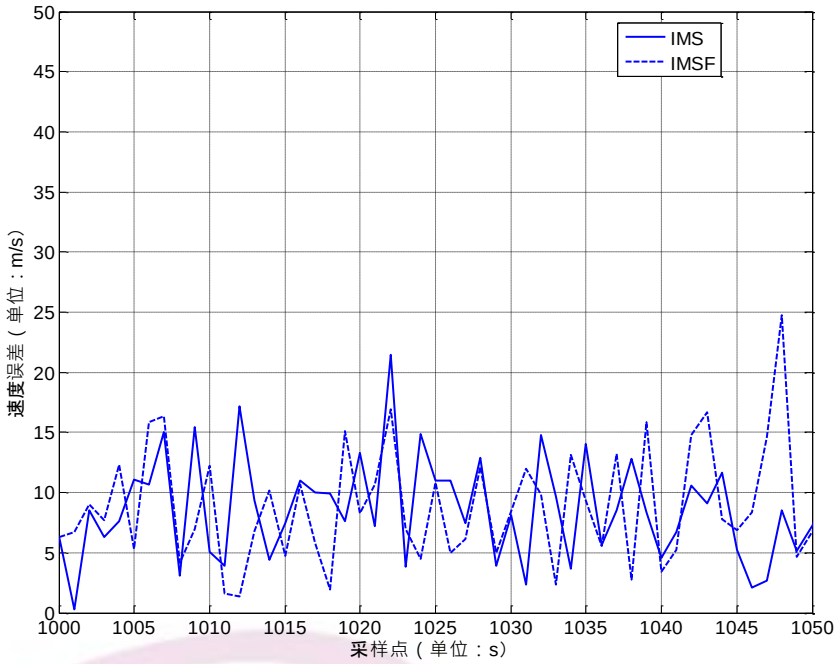

fig 3 RMSE of velocity error

The system probability trends of three UWB-cells in the whole process of simulation are shown infig 4. In the simulation, dynamic adjustment is processed to the three systems and their location performance is alternated. From the simulation, it, that the system probability alternate based on the performance, can be seen. But there are still some lag.

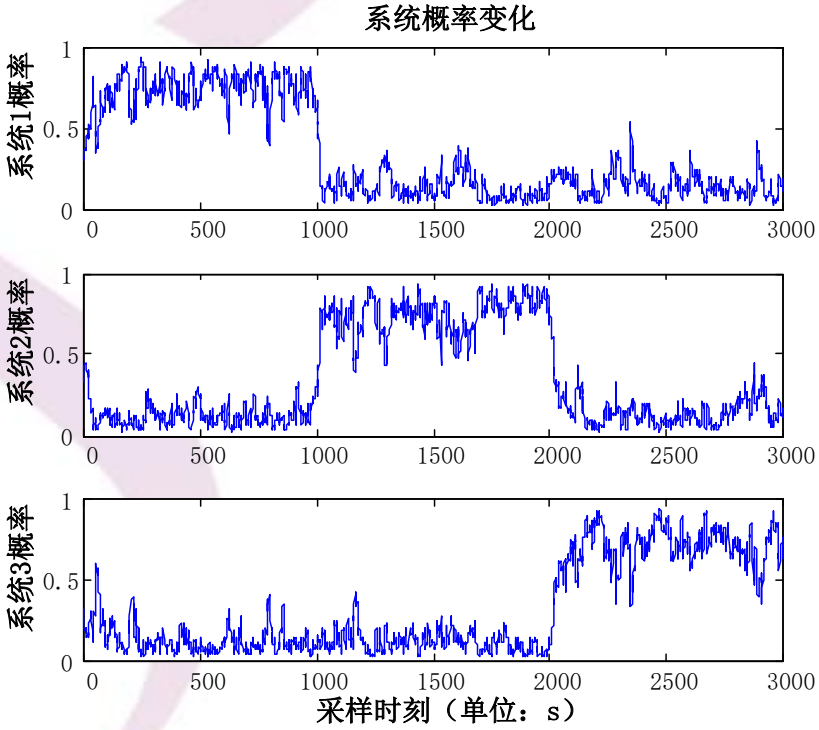

fig 4 the cross-cell probilities

REFERENCES

[1] Qin Lei, Li Jun-long, Zhou Di. Tracking for near space target based on IMM algorithm[J]. Systems Engineering and Electronics[J]. 2014, 36(7):1243-1249.
[2] Ma Xu. Research and application about a dynamic prediction model based on Bayesian Networks[D]. Harbin Engineering University.
[3] Blom H A P and Bar-shalom Y. The interacting multiple model algorithm for systems with Markovian switching coefficients[J]. IEEE Trans. on Automatic Control, 1988, AC-33 (8): 780-783.
[4] Sun Can, Xing Jian-ping, and Liang Hao-zhe, etal. S-IMM: Switched IMM algorithm for maneuvering target tracking[J]. Journal of Convergence Information Technology, 2012, 14(7):461-468.
[5] Chen Liang, Yang Jun-wei, Shu Xiao-di. Model-set adaptive algorithm of variable structure multiple-model based on K-L criterion[J]. Systems Engineering and Electronics, 2013, 35(12): 2459-2466.
[6] Luo Xiao-bing, Wang Hong-qiang, Li Xiang. Interacting multiple model algorithm with adaptive markov transition probabilities[J]. Jounal of Electronics & Information Technology, 2005, 27 (10): 1539-1541.
[7] Zhou Wei-dong, Cai Jia-nan, Sun Long. Interacting multiple model with optimal mode transition matrix[J]. Journal of Harbin Institute of Technology, 2014, 46(11): 101-106.
[8] He Jian, Wan Zhi-jiang, Liu Jin-wei. Indoor positioning technology based on powerline and location fingerprint[J]. Journal of Electronics & Information Technology. 2014,36(12): 2902-2908.
[9] Liu Zhi-gang, Wang Jin-kuan. Interacting multiple sensor filter for sensor networks[J]. Acta Electronica Sinica, 2012, 40(4): 724-728.
[10] Monica S, Ferrari G. UWB-based localization in large indoor scenarios: Optimized placement of anchor nodes[J]. IEEE Transactions on Aerospace & Electronic Systems, 2015, 51(2):987-999.
[11] Liu Zhi-gang, Wang Jin-kuan, Xue Yan-bo. Interacting multiple sensor filter[J]. Signal Processing, 92(2012): 2180-2186.

MODEL AND FRAMEWORK OF REAL-TIME FLOOD PROCESS DETECTION UNDER THE SENSOR WEB ENVIRONMENT

Kridsakron Auynirundronkool[1]
State Key Lab for Information Engineering in Surveying, Mapping and Remote Sensing (LIESMARS), Wuhan University, kron@gistda.or.th

Wenying Du[2*]
State Key Lab for Information Engineering in Surveying, Mapping and Remote Sensing (LIESMARS), Wuhan University, duwenying@whu.edu.cn

Nengcheng Chen[3]
State Key Lab for Information Engineering in Surveying, Mapping and Remote Sensing (LIESMARS), Wuhan University, cnc@whu.edu.cn

Zeqiang Chen[4]
State Key Lab for Information Engineering in Surveying, Mapping and Remote Sensing (LIESMARS), Wuhan University, zeqiangchen@whu.edu.cn

ABSTRACT

Flood occurred worldwide frequently, causing great causalities and economic losses. The occurrence and development of floods are process-based, while the state-of-art literature can only determine whether floods occur or not instead of judging flood phases, leading to coarse monitoring and delayed response. Therefore, it is imperative to construct the flood process detection (FPD) model and framework to implement the refined monitoring and provide decision information support for flood events. In this paper, floods were divided into four phases, including mitigation, preparedness, response, and recovery. Precipitation, water level, water flow and evaporation are variable indicators of floods, and their changes determine the flood occurrence or not in specific regions, thus the multi-dimensional vectors composed of precipitation, water level, water flow and evaporation are selected as flood indicators. The FPD model based on the support vector machine method was proposed in this paper to classify the flood indicators into four types, in correspondence with the four flood phases, respectively. The FPD framework conforming to the two standard information models, sensor model language, and observations & measurements, and the two service interfaces, sensor observation service, and sensor event service, of sensor web was proposed to achieve the real-time flood indicator access, filtering, and flood detection based on the aforementioned FPD model. The daily precipitation, water level, water flow, evaporation and the corresponding flood records data of Jiangxi, China from 1980 to 1989 were used as experimental data, firstly 80% of the data were used to construct the FPD model, and the left 20% were employed to verify the model precision, and secondly all the experimental observations were real-time accessed and filtered to validate the feasibility of the framework. The high accuracy of the flood detection results demonstrated the feasibility of the FPD model and framework proposed in this paper.

Keywords: *Flood Process Detection, Sensor Web, SVM, Real-time*

1. INTRODUCTION

Flood occurred worldwide frequently, causing great causalities and economic losses. Thus, it is of great urgency to propose a flood detection method for early flood alert and disaster prevention [1]. There are two kinds of early flood discovery methods in the current literatures, including the long-term or medium-to-long term flood probability prediction (FPP) method [2], and the real-time or near real-time flood detection method (FDM) [3, 4]. The occurrences of historic flood events all conform to the rule of "flood 1, silence, flood 2, silence, flood 3, …", which is exactly the basis of FPP. FPP is to discover the variation law of observations during the process of flood occurrence and development by analyzing the long time-series flood records and their corresponding hydrologic and meteorological observations, and then make the probability of flood occurrence predictions based on the probability density distribution function.

Predictions of flood events were usually made based on the correlation analysis between flood record and its corresponding hydrological and meteorological observation. The variation law of observation data during floods were discovered in the correlation analysis, based on which floods in the future were predicted. The river stages, rainfall-runoff, flow and flash flood predictions based on neural networks [5-9] all belong to this kind of predictions. While these studies are all long-time predictions based on historic data and probability distribution rules, all with the characteristics of poor stability, large errors and not process-based.

Different from prediction, the FDM is to employ the critical conditions of flood occurrence or not to filter the real-time observations, and flood is thought of to happen when the conditions are met. Auynirundronkool et al. (2012) [10] tried to use the monitoring of the flood area changes to detect floods, and the moderate-resolution imaging spectroradiometer (MODIS) and Radarsat data were used in the flood detection and mapping during their experiments in central plains of Thailand. Martinis et al. (2014) [11] proposed a fully automatic flood area mapping service method, implementing the automatic process from satellite data download, preprocessing, to the flood area extraction. But all these methods are based on satellite images, while limited by spatial or temporal resolutions, it often occurs that there is no data available in the spatial and temporal range of floods. Besides, there are some flood detection system developed, including Jongman et al. (2015) [12], Khalaf et al. (2015) [13], Garcia et al. (2015) [14], Shi et al. (2015) [15], Lai et al. (2013) [16] but some of them are based on low-reliability or restricted data source, some of them using quite simple and idealized filter conditions, and others being not flexible and extensible.

In a word, the problems of flood detection are faced with can be summarized but not limited to the three points: (1) Lack of flood process detection; (2) Not real-time based; and (3) Inflexible and unextendible. Therefore, to resolve the three abovementioned problems, the model and framework for real-time flood process detection (FPD) were proposed in this paper. The FPD model was constructed based on the support vector machine (SVM) method [17], which is a classical and mature model for feature classification of satellite images, and here it was used in the classification of flood observation dataset. The FPD framework was built based on Strom, a streaming data processing framework, and the senor web information models as well as service

interfaces, as the sensor web [18, 19] is recognized as the best candidate of implementing the unified while extensible real-time access, filter, and processing operations.

In the forthcoming sections, we illustrated the model and framework in Section II, performed the experiment and displayed the results in Section III. The discussion about the model and framework was provided in Section IV. Finally, Section V summarizes this work and describes future directions for this research.

2. METHODOLOGY

Real-time flood process detection under the sensor web environment was realized by the combination of the SVM-based FPD model and the real-time FPD framework. The former laid the model foundation for the determination of flood phases, and the latter provided a unified architecture for real-time data access, data filtering, and flood alert. The SVM-based FPD model was the core algorithm in the data filtering mechanism of the real-time FPD framework, and the real-time FPD framework provided a large-scale application scenario for the SVM-based FPD model.

2.1. SVM-based FPD model

The premise for the construction of SVM-based FPD model was that: (1) Floods were induced by the observable variables such as precipitation, and water level etc., for a specific region or watershed (with terrain, underlying surface, and drainage etc., remaining unchanged), and (2) Changes of the observable variables such as precipitation, and water level etc., during the occurrence and development of floods follow certain rules. The SVM-based FPD model was established based on the premise and the FLCNDEM proposed by Chen et al., 2015, in which floods are divided into four phases, including mitigation, preparedness, response, and recovery.

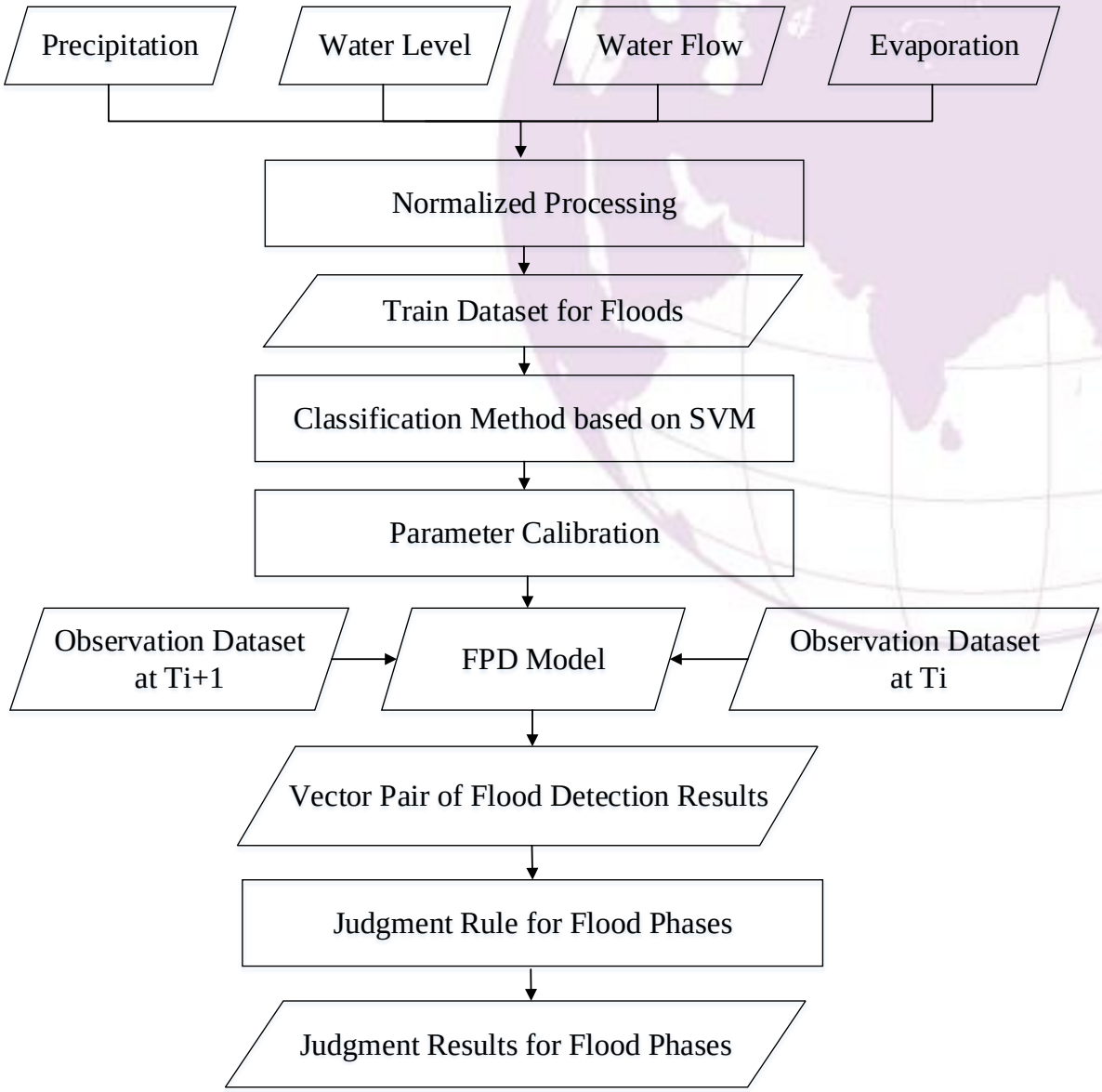

Fig. 1. Workflow of the SVM-based FPD model

In the SVM-based FPD model, as shown in Fig. 1, (1) the four observable variables of precipitation, water level, water flow, and evaporation were normalized according to the normalized observation calculation formula provided in Eq. (1); (2) each data record was composed of the normalized precipitation, water level, water flow, evaporation and their corresponding flood situation (FS) at the same day, FS = 1 represented there was flood while FS = 0 referred to there was no flood, and the FS values were determined by the authoritative flood records, all the data records consisted of the train dataset; (3) the FPD model was established based on the train dataset, the SVM model and the parameter calibration process; (4) Input the test observation dataset at the time T_i and T_{i+1}, and acquire the vector pair of flood detection results (FS_i, FS_{i+1}), where FS_i and FS_{i+1} refer to the FS at the time T_i and T_{i+1}, respectively; and (5) determine the flood phase according to the judgment rule demonstrated in Eq. (2).

$$\text{Normalized Observation} = \frac{\text{Observation - Average}}{\text{Max - Min}} \quad (1)$$

where observation refers to the original observation values of precipitation, water level, water flow, and evaporation, and average, max, and min refer to the average, max, and min value of them, respectively.

$$\text{Flood Phase} = \begin{Bmatrix} \text{Mitigation}, & \text{When}(FS_i, FS_{i+1}) = (0,0) \\ \text{Preparedness}, & \text{When}(FS_i, FS_{i+1}) = (0,1) \\ \text{Response}, & \text{When}(FS_i, FS_{i+1}) = (1,1) \\ \text{Recovery}, & \text{When}(FS_i, FS_{i+1}) = (1,0) \end{Bmatrix} \quad (2)$$

2.2. Real-time FPD Framework

The real-time FPD framework was able to implement the real-time observation data stream access, the FPD model based observation data stream filtering, the refined detection of flood phases, and E-mail alerts according to demands. It is composed of Storm, Sensor Observation Service (SOS), Sensor Event Service (SES), the connecting middleware of SOS and SES, SOS-SES-Feeder, and the SVM-based FPD model. Among these components, Storm and SOS takes charge of real-time observation data stream access, the SVM-based FPD model is used as the filtering algorithm of the observation data stream, SOS-SES-Feeder and SOS are to complete the data stream filtering and the flood phase determination.

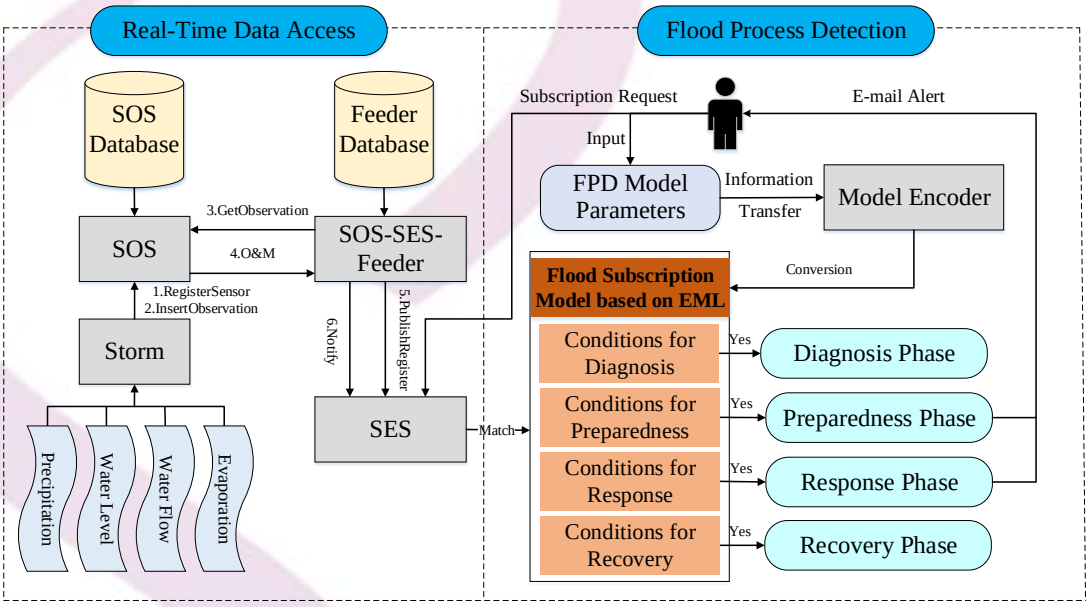

Fig. 2. Workflow of the Real-time FPD Framework

As demonstrated in Fig. 2, the workflow of the real-time FPD framework was: (1) Sensor Registration: the description information of the precipitation, water level, water flow, and evaporation sensors was encoded according to the Senor Model Language (SensorML), and was registered into SOS via the RegisterSensor operation; (2) Data Insertion: the observation data of the precipitation, water level, water flow, and evaporation sensors was encoded according to the Observations & Measurements (O&M), and was inserted into the SOS database through the InsertObservation operation; (3) Data Transfer: SOS-SES-Feeder sent the data request to SOS via the GetObservation operation, and SOS returns the data required to SOS-SES-Feeder in the format of O&M; (4) Data Registration in SES: SOS-SES-Feeder completed the

PublisherRegistration operation and notify the registration results to SES; (5) User Subscription: User submits the data subscription request and the FPD model parameters to SES, SES first received the parameters, encoded the model according to the EML format, formed the flood subscription model, then filtered the data stream according to the flood subscription model formed, and finally matched the data stream with the flood phase conditions, determined the flood phase and provided E-mail alert when necessary.

3. EXPERIMENTS AND RESULTS

3.1. Experimental Data

This paper used the precipitation, water level, water flow, and evaporation data in Jiangxi Province, China, from 1980 to 1989 (Download from the website of the National Earth System Science Data Sharing Infrastructure of China, URL: http://www.geodata.cn/data/), and the corresponding flood record data from the China meteorological disaster record collection (Jiangxi Volume) [20], and the flood records, precipitation, and water level observations of the Liangzi Lake flood occurring in Liangzi Lake, Wuhan, China from 1 July 2010 to 31 August 2010, as experimental data to test the validation and feasibility of the SVM-based FPD model and the real-time FPD framework, respectively. The reason why different dataset was used in the real-time FPD framework validation experiment was that the Liangzi Lake flood event lasted a longer time so that the results of different flood phases can be distinguished and displayed more clearly. The data frequency is one data record per day, and the flood records are specific to township. To be specific, there were 27 floods, totally lasting 68 days, covering 14 counties and 14 hydrological or meteorological stations, involved in our dataset. The space and time information of flood occurrence and their corresponding flood duration time and hydrological or meteorological station name information were displayed in Table 1. In contrast, non-flood days were also selected to consist of the dataset. There are in total 377 records in the dataset, 68 flood days (18%), 309 non-flood days (82%). Among the dataset, 299 records (79.3%) were used as the train dataset, and 78 records (20.7%) were used as the test dataset. For the train dataset, 54 records (18.1%) were flood days, while 245 records (81.9%) were non-flood days. And for the test dataset, 14 records (17.9%) were flood days, while 64 records (82.1%) were non-flood days. The summary of the record number and proportion for different types of dataset was shown in Table 2.

Table 1. Flood records and the corresponding stations

Location (County)	Time	Flood Duration (Days)	Station
Shangyou	8 May 1983	1	Anhe
	4-5 May 1984	2	
	2-3 July 1985	2	
Wanan	26 – 27 April 1980	2	Dongbei
	12 July 1980	1	
	14-15 May 1985	2	
	4 - 5 June 1985	2	
Longnan	26 July 1983	1	Dutou
	1 - 2 September 1984	2	
	3 July 1985	1	
Gaoan	14-18 June 1982	5	Jiacun
	7-9 July 1983	3	
Huichang	15-17 June 1983	3	Mazhou
Shanggao	7-9 July 1983	3	Niutoushan
	4 June 1985	1	
Lianhua	13-18 June 1982	6	Qianfang
	11-12 May 1983	2	
Wuning	27 June - 1 July 1981	5	Qingjiang
	30 May 1983	1	
Nanfeng	31 May - 1 June 1984	2	Shuangtian
Lean	13 - 18 June 1982	6	Wutou
	15 June 1983	1	
Xiushui	30 May 1983	1	Yangshuping
	5-10 July 1983	6	
Yifeng	6-9 July 1983	4	Yifeng
Yiyang	2 June 1983	1	Yiyang
Yongxiu	30-31 August 1980	2	Zhelin

Table 2. Summary of the record number and proportion for different types of dataset

	Total Records	Flood Days	Flood Frequency	Non-Flood Days	Non-Flood Frequency
Train Dataset	299	54	18.1%	245	81.9%
Test Dataset	78	14	17.9%	64	82.1%
Total Dataset	377	68	18.0%	309	82.0%

3.2. Detection results of the FPD Model

There are four parameters *s*, *t*, *c*, *g* involved in the FPD model, with *s* referring to the type of SVM, *t* representing the type of kernel function, *c* meaning loss function, and g referring to the gama function of the kernel function. In this paper, the parameter calibration process was performed by keeping one parameter changing while others remaining unchanged, and the parameter combination which could produce the highest overall accuracy of flood detection results were selected as the optimal parameters. The optimal parameters used in this paper were $s = 0$, $t = 2$, $c = 2$, and $g = 16$, respectively. Under the optimal parameter conditions, detection results of the FPD model were shown in Table 3, with 9 floods correctly detected while 5 floods not detected, and with 63 non-floods correctly detected while 1 non-floods mistakenly detected as flood.

Table 3. Detection results of the FPD Model

Class	Flood Record		Total
	Flood	Non-Flood	
Flood	9	5	14
Non-Flood	1	63	64

3.3 Real-time data access, filter, and alert

This section used the Liangzi Lake flood occurring from 1 July 2010 to 31 August 2010 as an example to test the feasibility of the real-time FPD framework. As the Liangzi Lake flood was a historic flood event, in order to test the real-time data access, filter, an alert, the data time was resampled to the system time of experiments, and the data frequency was resampled from one day to one minute to shorten the experimental time. A prototype was developed based on the real-time FPD model and framework proposed in this paper, and real-time data access interface was shown in Fig. 3. The real-time data access was realized by combing Storm and SOS, and what users need to do was to select the sensor you were interested in and clicked the finish sensor selection button, then the selected sensor would be registered into the system automatically, and its associated data could be accessed in real-time.

Fig. 3 Prototype interface for real-time data access

The result display interface for the Liangzi Lake flood was shown in Fig. 4, with different color representing different flood phases, cyan referring to the mitigation phase, orange representing to the preparedness phase, pink meaning the response phase, and green referring to the recovery phase. The detection results conformed to the flood occurrence rule, that was, first mitigation phase, then preparedness and response phase, and finally the recovery phase.

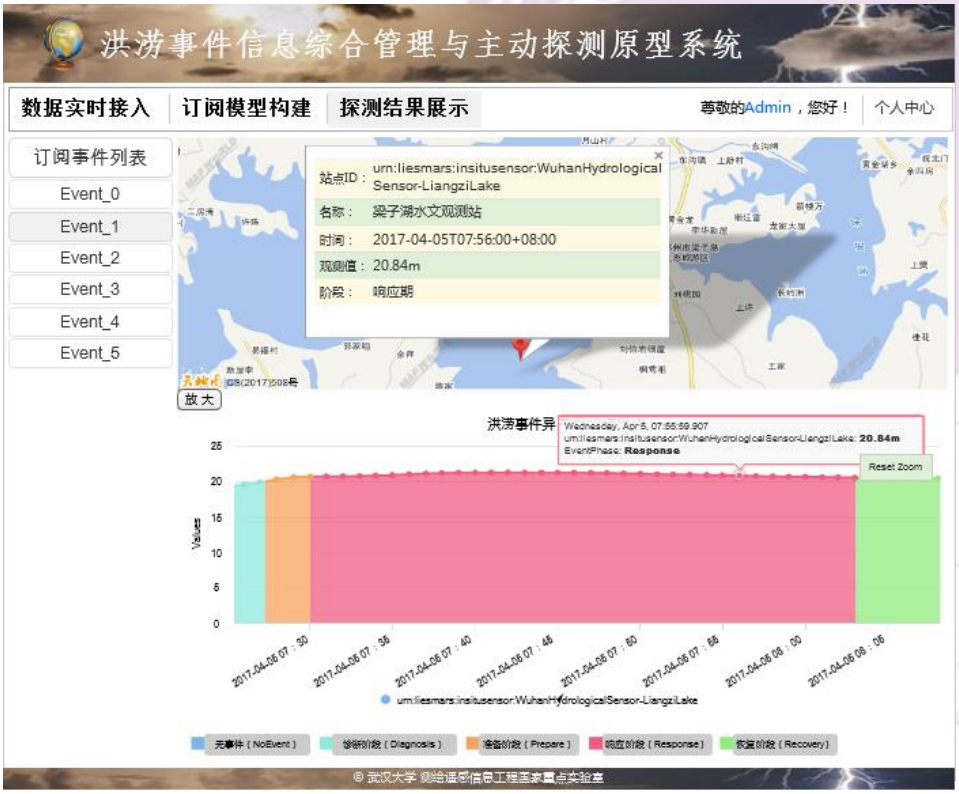

Fig. 4 Result display interface for the Liangzi Lake flood

Fig. 5 demonstrated the E-mail alert interface for the Liangzi Lake flood, (a) is the alert for the preparedness phase, while (b) is that for the response phase. Whether the E-mail alert was sent or not depended on the flood phase detection results. E-mail alerts would be sent to the subscriber only when the flood was detected to be in the preparedness or response phase.

(a) (b)

Fig. 5. E-mail alert interface for the Liangzi Lake flood

4. DISCUSSION

This section will be elaborated from the two perspectives of model accuracy evaluation as well as framework reusability and extensibility. The former performs quantitative evaluation for the SVM-based FPD model, and the latter discusses the reusability and extensibility of the real-time FPD framework.

4.1. Model Accuracy Evaluation

The accuracy of the FPD model determines the accuracy of flood detection. This section performs the quantitative accuracy evaluation for the SVM-based FPD models. The evaluation was performed based on the three quantitative indicators of overall accuracy (OA), Kappa Coefficient, Commission Error (CE), Omission Error (OE), Producer's Accuracy (PA), and User's Accuracy (UA) [21]. Based on the detection results provided in table 3, OA = 92.3%, CE = 7.1%, OE =35.7%, PA = 64.3%, and UA =92.9%, respectively.

4.2. Framework reusability and extensibility

The reusability and extensibility of the real-time FPD framework can be elaborated from the two perspectives of sensor providers and data consumers. Sensor providers publish their data through the framework, while data consumers use the data published by sensor providers. Data exchange and sharing can be achieved through the real-time FPD framework proposed in this paper.

4.2.1. Service reusability and extensibility for sensor providers

The real-time FPD model and framework implemented in section 3 just provide an instance of the process-based flood detection and service. The framework can be reused and extended by sensor providers. For sensor providers, they can use the service to publish their sensor information and the sensor associated observations. If sensor providers have new sensors to be published, what they need do is just firstly encoding their sensor description information according to the SensorML template, and secondly formatting their observations in accordance with the O&M template.

4.2.2. Service reusability and extensibility for data consumers

For data consumers, they can reuse the real-time FPD model and framework to subscribe flood events occurring in different regions or different time ranges. For the subscription of flood events occurring in the same region but different time ranges, what the data consumers are required to do is just changing the time ranges of the data, and then submit their new subscriptions. But for the subscription of flood events occurring in the different regions and different time ranges, the data consumer need to change both the spatial and temporal ranges in their subscriptions. Besides, the SVM-based FPD detection model proposed in this paper can be extended to any model of flood detection, only if the detection model is encoded according to the specification of EML.

4.3. Advantages

The real-time FPD model and framework proposed in this paper provide a unified and extensible solution for process-based flood detection and alert, via which the flood events occurring in any region or any time all can be detected. New sensors, flood detection algorithms or flood services can be added in the real-time FPD model and framework according to the method provided in section 4.2.1 and 4.2.2. The real-time FPD model and framework makes a flood detection model and system universally applied in multiple regions and organizations possible, and it can increase the reuse rate of the code, meanwhile save plenty of time and resources possibly wasted by repetitive coding.

4.4. Limitations

Parameters involved in the SVM-based FPD model was calculated based on the historic flood associated observations, and inappropriate parameters might lead to inaccurate flood detection results. In addition, the real-time FPD framework proposed in this paper could only provide alert service, and more service types need to be added in the framework to satisfy the needs from different phases of floods.

5. CONCLUSION AND OUTLOOK

In this paper, firstly, in combination with flood observation data and flood records, the SVM-based FPD model was proposed in this paper; secondly, the real-time FPD framework was put forward based on Storm, SOS, SES, and the SVM-based FPD model; and thirdly, the flood event process detection and alert prototype is designed and implemented based on the SVM-based FPD model and the real-time FPD framework. The water level, precipitation, water flow, and evaporation data of ** hydrological stations in Jiangxi, China from year 1980 to 1989 and their corresponding flood record data were used as experimental data to test the feasibility and effectiveness of the real-time FPD model and framework proposed in this paper, and the detection results demonstrated that the model and framework proposed in this paper could be used in the detection of flood process, proving that the feasibility and effectiveness of the SVM-based model and the real-time FPD framework.

ACKNOWLEDGEMENTS

This work was supported by grants from the National Nature Science Foundation of China program (no. 41771422), the Nature Science Foundation of Hubei Province (no. 2017CFB616), the Union Foundation of Ministry of Education of the People's Republic of China (no. 6141A02022318), the Creative Research Groups of Natural Science Foundation of Hubei Province of China (no. 2016CFA003) and the Fundamental Research Funds for the Central Universities (no. 2042017GF0057).

REFERENCES

[1] GuhaSapir, et al., "Annual disaster statistical review 2014: the numbers and trends," Region II - Asia, 2015.

[2] Saini, S.S., S.P. Kaushik, and R. Jangra, "Flood-risk assessment in urban environment by geospatial approach: a case study of Ambala City, India," Applied Geomatics, 8(3): pp. 1-28, 2016.

[3] Cornelia, G. and R. Peter, "Multitemporal and Multispectral Remote Sensing Approach for Flood Detection in the Elbe-Mulde Region 2002," CLEAN - Soil, Air, Water, 33(5): pp. 395-403, 2010.

[4] Rudolfbrãzdil, Z. Kundzewicz, and Gerardobenito, "Historical hydrology for studying flood risk in Europe," International Association of Scientific Hydrology Bulletin, 51(5): pp. 739-764, 2006.

[5] Alvisi, S. and M. Franchini, "Grey neural networks for river stage forecasting with uncertainty," Physics & Chemistry of the Earth, 42-44(208): pp. 108-118, 2012.

[6] D. Herr, H. and R. Krzysztofowicz, "Addendum to Bayesian ensemble forecast of river stages and ensemble size requirements,". 387: pp. 151-164, 2010.

[7] Khan, M.S. and P. Coulibaly, "Bayesian neural network for rainfall-runoff modeling," Water Resources Research, 420(7): pp. 379-393, 2006.

[8] Piotrowski, A., J.J. Napiórkowski, and P.M. Rowiński, "Flash-flood forecasting by means of neural networks and nearest neighbour approach – a comparative study," Nonlinear Processes in Geophysics, 13(4): pp. 443-448, 2006.

[9] Sahoo, G.B. and C. Ray, "Flow forecasting for a Hawaii stream using rating curves and neural networks," Journal of Hydrology, 317(1–2): pp. 63-80, 2006.

[10] Auynirundronkool, K., et al., "Flood detection and mapping of the Thailand Central plain using RADARSAT and MODIS under a sensor web environment," International Journal of Applied Earth Observations & Geoinformation, 14(1): pp. 245-255, 2012.

[11] Martinis, S., J. Kersten, and A. Twele, "A fully automated TerraSAR-X based flood service,". ISPRS Journal of Photogrammetry & Remote Sensing, 104(2013): pp. 203-212, 2015.

[12] Jongman, B., et al., "Early Flood Detection for Rapid Humanitarian Response: Harnessing Near Real-Time Satellite and Twitter Signals,". ISPRS International Journal of Geo-Information, 4(4): pp. 2246-2266, 2015.

[13] Khalaf, M., et al. "Advance flood detection and notification system based on sensor technology and machine learning algorithm," International Conference on Systems, Signals and Image Processing. 2015.

[14] Garcia, F.C.C., A.E. Retamar, and J.C. Javier. "A real time urban flood monitoring system for metro Manila," in TENCON 2015 - 2015 IEEE Region 10 Conference. 2016.

[15] Shi, H., et al., "A service-oriented architecture for ensemble flood forecast from numerical weather prediction," Journal of Hydrology, 527: pp. 933-942, 2015.

[16] Lai, H.C., et al., "A Developing Flood Automation System," Applied Mechanics & Materials, 457-458: pp. 1220-1223, 2013.

[17] Cortes, C. and V. Vapnik, "Support Vector Network," 20(3): pp. 273-297, 1995.

[18] Botts, M., et al. "OGC® Sensor Web Enablement: Overview and High Level Architecture," in Autotestcon. 2008.

[19] Arne, B., et al., "New Generation Sensor Web Enablement," Sensors, 11(3): pp. 2652-99, 2011.

[20] Wen, K., China Meteorological Disaster Records (Jiangxi Volume) (In Chinese). Beijing, China: Meteorological Press, 2006.

[21] Fitzgerald, R.W. and B.G. Lee, "Assessing the classification accuracy of multisource remote sensing data," Remote Sensing of Environment, 47(3): pp. 362-368, 1994.

DEVELOPMENT OF SPECTRAL LIBRARY FOR TRACE DETECTION OF EXPLOSIVES USING HYPERSPECTRAL SENSOR

Siddharth Chaudhary[1], Dr. Sarawut Ninsawat[1], Dr. Tai Nakamura[1]
[1]Remote Sensing and GIS (FOS), School of Engineering and Technology
Asian Institute of Technology, Pathum Thani, Thailand
siddharth.chaudhary@ait.asia , sarawutn@ait.asia , nakamura-tai@ait.asia

ABSTRACT

Determining the traces of chemicals is an important factor for identifying the explosive materials which are in the form of improvised explosive devices (IED). Due to the national security the research community has escalated the research in the field of detection of explosives. However, little information is known about identifying traces of chemicals using hyperspectral imaging. It is a combination of spectroscopy and imaging technique which gives information about the spatial distribution and chemical properties of the objects. The study provides a fast, non-contact and non-destructive method using visible and near infrared (400-1000nm) hyperspectral imaging (VNIR-HSI) for trace detection of chemicals used as a part of IED. The various explosives used in the research for this purpose are ANFO, C4 and TNT. A spectral library of these chemicals along with the background material is built. Identification of the chemicals ANFO, C4 and TNT is achieved using a high sensitive model developed in this study which leads to insitu detection of explosives using VNIR-HSI.

***Keywords**: Trace explosives, Visible Near Infrared, Hyperspectral Imaging, Spectral Library*

1. INTRODUCTION

The threat of explosive is increasing due to the large number of conflicts taking place across the world due to which there is increase in number of warzones. This is a serious issue that is affecting socio-economy of many countries like public security, unused arable land, closing of trade routes, isolation of villages. Such problems act as a hindrance in the development of the country as discussed in [1]. These problems motivate the government and research community to develop a technique for fast and accurate detection of explosives.

To minimize the risk of destruction and contamination of traces Hyperspectral imaging (HSI) is most suitable as it provides non-contact identification of evidence. HSI is an integration of spectroscopy and digital imaging technique to create three-dimensional data set containing both spatial and spectral information of the target. HSI was initially used for remote sensing applications utilizing satellite imaging data of the earth [2] but has since found application in such diverse fields as food science [3], pharmaceuticals [4] and medical diagnostics [5]. Hyperspectral images are analogous to a stack of images, each acquired at a narrow spectral band. Like spectroscopy, HSI can be applied in different parts of the electromagnetic spectrum, e.g. ultraviolet (UV),

visible (VIS), near infrared (NIR), mid infrared (IR) or even the thermal infrared range. HSI is advantageous over other techniques due its speed of data acquisition, reduction of human error, no destruction of traces, no specimen preparation, and the ability to illustrate the results. Chemicals like ammonium nitrate, tri nitro toluene, C4 are used as explosive material. Ammonium nitrate is one of most common fertilizer used for agriculture but a mixture of ammonium nitrate and fuel oil in the ratio of 94:6 results in an explosive which is used widely [6].

2. OBJECTIVE

The main objective of the study was to develop a hyperspectral imaging technique to determine the traces of chemicals used in explosives because this system can give spatial and spectral information about the target. This objective was achieved by developing a spectral library for the chemicals and the background materials from the acquired hyperspectral images. Information was distributed in large number of bands and had data redundancy thus a suitable preprocessing technique was applied to reduce data redundancy and noise in the hyperspectral images. Specific objective of the system was:

- Acquire hyperspectral image
- Preprocessing of image for noise removal
- Acquire pure spectral response
- Build spectral library

3. METHODOLOGY

3.1. Chemical Samples

A total of 30 samples of pure chemical were used in this study which includes 10 samples each of Ammonium nitrate (AN), Trinitrotoluene (TNT) and Cyclotrimethylene trinitamine (C4). All the samples were collected by Foundation Innovation for Happiness and was stored safely in the laboratory.

3.2. Hyperspectral Imaging System

Images were acquired using hyperspectral camera manufactured by BaySpec. The instrument has two sensors visible and near infrared which provides images over 144 spectral bands with a spectral resolution of about 4.2 nm over the spectrum of 400-1000nm. The chemical samples prepared were placed on black color platform to reduce to the reflectance from the background. The movement of the platform was controlled using a potentiometer attached to the motor. Technical specification of the hyperspectral camera is described in Table 3.1 and laboratory setup is shown in Figure 3.1. Two artificial light sources one halogen lamp of 60 W and one IR lamp of 60 W was placed in opposite direction at angle of 45 covering the spectrum from 400-1000nm as shown in Figure 3.3. The light sources were arranged in such a way that light intensity was uniformly distributed around FOV shown in Figure 3.2. Light intensity was measured in Lux using a luxmeter at 13 different points in the field of view. SpecGrabber software was used to control and capture the raw images and CubeCreator was used to process the raw images to create hyperspectral image in 144 bands.

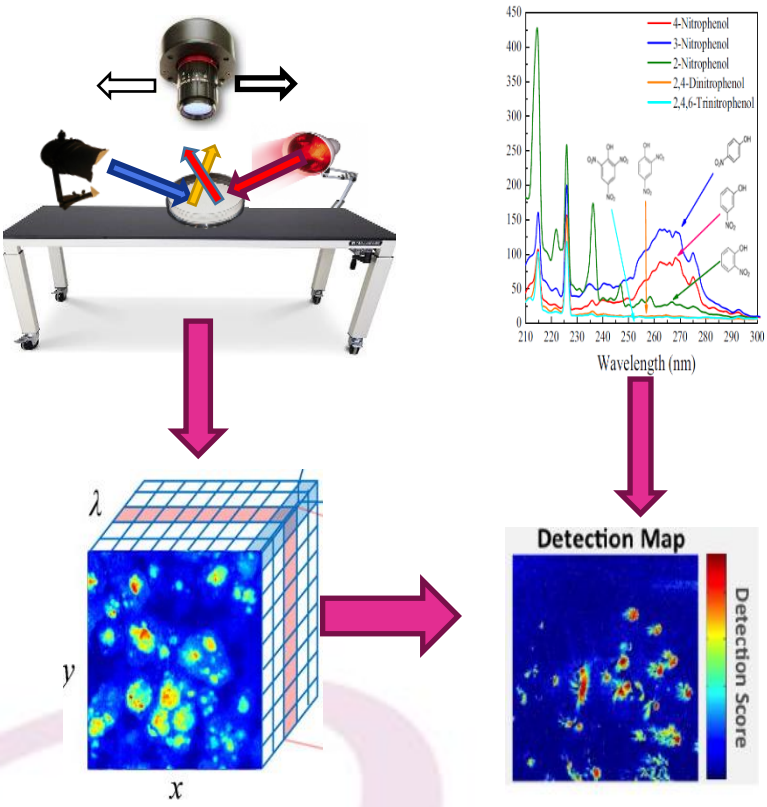

Figure 3.1: Graphical representation

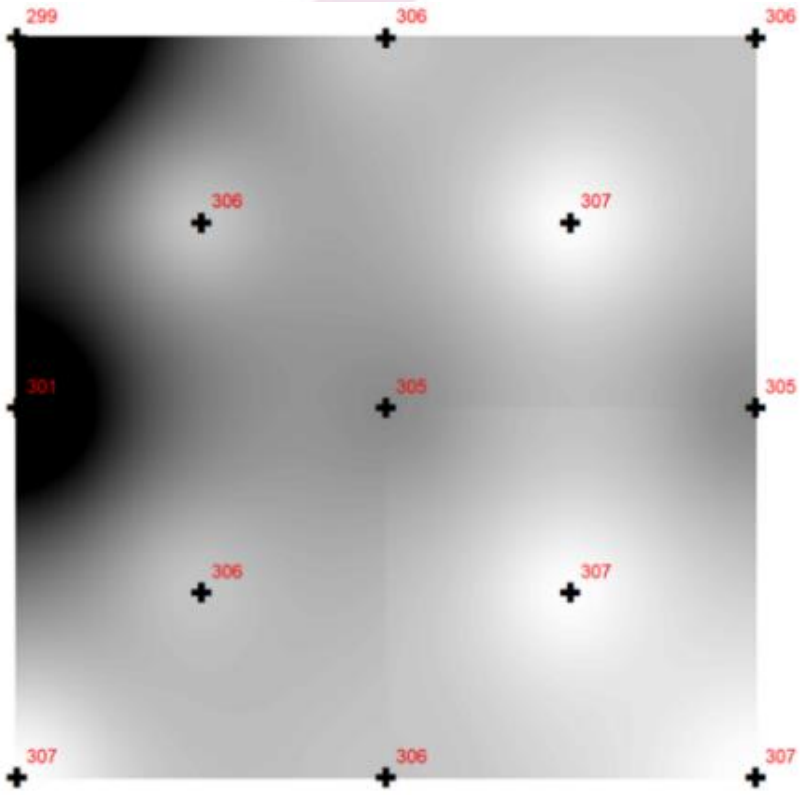

Figure 3.2: Distribution of light intensity

Scanning Technique	Push Broom
Field of View (FOV)	22°
Focal Length	16mm
Frame Per Second (FPS)	45
Swath	15.4 cm*12.3 cm
Spatial Resolution	0.012 cm
Spectral Bands	144
Spectral Resolution	4.16
Height of Sensor	40 cm

Table 3.1: Sensor specifications

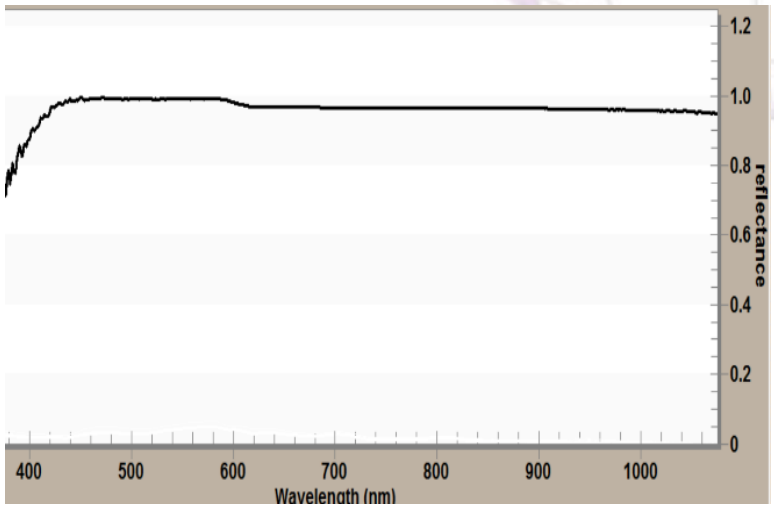

Figure 3.3: Spectrum of light source

3.2. Analysis of hyperspectral data and building spectral library

The hyperspectral cube created was analyzed on ENVI and IDL. To create the spectral reflectance and spectral library of various chemicals used in explosives following steps were carried out:

- Identification of chemicals on the platform
- Reflectance data was calculated
- Spikes or noises was removed by identifying the outliers
- Statistical analysis for each chemical sample

After processing the data spectral reflectance of each chemical samples and background material were calculated and saved as ASCII file format and *.lib format which was used as spectral library for explosives as shown in Figure 3.4. Such library will enable in prediction of spatial variation of traces of chemical in the scanned image.

4. RESULTS

All chemical samples were subjected to hyperspectral imaging. Raw spectrum was generated from the hyperspectral image which was later processed by removing the spikes and outliers to generate a processed spectrum as shown in Figure 4.1. The spectra of all three chemicals are different specially from 525nm – 975nm. The pure sample of TNT has lower reflectance throughout the spectrum as compared to pure ammonium nitrate and C4. TNT and C4 show similar peaks and falls in the spectral reflectance at 600nm, 725nm and 875nm due to the presence of NO_2. Whereas Ammonium nitrate can be distinguished between 600nm to 875nm as shown in Figure 4.2 because of constant rise in the spectral reflectance without any major peaks and falls as compared to C4 which also has lower reflectance. Ammonium nitrate can also be distinguished at 925 nm when there is a major fall in the reflectance. Further this library of explosives can be used for performing image classification and classifying the object in explosive and non-explosive.

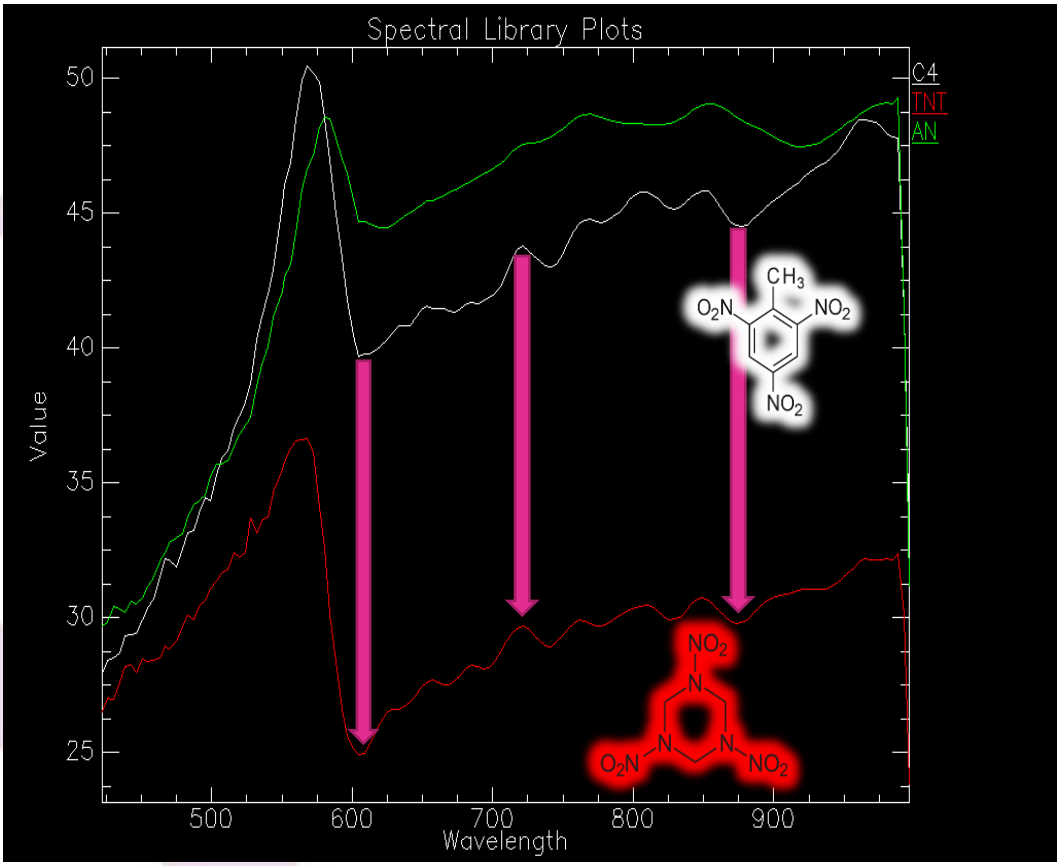

Figure 4.1: Processed spectral reflectance

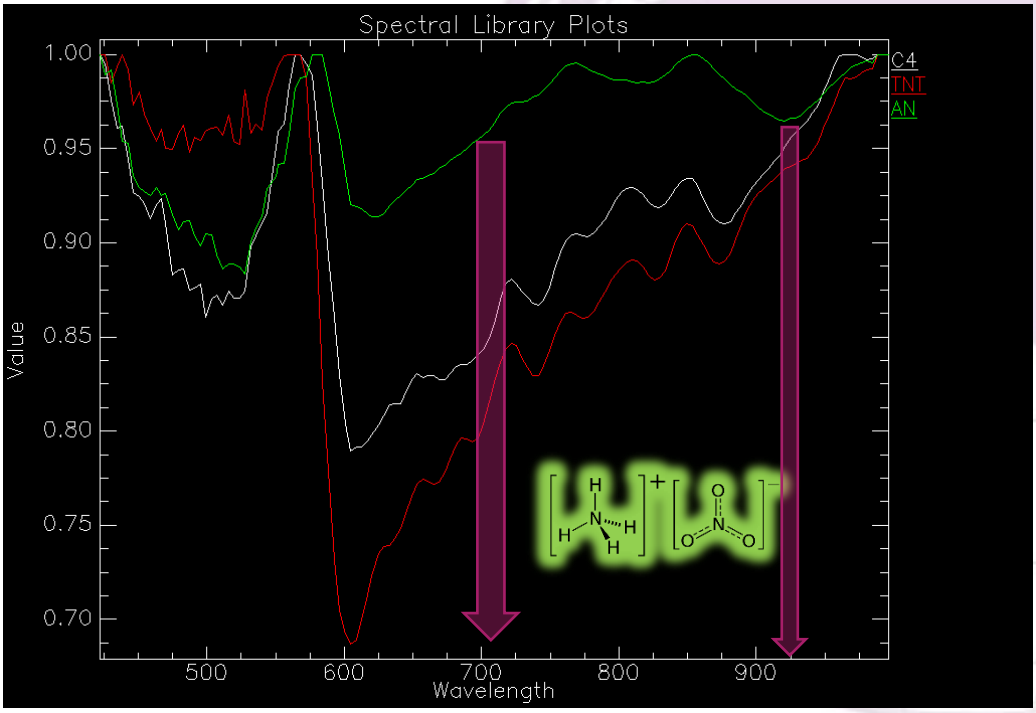

Figure 4.2: Normalized spectral reflectance

5. CONCLUSION AND DISCUSSION

The research was carried out to study the capability of the hyperspectral imaging system for trace detection of chemical by building a spectral library of the chemicals used in the explosives along with the background materials. Hyperspectral imaging system used in this study was a combination of digital imaging and spectroscopy which gives information regarding spatial distribution and properties of the chemicals. HSI is used increasingly in many applications but due to push broom scanning the system face a technical challenge like signal disturbance due to the relative movement between imaging platform and samples. But still the system is a promising tool for trace detection of chemicals because this technology is fast, non-contact nondestructive and presents advantage of remote and real-time measurements.

REFERENCES

[1] Makki, I.; Younes, R.; Francis, C.; Bianchi, T.; Zucchetti, M. A survey of landmine detection using hyperspectral imaging. ISPRS J. Photogramm. Remote Sens. 2017, 124, 40–53.

[2] M. Govender, K. Chetty, H. Bulcock, A review of hyperspectral remote sensing and its application in vegetation and water resource studies, Water Sa 33 (2007) 145–151.

[3] A.A. Gowen, C.P. O'Donnell, P.J. Cullen, G. Downey, J.M. Frias, Hyperspectral imaging – an emerging process analytical tool for food quality and safety control, Trends Food Sci. Technol. 18 (2007) 590–598.

[4] A.A. Gowen, C.P. O'Donnell, P.J. Cullen, S.E. Bell, Recent applications of chemical imaging to pharmaceutical process monitoring and quality control, Eur. J. Pharm. Biopharm. 69 (2008) 10–22.

[5] R.M. Levenson, E.S. Wachman, W. Niu, D.L. Farkas, Spectral imaging in biomedicine: a selective overview, in: Proceedings of SPIE, Imaging Spectrometry IV, vol. 3438, 1998, pp. 300–312

[6] Almeida, M. R., Logrado, L. P., Zacca, J. J., Correa, D. N., & Poppi, R. J. (2017). Raman hyperspectral imaging in conjunction with independent component analysis as a forensic tool for explosive analysis: The case of an ATM explosion. *Talanta*, *174*, 628-632. doi:10.1016/j.talanta.2017.06.064